SYNTHESES AND INVESTIGATION OF OPTOELECTRONIC PROPERTIES OF 5,6-BIS(OCTYLOXY)BENZO[c][1,2,5]OXADIAZOLE DERIVATIVES

A THESIS SUBMITTED TO
THE GRADUATE SCHOOL OF NATURAL AND APPLIED SCIENCES
OF
MIDDLE EAST TECHNICAL UNIVERSITY

BY

SEZA GÖKER

IN PARTIAL FULFILLMENT OF THE REQUIREMENTS
FOR
THE DEGREE OF MASTER OF SCIENCE
IN
CHEMISTRY

AUGUST 2014

Approval of the thesis:

SYNTHESES AND INVESTIGATION OF OPTOELECTRONIC PROPERTIES OF 5,6-BIS(OCTYLOXY)BENZO[c][1,2,5]OXADIAZOLE DERIVATIVES

submitted by **SEZA GÖKER** in partial fulfillment of the requirements for the degree of **Master of Science in Chemistry Department, Middle East Technical University** by,

Prof. Dr. Canan Özgen ______________________
Dean, Graduate School of **Natural and Applied Sciences**

Prof. Dr. İlker Özkan ______________________
Head of Department, **Chemistry**

Prof. Dr. Levent Toppare ______________________
Supervisor, **Chemistry Dept., METU**

Examining Committee Members:

Assoc. Prof. Dr. Ali Çırpan ______________________
Chemistry Dept., METU

Prof. Dr. Levent Toppare ______________________
Chemistry Dept., METU

Assoc. Prof. Dr. Yasemin Udum ______________________
Advanced Technologies Dept., Gazi University

Assist. Prof. Dr. İrem Erel Göktepe ______________________
Chemistry Dept., METU

Dr. Görkem Günbaş ______________________
Chemistry Dept., METU

Date: 05.08.2014

I hereby declare that all information in this document has been obtained and presented in accordance with academic rules and ethical conduct. I also declare that, as required by these rules and conduct, I have fully cited and referenced all material and results that are not original to this work.

Name, Last name: Seza GÖKER

Signature:

ABSTRACT

SYNTHESES AND INVESTIGATION OF OPTOELECTRONIC PROPERTIES OF 5, 6- BIS (OCTYLOXY) BENZO[c][1,2,5]OXADIAZOLE

Göker, Seza
M. S., Department of Chemistry
Supervisor: Prof. Dr. Levent Toppare

August 2014, 136 pages

As an acceptor unit, strong electron withdrawing moeities decrease LUMO levels resulting in low band gap polymers. Benzoxadiazole is one of the strongest electron acceptor units in the literature. Air stable polymers of this moeity can be synthesized on account of ability to adopt quinoid form and strong electron accepting property. 2,1,3-Benzooxadiazole bearing conjugated polymers are used for potential applications including organic light emitting diodes, solar cells, electrochromic devices and organic field effect transistor. Besides, alkoxyl substitution of benzooxadiazole unit is very helpful for the construction of the conjugated polymers with better solubility and higher molecular weight. Meanwhile, the polymer chain could have a planar conformation. On account of planar structure, π-conjugation is enhanced which results in extended absorption and low band gap when incorporated into the polymer backbone. In this thesis, 2,1,3-benzooxadizole was coupled with donor groups via both Stille and Suzuki polycondensation reactions. Oxidation and reduction behavior of the polymers were studied using cyclic voltammetry. The effect of thermal annealing on morphology was determined for selenophene containing polymer. After optimizing thickness and morphologies of polymer: PCBM, device production and current/voltage property measurements were conducted in a nitrogen-filled glovebox system. The analysis of the photovoltaic devices (ITO/PEDOT:PSS/Polymer:$PC_{70}BM$/Metal) were performed by means of the energy conversion efficiency measured under standard AM 1.5G illumination.

Keywords: Donor-Acceptor Approach, Benzooxadiazole, Conducting Polymers, Photovoltaic

ÖZ

5,6-BİS(OKTİLOKSİ)BENZO[c][1,2,5]OKZADİYAZOL TÜREVLERİNİN SENTEZİ VE OPTOELEKTRONİK ÖZELLİKLERİNİN İNCELENMESİ

Göker, Seza
Yüksek Lisans, Kimya Bölümü
Tez Yöneticisi: Prof. Dr. Levent Toppare

Ağustos 2014, 136 sayfa

Akseptör ünitesi olarak, güçlü elektron alıcı üniteler LUMO enerji seviyesini azaltarak düşük bant aralıklı polimerlerin eldesini sağlarlar. Benzookzadiazol, literatürdeki en kuvvetli elektron çeken gruplardan biridir. Bu ünitenin kinin yapısına sahip olabilme ve kuvvetlice elektron alabilme özellikleri sayesinde kararlı polimerler sentezlenebilir. 2,1,3-Benzookzadiazol içeren konjuge polimerler son zamanlarda organik güneş pillerinde, ışık saçan diyotlarda, elektrokromik malzemelerde ve organik transistörlerde kullanılmaktadır. Ayrıca, benzookzadiazole ünitesine alkoksi grupların ikame edilmesi daha iyi çözünürlüğe ve daha yüksek moleküler ağırlığa sahip polimerlerin üretilmesinde yardımcıdır. Bu sayede, polimer zinciri düzlemsel bir konformasyona sahip olabilir. Düzlemsel yapı sayesinde, π-konjugasyonu iyileştirilerek absorpsiyonda genişleme ve bant aralığında azalma ile sonuçlanmıştır. Bu tezde, 2,1,3-Benzookzadiazol ünitesi Stille ve Suzuki kenetlenme reaksiyonları ile bir çok donör ünitesi ile eşleştirilmiştir. İndirgenme ve yükseltgenme davranışları dönüşümlü voltametri ile çalışılmıştır. Termal ve çözelti tavlama yöntemlerinin morfolojiye etkisine bakılmıştır. Son olarak kalınlığın ve morfolojinin optimizasyonu yapıldıktan sonra, pilin üretimi ve akım/gerilim özelikleri azot dolu eldivenli kabin sisteminde gerçekleştirilmiştir. Güneş pillerinin (ITO/PEDOT:PSS/Polimer:PCBM/Metal) analizleri güç çevirim verimi AM 1,5G aydınlatma ile hesaplanmıştır.

Anahtar kelimeler: Donör-Akseptör Yaklaşımı, Benzookzadiazol, İletken Polimerler, Fotovoltaik

To Sezgi, My Family and Özgür

ACKNOWLEDGMENTS

I would like to thank Prof. Dr. Levent Toppare for his guidance and continuous support. He is not only a professor leading me but also a second father to me. His invaluable discussions, criticism, encouragement and advices showed that I could always succeed.

I would like to thank Assoc. Prof. Dr. Ali Çırpan for always answering my questions, his guidance and support.

I would like to to thank Assoc. Prof. Dr. Yasemin Arslan Udum and Şerife Özdemir Hacıoğlu for electrochemical, spectroelectrochemical characterizations and also for their valuable discussions.

I would like to thank Dr. Görkem Günbaş for always answering my questions persistenly, his patience, encouraging me, making molecular design more fun, coffee breaks and friendship.

I would like to thank Gönül Hızalan not only for teaching me everything but also for being a sister to me, giving a shoulder to cry and a hug for great moments.

I would like to thank Öykü Akçay, Ozan Erlik and Özde Ceren Hızal for their beautiful friendship and sharing years together. Their support and the memories we have helped me to handle difficulties.

I would like to thank my Melis Kesik and Nehir Utku for their friendship, supporting me every single time. I wish I could spend time with them from the first year of college.

I would like to thank Esra Özdemir, Esra Öğün, Hande Ünay, Sinem Toksabay, Şevki Can Cevher for providing such a nice friendship. They made these years both funny and endurable.

I would like to thank my little girls Merve İleri, Ebru Işık and Çağla İstanbulluoğlu for their support, listening to me relentlessly, coffee breaks, sharing great moments and providing a perfect working enviroment.

I would like to thank Görkem Eşsiz, one of my best friends. His understanding, encouragement, true friendship, our memories and laughters will always leave a smile on my face. I know our friendship will never grow old.

I would like to thank my chocholate pudding Leyla Deniz for being the third daughter of our family and a friend. Since 2002, we grew up together, shared perfect moments. The memories we have are incomporable to nothing. Our real friendship will overcome all difficulties even if her illness and distance between us.

I owe my special thanks to Özgür Şahin for his true love, patience, support and every single thing. He was always the role model for me, the reason to deal with desperate moments. It was very hard to proceed without him but his love gave me the strength I need. I know he will continue to encourage and support me till the day we meet again.

Special thanks go to Sezgi Göker, my other half, my sister, friend, parent and everything. She made this life meaningful. Words cannot express what she means to me.

Last but not least, words fail to express my gratitude to my father and my mother. They did more than their best for our education and life. Without their love and understanding, I could not succeed anything.

TABLE OF CONTENTS

LIST OF TABLES

TABLES

LIST OF FIGURES

FIGURES

LIST OF ABBREVIATIONS

ACN	Acetonitrile
Ag	Silver
BHJ	Bulk Heterojunction Solar Cell
CB	Conduction Band
CE	Counter Electrode
CIE	La Commission Internationale de l'Eclairage
CP	Conducting Polymer
CV	Cyclic Voltammetry
DCM	Dichloromethane
DMF	Dimethylformamide
ECD	Electrochromic device
EDOT	3,4-Ethylenedioxythiophene
E_g	Band gap
EPR	Electron paramagnetic resonance
HRMS	High Resolution Mass Spectrometer
HOMO	Highest Occupied Molecular Orbital
ITO	Indium Tin Oxide
L, a, b	Luminance, hue, saturation
$LiClO_4$	Lithium perchlorate
$NaClO_4$	Sodium perchlorate
NMR	Nuclear Magnetic Resonance Spectrometer
OLED	Organic Light Emitting Diode
PLED	Polymer Light Emitting Diode
Pt	Platinum
$(SN)_x$	Poly(sulfurnitride) / Polythiazyl
TBAB	Tetrabutylammonium bromide
$TBAPF_6$	Tetrabutylammonium hexafluorophosphate
THF	Tetrahydrofuran

TLC	Thin Layer Chromatography
PA	Polyacetylene
PAn	Polyaniline
PPV	Polyphenylene vinylene
PPy	Polypyrrole
VB	Valence Band

CHAPTER 1

INTRODUCTION

1.1. Conjugated Polymers

Conjugated polymers have attracted an overwhelming interest all around the world for the last few decades due to their solution processability, ease in band gap engineering via structural modification, low cost and flexibility. The modern study on this field began in 1977 with the preparation of polythiazyl in the form of shiny adherent films. It was the first synthetic conjugated polymer which is an explosive insoluble superconducting black powder at 2K. The plastic had not drawn much interest because it was only black powder for scientists which difficult to work with. Alan J. Heeger, Hideki Shirakawa and Alan G. MacDiarmid made all the difference in the field of conducting plastics by showing how a plastic can conduct electricity in its oxidized and reduced states. Polyacetylene was synthesized from ethyne using high amount of Ziegler-Natta catalyst accidentally resulting in a metal-like silvery black film. With this discovery, polyacetylene achieved a remarkably high electrical conductivity (10^3 S/cm) upon doping with iodine vapor at room temperature. Shirakawa *et al.* showed that the trans polyacetylene is the thermodynamically stable form having a high conductivity. For a polymer to be conductive, π-conjugation is the main prerequisite. Doping is the addition of chemicals with an electron-withdrawing property such as halogens. This process can increase the plastic conductivity levels up to a billion times of which matches the conductivity of metallic materials. Doping provides free movement of electrons resulting in conduction. In 2000, Heeger, Shirakawa and MacDiarmid were awarded with the Nobel Prize in chemistry for the discovery and development of conductive polymers. However polyacetylene is insoluble, sensitive to air and humidity therefore it is impossible to characterize and also not favorable for practical applications in daily life. This led to the development of more stable conjugated polymers which can be used as an active layer in many applications such as solar cells (OPVs), organic light emitting diodes (OLEDs), organic field effect transistors (OFETs), biosensors and electrochromics (ECs). Thiophene, furan, fluorene, pyrrole, benzene, aniline, and carbazole were some examples of common aromatic and heteroaromatic compounds studied in polymer science since they are not much sensitive to air and humidity like polyacetylene.

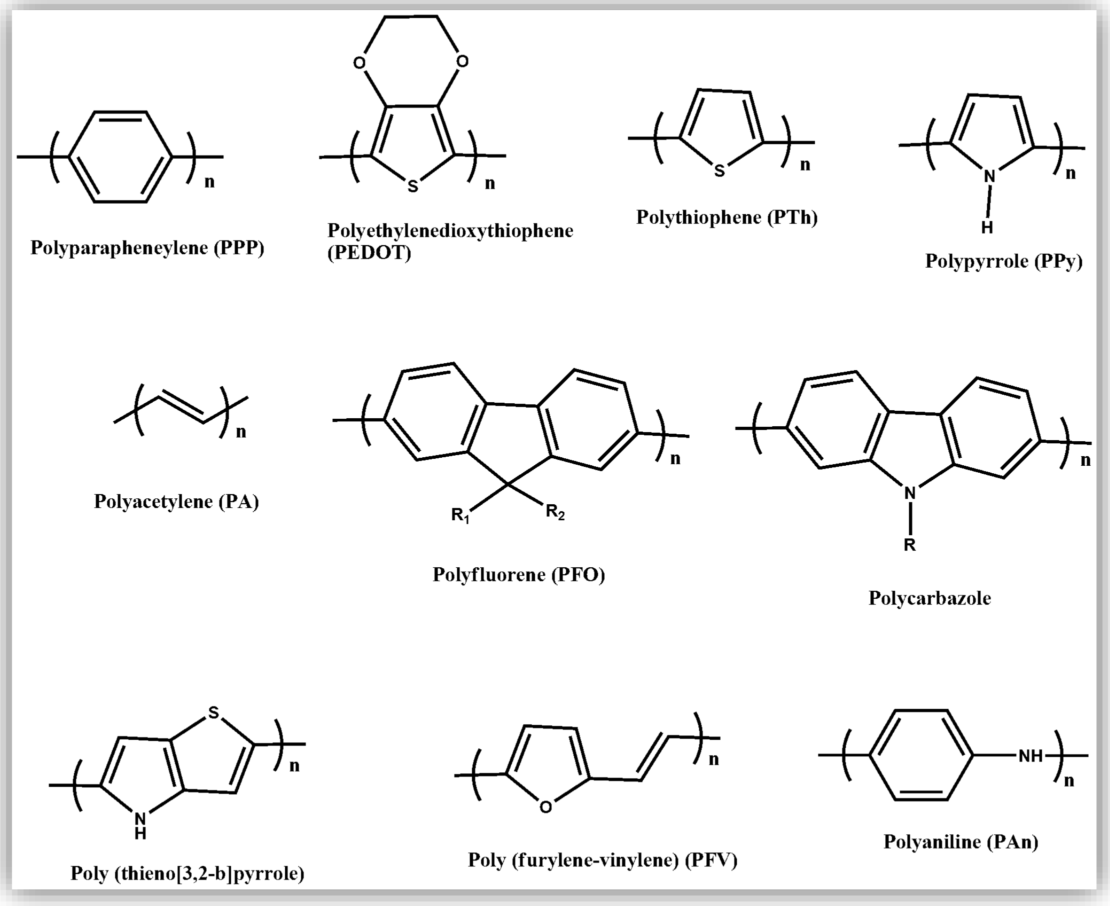

Figure 1.1: Structures of common conducting polymers

1.2. Band Theory

Band gap can be defined as the energy spacing between valence band (VB) which is also known as highest occupied molecular orbital (HOMO) and conduction band (CB) which is also known as lowest unoccupied molecular orbital (LUMO). Band theory explains the characteristics of insulator, semiconductors and metals. According to this theory, conducting polymers lie between metals and insulators according to their conductivity. Holes (p-type) and electrons (n-type) are the two types of charge carriers. For insulators, there is a large band gap between two bands resulting in no movement of charge carriers and hence conductivity. In metals, there is no band gap between empty conduction band and partially filled valence band therefore charge carriers can easily move between these two overlapped bands leading to conductivity. In the case of semiconductors, there is a small gap between filled valence band and empty conduction band therefore electrons can move from valence to conduction band resulting in conduction at ambient temperature. The band gap can be calculated in the UV-Vis spectrum from the onset of the π-π^* transition. The other way to determine band gap is to measure the oxidation and reduction onset values only if the polymer is both p and n dopable.

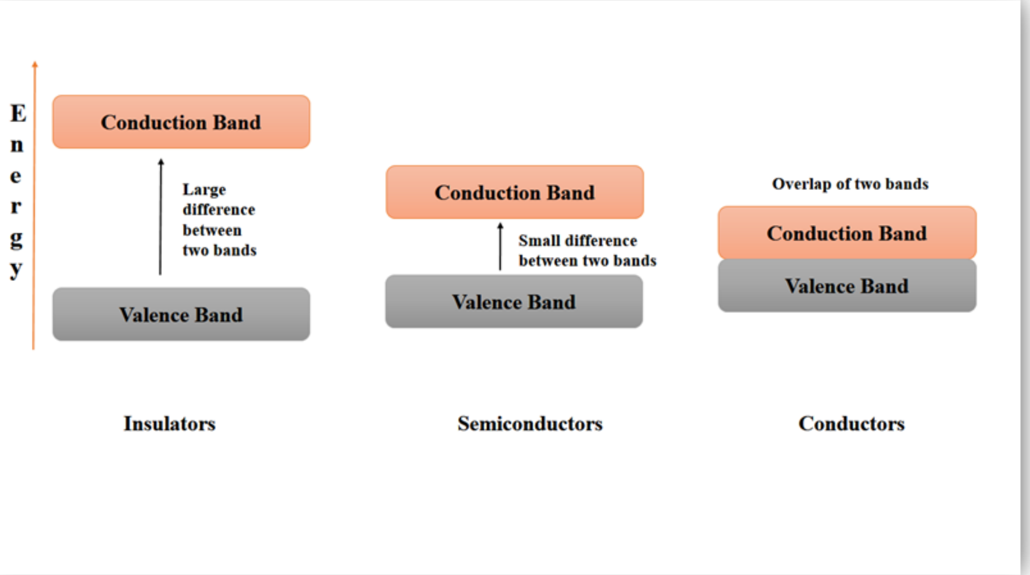

Figure 1.2: Band structures of materials

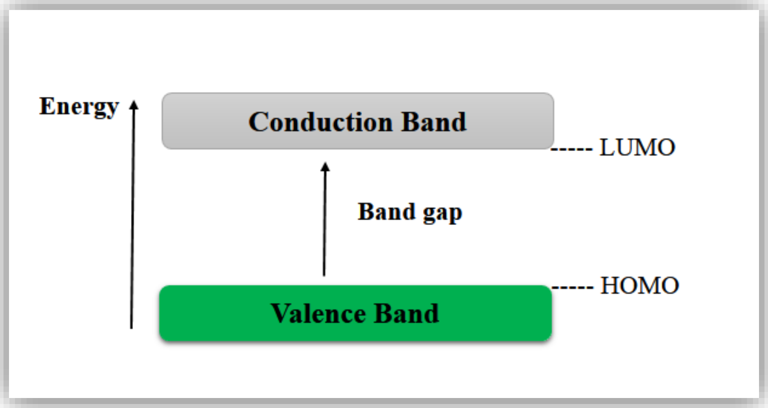

Figure 1.3: Representation of band structure in organic semiconductors

1.3. Conduction in Conjugated Polymers

Conducting polymers can be synthesized according to two widely employed methods: chemical and electrochemical polymerization. There are several other techniques carried out such as photochemical polymerization, solid state polymerization, pyrolysis [10]. Conductivity, processability, defined three dimensional structures, solubility and stability of the conducting polymers should be considered to determine the polymerization methods for a target design.

1.3.1. Solitons, Polarons and Bipolarons

Unlike polyacetylene, most of the conducting polymers do not have degenerate ground states as is the case for polyacetylene therefore there is not any indication for the formation of solitons. A neutral soliton is a free radical formed in the polymers with a degenerate ground state energy like polyacetylene. Polymers with nondegenerated ground state such as PPy and PPV, polarons and bipolarons form. Su *et al*. stated that formation of charge radicals during polymerization causes structural defects in the backbone. In trans polyacetylene which is thermodynamically favorable, the defect is called as neutral soliton since it moves as a solitary wave [1].

Oxidation of the polymer raises the energy of the orbital by removing electrons. Removal of one electron produces a radical cation namely ‘polaron’. Polarons have both spin and charge [2, 3]. Dications namely bipolarons form with exothermic chain reactions in further oxidation [4]. In such reactions, two polarons could also form however bipolarons are thermodynamically more stable because two charges cause electronic repulsion. Such positive charges in the polymer chain provides conduction in polymers.

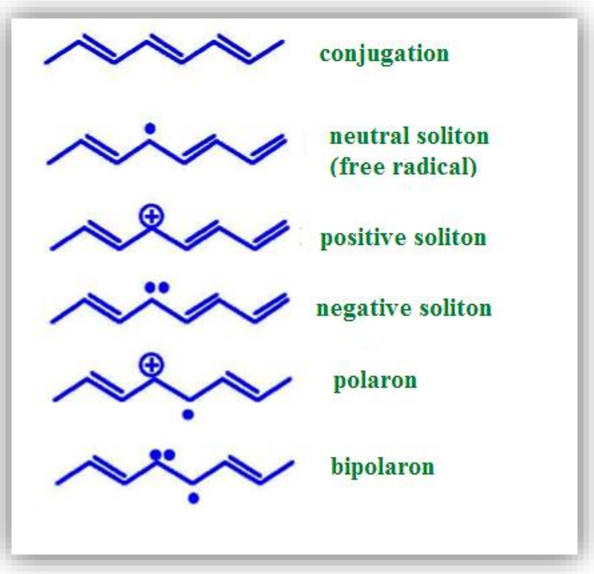

Figure 1.4: Charge carriers

1.3.2. Doping Process

When exposed to oxidative agents, twelve order of magnitude increase in the conductivity of polyacetylene was achieved due to its extended π system resulting in easy electron removal or gain in the polymer backbone. Doping can be defined as the introduction of charges to the polymer chain by a redox process. Removing an electron from the polymer chain is called p-doping whereas adding an electron to the polymer chain is called n-doping. There is no net spin in both neutral and heavily doped states since they are diamagnetic in nature. For slightly doped materials, there are unpaired electrons which were proven by EPR studies. Most heavily doped materials conduct electricity. [4]

Doping lead conjugated polymers to become conductors by forming interbands between conduction and valence bands. This process can completely change optical, magnetic, and mechanical properties of the polymers resulting from polaronic and bipolaronic bands [1]. Anions are relatively more sensitive to oxygen and air compared to cations, therefore n-doped conjugated polymers are not common as p-type ones.

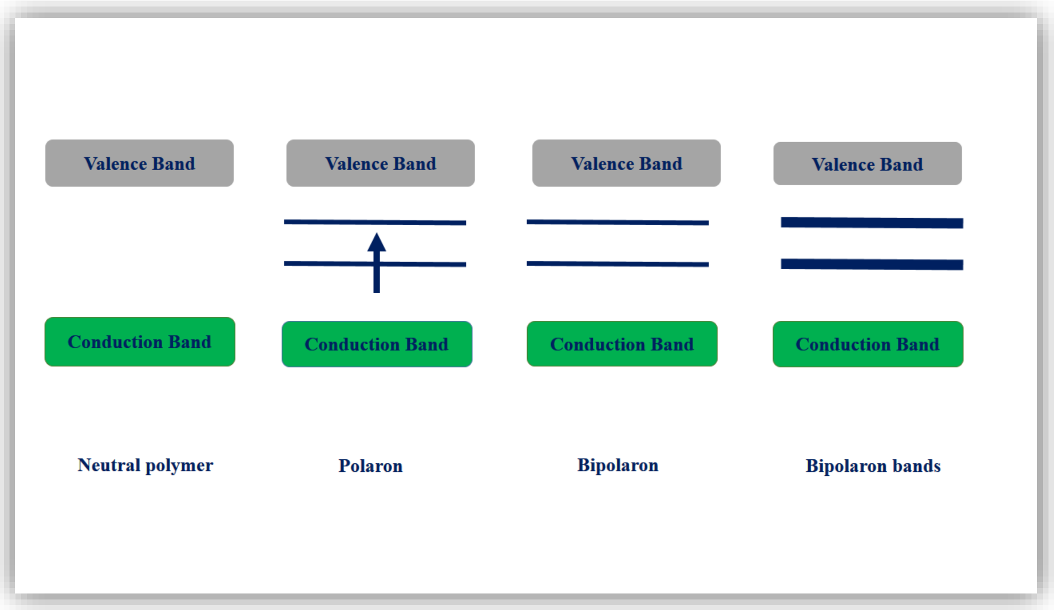

Figure 1.5: Energy bands

1.4. Polymerization Methods

1.4.1. Electropolymerization

Electrochemical synthesis of conjugated polymers are achieved by self-coupling of a monomer in an inert organic solvent system containing a supporting electrolyte. In anodic polymerization, irreversible oxidation proceeds whereas irreversible reduction occurs in cathodic polymerization. To synthesize homopolymers of electron rich units such as pyrrole, anodic polymerization is used since they have tendency for oxidation [4]. Electropolymerization is advantageous since there is no requirement for further purification. In this method, solvent and electrolyte types, concentration of monomer and electrodes strongly affect the properties of the polymer. Easy production of an electrochemically active conductive polymer film and control of film thickness, morphology and conductivity upon the applied potential, scan rate and time are some advantageous of oxidative electropolymerization [5]. Platinum, gold, glassy carbon, and indium–tin oxide (ITO) coated glass are some examples of anodes used in the electropolymerization. Generally, the electropolymerization is carried out potentiostatically or galvanostatically. In potentiodynamic techniques, constant potential is applied at the electrode surface like in cyclic voltammetry and a repetitive potential waveform is observed. Galvanostatic techniques provides qualitative information about the redox processes in the polymerization reaction. Moreover, the electrochemical behavior of the polymer film can also be examined by this method [6]. The monomer is dissolved in an appropriate solvent and supporting electrolyte couple. Anodic potential is applied for oxidation of monomer on an electrode surface. Solvent and electrolyte choice is important therefore they should be stable at the oxidation potential of the monomer. Since acetonitrile and propylene carbonate have high relative permittivity and large potential range, these are the solvents of choice for electropolymerization. The monomer is initially oxidized and the radical cation of the monomer is formed. Then, a neutral dimer is formed via reaction of radical cation with other monomers present in solution with the loss of another electron and two protons. The oxidized radical cations react with monomers to form oligomers until the polymer is formed [7, 8]. While the polymer is synthesized electrochemically, it is also doped at the same time. The oxidation potential of the polymer is lower than monomers due to extended conjugation in the system. The mechanism of electropolymerization is shown in Figure 1.6.

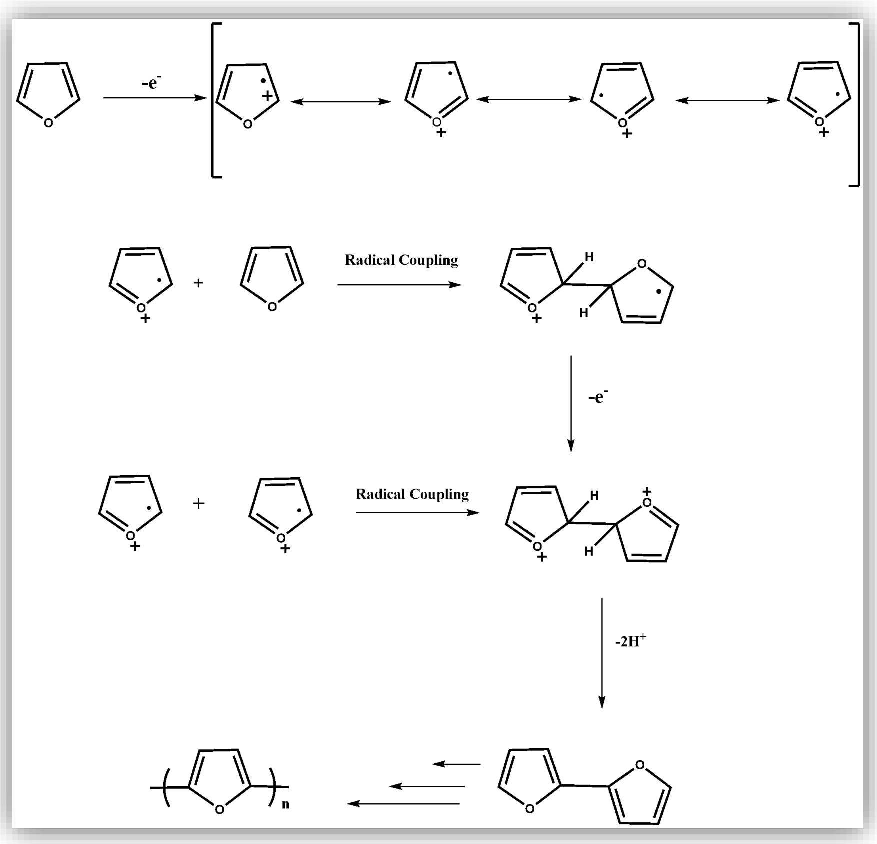

Figure 1.6: Mechanism of Electropolymerization

1.4.2. Oxidative Chemical Polymerization

In chemical oxidation polymerization, heterocyclic compounds react with anhydrous Lewis acid catalysts like $MoCl_5$, $FeCl_3$, $RuCl_3$ to obtain high molecular weight polymers with relatively high conductivity. Anhydrous chloroform or dioxane are used as solvents. The properties of chemically synthesized polymers are very similar to electrochemically synthesized ones. Polymers of furan, thiophene, pyrrole or alkyl substituted thiophene can be prepared by oxidative cationic polymerization [9].

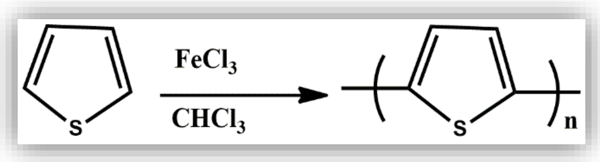

Figure 1.7: Chemical oxidation polymerization

1.4.3. Suzuki-Miyaura Coupling

Suzuki-Miyaura Coupling is used for selective formation of C-C bonds via reactions of organic halides with organometallics in the presence of transition metal catalysts [10, 11].

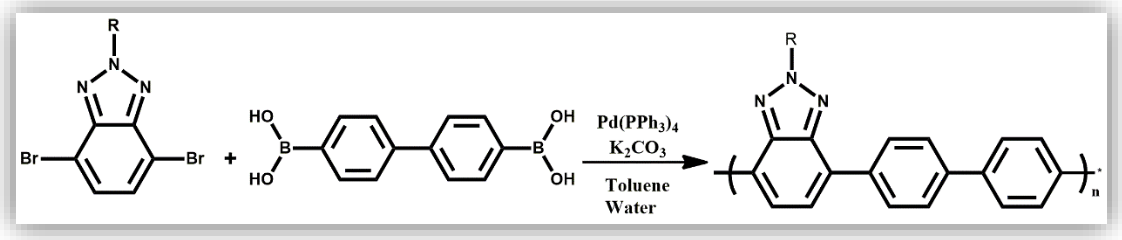

Figure 1.8: Suzuki Coupling

1.4.4. Stille Coupling

The Stille Coupling is one of the most efficient C-C bond forming reaction which utilizes two distinct monomers, stannanes and halides, to synthesize alternating and random copolymers [12].

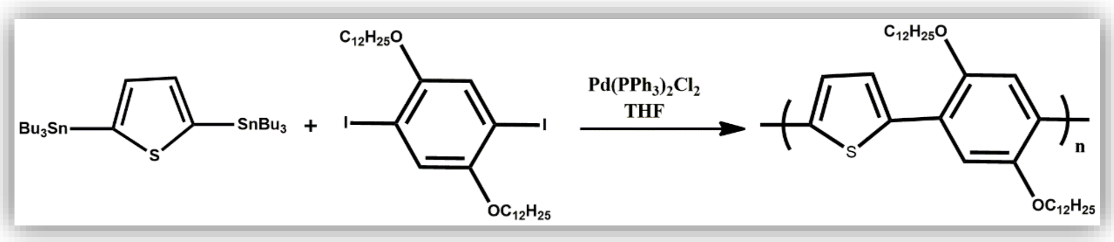

Figure 1.9: Stille Coupling

1.4.5. Yamamoto Coupling

In Yamamoto type polycondensation reactions, organometallic C-C couplings are promoted with $NiCl_2$/bpy/Mg/DMF system. $NiCl_2$, 2,2'-bipyridine (bpy), and Mg are mixed in DMF. Mg is believed to serve as a reducing reagent for [Ni^{II}Lm] to form [Ni^0Lm]; the polymer is formed by the polycondensation of the formed [Ni^0Lm]. Zinc can also be used as a reducing metal to generate [Ni0Lm] from [Ni^{II}Lm] for basic C -C coupling and dehalogenative polycondensation, generally carried out in solvents like N,N-dimethylacetamide (DMAc) and DMF. Moreover, $NiBr_2$, PPh_3 and bipyridine can also be used in dimethylacetamide for this type of polycondensation [13].

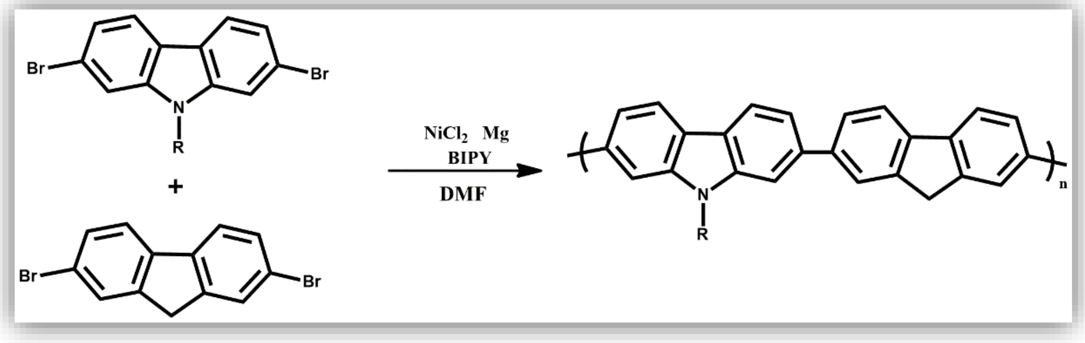

Figure 1.10: Yamamato Coupling

1.4.6. Knoevenagel Condensation

Knoevenagel condensation is the C-C bond formation between carbonyl compounds and active methylene species. Knoevenagel reaction products can be formed using heterogeneous catalysis with high yields. Alkali metal hydroxides or organic bases like primary, secondary and tertiary amines are used as catalysts [14, 15].

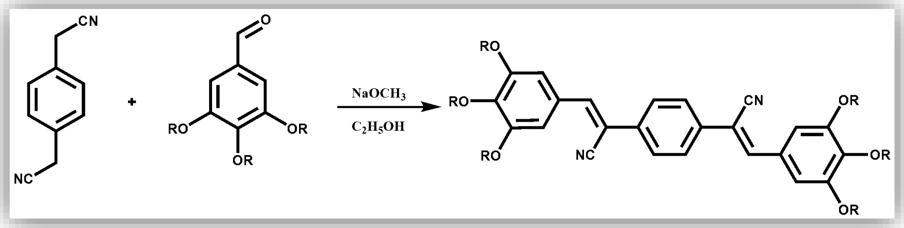

Figure 1.11: Knoevenagel Condensation

1.4.7. Tamao-Kumada-Corriu Coupling

Tamao-Kumada-Corriu coupling is a type of polycondensation reaction of an alkyl or aryl Grignard reagent with an aryl or vinyl halocarbon using nickel or palladium catalysis [16, 17, 18, 19]. An example is shown below (Figure 1.12).

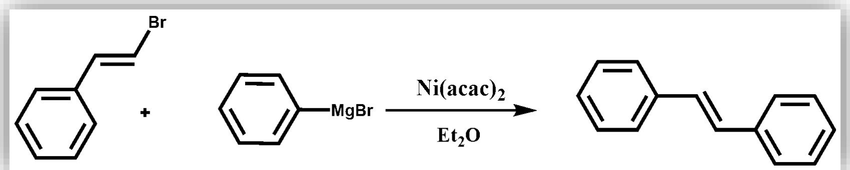

Figure 1.12: Kumada-Corriu Coupling

1.4.8. Sonogashira Coupling

Sonogashira coupling is the substitution of acetylenic hydrogen with iodoarenes, bromoalkenes or bromopyridines in the presence of tetrakis(triphenylphosphine)palladium(0) catalyst with cuprous iodide as cocatalyst under a very mild condition. Kenkichi Sonogashira and Nobue Hagihara firstly reported this type of cross coupling in 1975 [20].

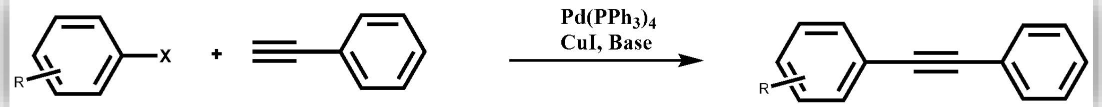

Figure 1.13: Sonogashira Coupling

1.5. Factors Affecting The Band Gap

There are numerous synthetic strategies in the synthesis of conducting polymers, mainly for controlling the band gap of conjugated polymers to achieve desired applications. The band gap determines the color, conductivity and the optoelectronic properties of the materials. It can be controlled by changing planarity, bond length alternation, resonance effects along the polymer backbone, interchain effects and through donor-acceptor approach.

1.5.1. Resonance Energy

To synthesize low band gap π-conjugated polymers, aromatic systems have the most proper basic structures due to their stability and structural flexibility. Double bond introduction to aromatic ring is one of the simplest and most straightforward way to reduce band gap. For instance, ethylene linkages reduce the torsion angle resulting from steric interactions between adjacent phenyl rings providing a planar structure for the conjugated system as in the case of paraphenylenevinylene (PPV). Moreover, the rotational freedom around the single bonds like in thiophene ring is reduced by the double bonds, thus leading a planar geometry. As the aromaticity increases, band gap increases due to increase in rigidity of the system. Thus, double bonds in the π-conjugated system reduces the band gap by decreasing total aromaticity. Band gap of paraphenylenevinylene is reduced from 3.20 eV to 2.60 eV due to double bond insertion [21].

Electron-Withdrawing Groups

Electron-donating and electron-withdrawing groups alter the HOMO and LUMO energy levels of a conjugated system. For instance, oxidation potential of thiophene increases with the insertion of electron withdrawing groups such as nitro or cyano to the 3-position [22]. Based on the work of Roncali's group, a cyano group introduction to the vinylene linkage of dithienylethylene may lead to the band gap reduction for the corresponding polymers. High lying HOMO levels cause unstable neutral state of the system. The electron-withdrawing groups such as cyano helps decreasing HOMO level that results in a stabilization of neutral state sytem. According to theoretical studies, increase in the quinoid character of the ground state provides a low band gap system [23]. However, one of the drawbacks of this approach is the increase in the oxidation potential which may cause difficulty in electrochemical or chemical polymerization.

Electron-Releasing Groups

Electron-donor groups in a conjugated system increase the HOMO level which results in a reduced band gap. It has been shown that the oxidation potential of the materials decreases due to the inductive effect of alkyl groups [24]. Linear alkyl chains with a proper length reduce the band gap of the materials due to increase in lipophilic interactions between the alkyl chains in the polymer [25, 26]. Strong electron donors such as alkoxy groups increases the HOMO level effectively. Oxygens attached to thiophene with an ethylene bridge as electron releasing groups results in the formation of a highly strong donor. This unit can easily be polymerized by chemical or electrochemical methods producing highly-conductive polymer with a lower band gap than polythiophene [27, 28].

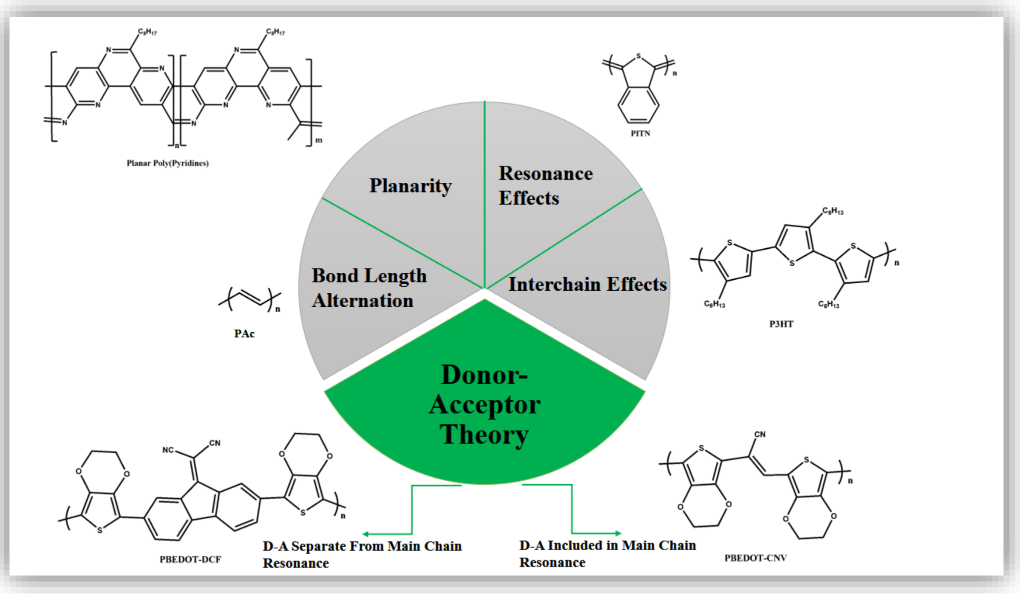

Figure 1.14: Factors affecting the band gap of the polymer

1.5.2. Donor Acceptor Approach

In 1992, Havinga et al. proposed the donor-acceptor (D-A) concept to reduce band gap of conducting polymers [29]. Intrinsic conduction requires small band gaps and high chain mobility is obtained via wide bandwidths. Therefore Havinga drew attention to donor- acceptor systems to adjust band gap and obtain such requirements. In D-A approach, electron rich donor unit is combined with electron poor acceptor unit in close conjugation. Donor and acceptor groups with regular alternation result in the valence and conduction band broadening and therefore band gap is reduced [30]. By this approach, the highest occupied molecular orbital (HOMO) of the donor unit contributes to HOMO level of the polymer whereas the lowest unoccupied molecular orbital (LUMO) of the acceptor group contributes to the LUMO level of the polymer. Tuning band gap provides color change in light emitting systems increasing in the efficiency of photoluminescence and increase in intrinsic conductivity [31].

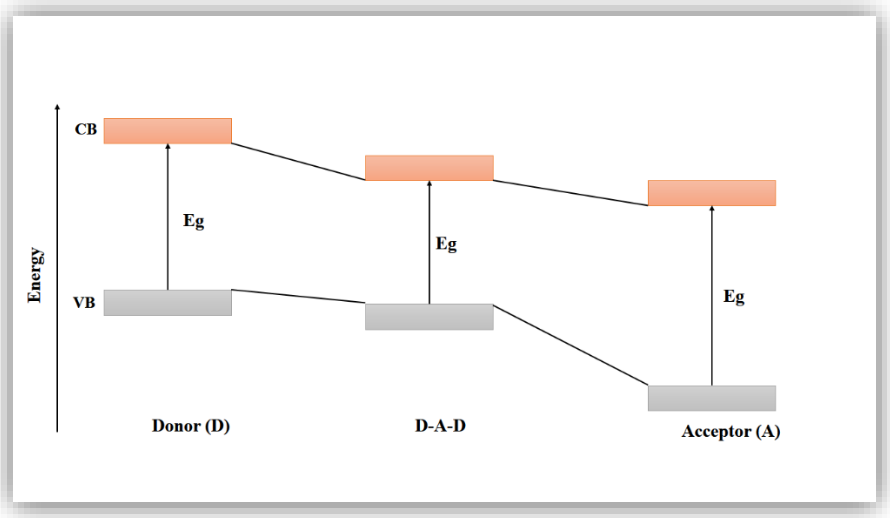

Figure 1.15: A polymer having combined optical properties of the donor or acceptor units via Donor-Acceptor Approach

1.6. Characterization of Conducting Polymers

Conducting polymers can be characterized using cyclic voltammetry, spectroelectrochemistry, kinetic studies, gel permeation chromatography and NMR spectroscopy. In cyclic voltammetry studies, redox properties of polymers are detected. In spectroelectrochemistry experiments electrochemical and spectroscopic techniques are operated simultaneously providing valuable information such as the band gap (E_g), λ_{max}, and polaron and bipolaron formation of the polymer upon oxidation. Kinetic studies reveal percent transmittance changes and switching times of the polymer by stepping repeated potential between the neutral and oxidized states. Percent transmittance changes are recorded as a function of time and switching times are calculated for wavelengths at which polaron and bipolaron bands form. Gel permeation chromatography determines the number average molecular weight, weight average molecular weight and polydispersity index of the polymer. ^{1}H NMR spectra of the polymers give broad peaks proving information about polymer formation. Also, ^{1}H NMR spectroscopy provides an idea about copolymer ratio for random copolymers.

1.7. Chromism

Reversible color change of materials upon external stimulus is defined as chromism. There are several types of chromism such as thermochromism based on change in temperature, piezochromism based on mechanical effects, solvatochromism based on different types of solvents, halochromism based on pH change and electrochromism based on change in applied potential or electrochemical reaction by redox processes.

1.7.1 Electrochromism

The reversible change in optical properties of a material upon external potential can be defined as electrochromism. Different absorption bands during redox processes result in electrochromism. The color change occurs between either in two colored or one bleached one colored states [32]. In 1969, electrochromism was firstly observed in the films of WO_3 and MoO_3 [33]. The color change can be detected by human eye in optical devices. Their potential to be used in optical devices makes electrochromic materials popular and opened the way for the development of new materials. Electrochromic materials can be classified as metal oxides, viologens, metal hexacyanometallates, metal coordination complexes and conjugated conducting polymers [34]. Since conducting polymers have good UV stability, large operation temperature range and low cost in production, these materials are excellent choices for the construction of electrochromic devices. For polymer based electrochromic devices, high coloration efficiency, good stability, high optical contrast, optical memory and short response time are some important parameters required. To satisfy most of these parameters simultaneously, molecular design of new materials is very important. Car rear view mirrors, protective eyewear, sunglasses, data storages, smart windows are some examples of applications where electrochromic devices can be utilized [35, 36].

1.7.1.1. Electrochromic Material Types

1.7.1.1.1. Viologens (1,1'-disubstituted-4,4'-bipyridylium salts)

1,1'-Disubstituted-4,4'-bipyridylium salts are synthesized from 4,4'-bipyridyls via diquaternisation. The name of the compounds come from the identity of substituents on nitrogen atom. When the substituents on nitrogen atom are same, the compound is named as 1-substituent-1’-substituent-4,4’-bipyridylium. The widely used viologen is methyl viologen. Radical cations form upon reductive electron transfer and they are colored due to intramolecular electronic transition in a delocalized positive charge. Figure 1.16 shows the three common viologen redox states. The colorless and the most stable state belongs to dication [32].

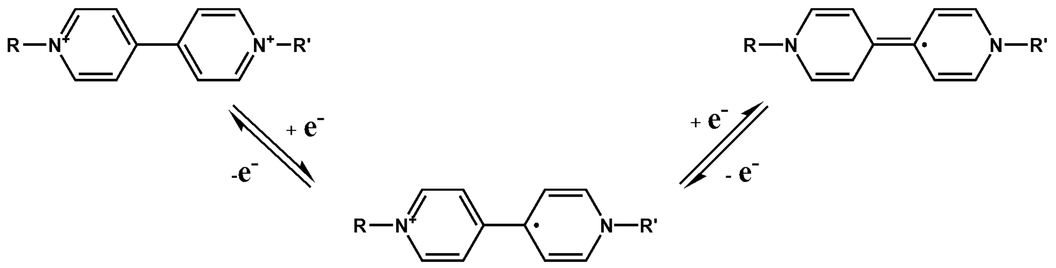

Figure 1.16: Viologen Redox States

Aryl substituents incite a green color to radical cation whereas alkyl groups promote a violet-blue color.

1.7.1.1.2. Prussian Blue System

The electrochemistry of Prussian blue dates back to 1986. Prussian blue were used in carbon paper, in the paint formulation and printings. It was the earliest synthetic pigment due to its intense blue color stems from iron(III) hexacyanoferrate(II) [37]. Iron(III) hexacyanoruthenate (III) and iron(III) hexacyanoosmate (II) were the only examples of early prototype electrochromic devices. Prussian blue have yellow, green, blue and colorless forms at different applied potentials.

1.7.1.1.3. Metal Oxides

Oxides of the metals like cerium, chromium, cobalt, iridium, iron, manganese, molybdenium, nickel, palladium, ruthenium, tungsten and vanadium possess electrochromism [38]. Tunsgten, molybdenium, nickel and iridium oxides reveal the most intense color change in all the metallic electrochromic materials. The thin films of those metal oxides are transparent and they show an intense electronic absorption band upon reduction. The most popular electrochromic material is tungsten trioxide, WO_3, having a high band gap. In 1815, color change of pure tungsten trioxide by reduction under hydrogen gas was shown by Berzelius [39]. Wöhler conducted a similar experiment using sodium metal to show a color change in the reduction of WO_3 in 1824 [40]. In its oxidized form, WO_3 shows a colorless or very pale yellow color having a oxidization state of six (W^{VI}) whereas W^{V} sites are formed giving a deep blue color upon electrochemical reduction. Moreover, molybdenium and vanadium oxides are also electrochromic materials giving the reactions below: [41, 42]

$MoO_3 \quad + \quad y(M^{+}+e^{-}) \quad H_yMo^{VI}_{(1-y)}Mo_x{}^{V}O_3$

Colorless deep blue

$V_2O_5 \quad + \quad y(M^{+}+e^{-}) \quad M_xV^{IV}_{(1-y)}V_y{}^{V}O_5$

Brownish yellow very pale blue

1.7.1.1.4. Conjugated conducting polymers

Thiophene, aniline, pyrrole, carbazole are some examples of electrochemically or chemically oxidized molecules leading to electrochemically active conducting polymers

[43].The conducting polymers are advantageous for electrochromic devices due to possibility of tuning spectral properties of materials. In p-doped states, polymers have delocalized π electron systems and positive charge carriers balanced with anions. Polarons which are major charge carriers form in the oxidation. Cation addition via cathodic doping to balance injected charge is called p-doping. N-doped states are not as stable as p-doped ones [32]. Reduction of the polymer electrochemically results in electrically insulator materials due to removal of conjugation [44]. Band gap of the molecules determines the electrochromic properties in their neutral states. Most of the polymers are colored in undoped form. Materials having a large band gap (higher than 3 eV) reveal no color in the undoped form. However, they absorb visible region of light in their doped form. Materials with moderate band gaps which are in the range between 1.7-1.9 eV absorb in their neutral form whereas absorption is very weak in the visible region and free charge carriers are shifted to near IR region in the doped form. Smaller band gap materials have different colors.

1.8. Applications of Conducting Polymers

1.8.1. Biosensors

Since they can be used in many applications such as diagnosis, biotechnology and genetic engineering, biosensors gained significant attention for the last few decades. A biosensor is a device that converts chemical information into an analytical signal using a mechanism in a biochemical way. These devices include a biorecognition element and a transducer. The biological element part of a biosensor can be enzymes, microorganisms, antibodies, tissues and nucleic acids. To read the biological signal, a transducer is required. Amperometric, optical, colorimetric and acoustic transducers are some types used in the fabrication of a biosensor.

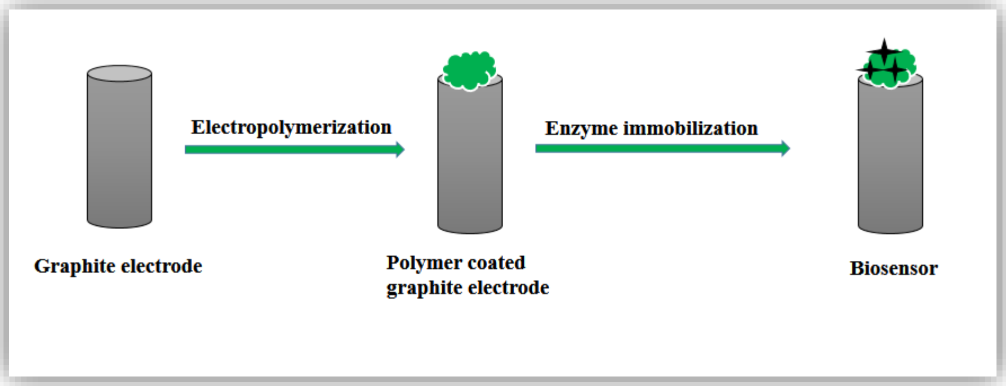

Figure 1.17: Construction of a conducting polymer based biosensor

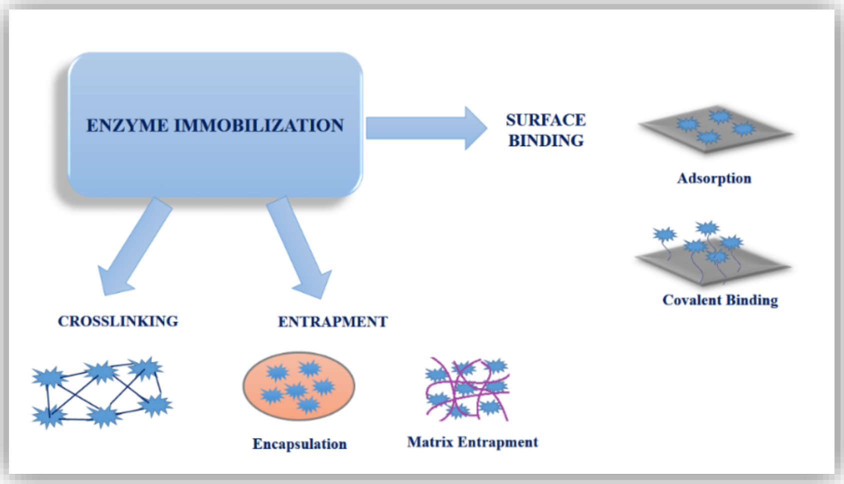

Figure 1.18: Enzyme Immobilization Techniques

Since they are able to catalyze a wide range of reactions, enzymes have been indispensable for science [45]. Controlling reaction rate, reusability for the same reaction with longer half-lives and less degradation make enzyme immobilization particularly valuable. Enzyme immobilization provides low cost purification by prevention of the contamination of the substrate with enzyme/protein. Immobilization provides an effective relation between the biological molecule and the electrode surface by improving its stability [46]. There are several techniques for enzyme immobilization which can be classified as adsorption, entrapment, and cross-linking or covalently binding to a support. Regardless of the method of immobilization, the material in which the enzyme is immobilized should be insoluble in the solvent.

The simplest method for enzyme immobilization is the physical adsorption. In the adsorption method, the enzyme is physically adsorbed onto the backbone or support material which is generally a polymer matrix. To achieve physical adsorption, reversible surface interactions such as hydrogen bonding, Van der Waals forces or ionic interactions between enzyme and various supporting materials are required [47]. Simplicity, low cost, not damaging to enzyme, and no chemical change for support/ enzyme cell are some advantageous for this technique. The biological components and a support with adsorption properties are mixed and incubated under suitable pH, ionic strength. To get rid of nonbound components in the media, washing is needed after collecting immobilized material [48, 49]. This technique has some drawbacks such as leaching of the enzyme while reacting, thereby, contaminating the substrate [50]. Denaturation of the enzyme due to the surface chemistry of the support material may be observed in physical adsorption method.

Entrapment is different from other techniques where enzyme molecules are free in the solution [51].The simplicity, single step preparation and minimal leaching of enzyme are the advantages whereas diffusional restrictions and long response time are the disadvantages of this method. Mixing of an enzyme, an ionic polymer and crosslinking agent produces multivalent cations in ion-exchange reaction resulting in a lattice structure and trapping the enzyme. Moreover, monomers can be polymerized and mixed with enzymes to form a cross-linked lattice structure providing the entrapment of the enzyme. The second method is more widely used because there are various numbers of acrylic monomers available for polymer formation. In this technique, a crosslinking agent is added during polymerization to create a three- dimensional network on the surface of the electrode. To ease substrate and product diffusion, the porosity of the network is important. It should prevent the leakage of enzymes and also be large enough in size for movement of products and substrates [52, 53].

Crosslinking is the support-free enzyme immobilization type with the formation of large, three-dimensional complex structure by the enzymes or the cells. There are both chemical and physical methods for crosslinking [54]. Albumin, glutaraldehyde (GA) or carbodiimide are some proteins used to minimize the close proximity problems that can be caused by crosslinking a single enzyme by this method. The toxicity of reagents like toluene diisocyanate or gluteraldehyde is a limiting factor for application of this method to living cells and that enzymes. Moreover, the other disadvantage of this method is the activity loss may be observed on account of strong crosslinking. Due to limited mechanical properties and poor stability, crosslinking is not preferentiably used. Crosslinking is mostly used to enhance other immobilization types to reduce cell leakage in these systems.

The mostly preferred technique for immobilization is covalent binding [55] via functionality of supporting such as a carboxylic acid [47]. To have a covalent bond formation between an enzyme and a support material, a number of functional groups such as the amino group (NH_2) of arginine, the carboxyl group (CO_2H) of glutamic acid, the hydroxyl group (OH) of serine or threonine, and the sulfydryl group (SH) of cysteine can be used [56]. Free amino and carboxylic acid groups present in the enzyme structure provides covalent bonding with functional groups on the electrode surface. Functionalization of the support can be achieved such as coating the electrode with a functional polymer [57], formation of self-assembled monolayers (SAM) [58]. Long life time and high stability of the biosensor are the reasons to prefer covalent binding between the enzyme and the support matrix [59].

1.8.2. Organic Light Emitting Diodes

Organic light emitting diodes (OLEDs) are considered as one of the most promising technologies for future displays. Tang and Van Slyke first opened this era in 1987 [60]. The idea of replacement of conventional lighting with more efficient semiconducting light sources, has already an impact [61]. Some of the advantages of solid state lightening are a reduced ecological footprint on environment, potential to be used in flexible substrates and self-sustainability [62]. The main advantages of OLEDs are their high luminance efficiency, full- color capability, high contrast, low power consumption, light weight [63].

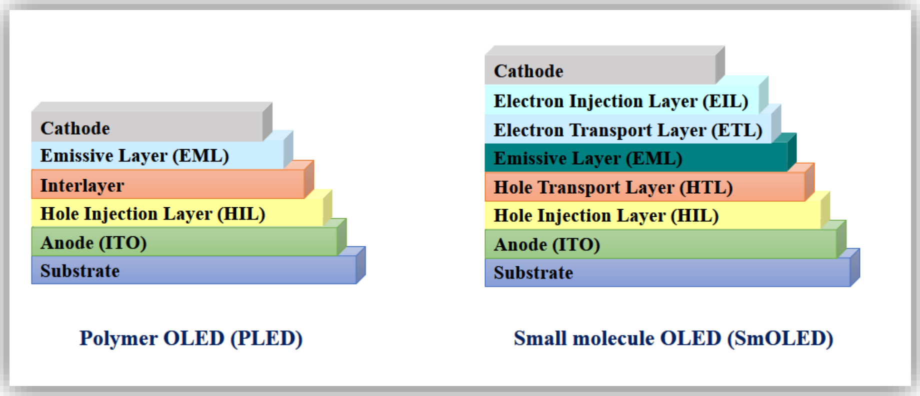

Figure 1.19: Schematic representation of organic light emitting diode

There are mainly two types of organic molecule light emitting diodes which are polymer based (PLEDs) and small molecule based (SmOLEDs). Figure 1.19 illustrates the difference in architectures of PLEDs and small molecule OLEDs. PLEDs are composed of one emissive layer sandwiched between two electrodes which are cathode üand anode, respectively whereas small molecule organic light emitting diodes have functional multi layers. When the materials are properly stacked, high efficiency and long lifetime devices can be fabricated. [60]

1.8.1.2. Working principle of an organic light emitting diode

The emission of light from other sources of energy is called luminescence. There are several types of luminescence according to excitation sources. Electroluminescence is the emission of light from materials in an electric field. For organic light emitting diodes, electroluminescence is the source of excitation and can be classified into two depending on the mechanism which are fluorescence and phosphorescence. External voltage is applied to device providing the injection of charge carriers from anode and cathode electrodes. The holes are injected from anode while electrons are injected from cathode. With the formation of excitons due to attraction between charge carriers, light is emitted by radiative decay in the emissive layer [64]. Figure 1.20 illustrates the operation principle of organic light emitting diodes.

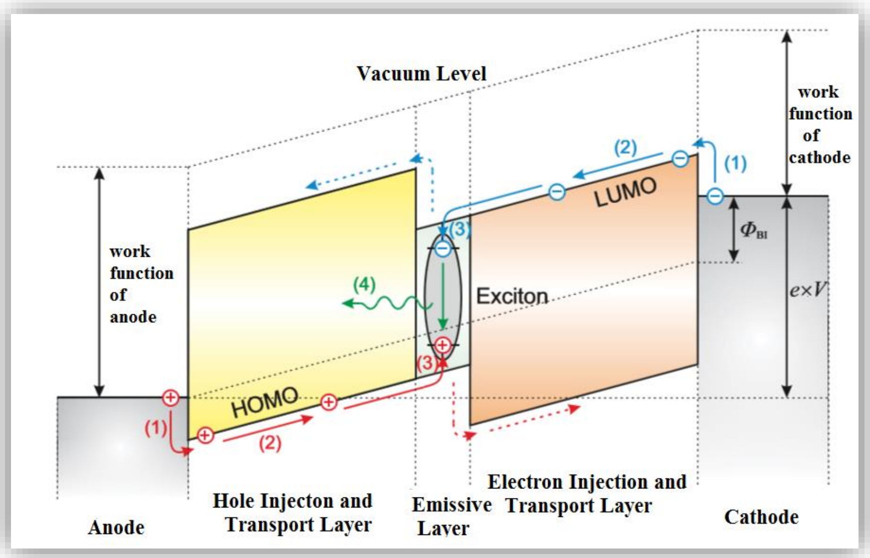

Figure 1.20: OLED working principle

The steps of the operation principle of OLEDs are

- injection of charge carriers
- charge transport
- generation of excitons
- radiative decay leading to emission of light

Emission of light depends on the band gap of the material.

1.8.2.2. Device Fabrication

The basic structure of a PLED consists of a thin film of organic material sandwiched between two electrodes. π-Conjugated organic molecules are active materials in light emissive layer. Light is produced by recombination of holes and electrons in the emissive layer, followed by their radiative decay. The anode is transparent and is usually made of indium doped tin oxide (ITO) while the cathode is metal which is reflective. One of the most crucial step in the construction of an OLED or PLED device is ITO cleaning part. Toluene, distilled water, acetone and isopropyl alcohol are used in the cleaning step. Ultrasonic bath and plasma are also used. PEDOT: PSS is filtrated to elude particles for a homogeneous film during coating onto ITO. PEDOT: PSS is spin casted onto ITO coated substrate as a hole injection layer material after substrate cleaning process. The emissive active layer is spin casted with different solvents and speeds in order to obtain required thickness. For cathode deposition, Ca and Al are thermally evaporated. The devices are encapsulated to protect against oxygen and moisture. Characterization of a device is performed after encapsulation to determine luminance, quantum efficiency, luminance efficacy, color temperature and color point.

1.8.3. Organic Solar Cells

A solar cell is a device that produces electricity from sunlight. Organic photovoltaics have been very popular for the last two decades since they are the key materials for low cost power production. Conducting polymers are used as the active materials in photovoltaics since they can absorb sunlight, generate and transport the charge carriers due to a delocalized π electron system in the polymer chain [65]. Solution processability, easy purification, potential to be used in flexible substrates and low cost production make conjugated polymers more popular than their inorganic counterparts. There are several device architectures in literature. In bilayer devices, donor (p-type) semiconducting polymers and acceptor (n-type) semiconducting molecules are put on top of each other alternately by vacuum deposition [66]. Electron and hole pairs namely excitons are created in donor molecule and dissociation into free charge carriers occurs at the heterojunction interface. For efficient charge generation, approximately 100 nm film thickness is required. However, excitons can only diffuse in short ranges like 10-20 nm in bilayer devices resulting in the loss of absorbed photons while reaching to donor-acceptor interface and the loss of quantum efficiencies. To overcome exciton diffusion length problem, Heeger et al. designed a different architecture namely Bulk Heterojunction in 1995 [67]. Donor/acceptor bulk heterojunction type devices reveal higher efficiency than others. In this architecture, a semiconducting donor polymer is blended with acceptor fullerene. Charge separation is not effective in large domains while small domain size causes recombination of the separated charges [68]. Domain size of the donor and acceptor is required to be in the range of exciton diffusion length which lies between 5 to 20 nm. For bulk heterojunction type devices, domains are optimum providing better charge separation than other type architectures. Continuous morphology is present in BHJ type solar cells which is important to prevent exciton recombination. The buckminsterfullerene (C_{60}) is one of the best electron acceptors since it can gain up to 6 electrons electrochemically. PCBM derivative was synthesized by Wudl et al to overcome solubility problem of the buckminsterfullerene [65]. To provide efficient electron transfer, a highly soluble fullerene derivative, phenyl-C_{61}-butyric acid-methyl ester (PCBM), was used by Yu et al. [69].

1.8.3.1. Working principle of a solar cell

In a bulk heterojunction organic solar cells, anode material is generally ITO coated substrates. Organic molecules' work function should match with the work function of ITO which is 4.8 eV for an efficient charge transfer. There are five steps for photoinduced charge transfer [70].

- light absorption and exciton generation
- exciton diffusion to the interface between the two semiconductors via electric field
- exciton dissociation
- charge transport to the corresponding electrodes
- charge collection in the electrodes and recombination of electrons and holes in the polymer [71].

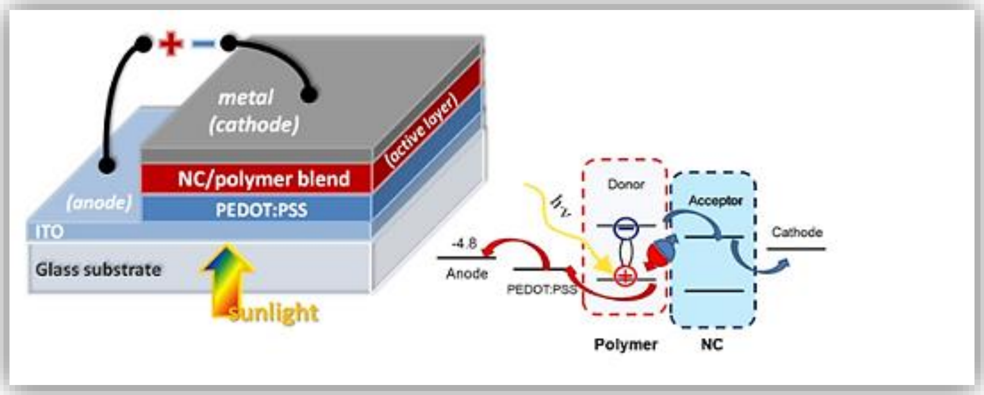

Figure 1.21: Device architecture and working principle of a polymer solar cell

1.8.3.2. Device Fabrication and Characterization of a Bulk Heterojunction Solar Cell

In BHJ solar cells, semiconductor donor and acceptor molecules are blended as photoactive layers and sandwiched between two electrodes. A typical device structure is glass /indium tin oxide (ITO)/ polyethylenedioxythiophene: polystyrene sulfonate (PEDOT: PSS)/photoactive blend layer /cathode metal. ITO coated glass or plastic substrates are generally used. On top of transperent conducting oxide coated substrate, PEDOT: PSS is spin casted to raise the work function of the bottom electrode in order to accept holes. Morever, PEDOT: PSS layer creates a smoother layer on ITO which generally have surface imperfections. PEDOT: PSS has a work function nearly 5 eV vs. vacuum, whereas ITO has a work function between 4.7 and 4.9 eV depending on the treatment method. [72, 73]. ITO and PEDOT:PSS have high transparency in the region between 350 and 900 nm. The photoactive polymer blend is spin coated onto PEDOT: PSS layer with varying speeds to obtain desired thicknesses and film quality. Then metal layer is thermally evaporated as the cathode layer which generally have a thickness around 100 nm. Aluminum is generally used with a work function of 4.2 eV. In order to lower work function of aluminum (Al), calcium (Ca) or lithium fluoride (LiF) can also be evaporated. By this way, the electrons are transferred to the metal electrode easily.

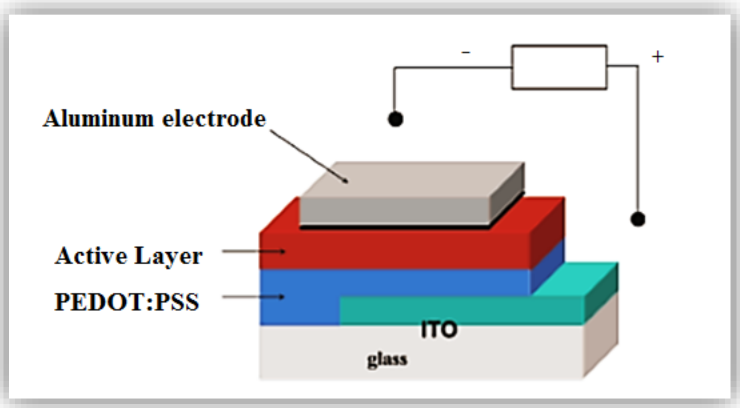

Figure 1.22: Schematic device structure for bulk heterojunction solar cells

The path length that light takes through the atmosphere is Air Mass (AM) which is inversely related to the angle from the zenith angle. For AM 1.5 spectrum, the zenith angle is 48^0 and the incident light power is generally 100 mW/cm^2 to characterize a photovoltaic device. Current vs. voltage curve is constructed both under illumination and dark for a photovoltaic device characterization. Figure 1.21 shows the current-voltage curve of an organic solar cell.

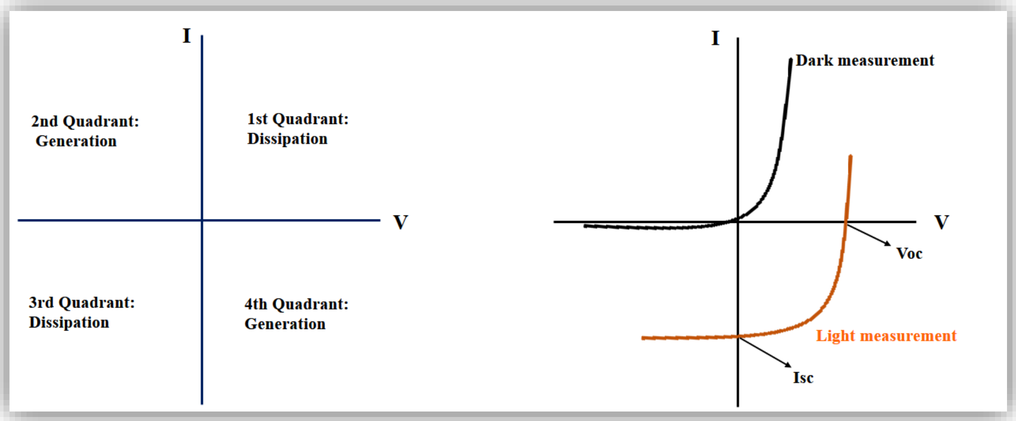

Figure 1.23: Current-Voltage curve of a solar cell

The power conversion efficiency of a photovoltaic device is affected by open circuit voltage (V_{OC}), short circuit current (I_{SC}), the fill factor (FF). Open circuit voltage can be defined as difference between HOMO level of donor unit and LUMO level of the acceptor unit in the polymer blend. The band gap of the material determines the short circuit current. Energy level matching is important to get high Voc and Isc. Fill factor illustrates the quality of the photovoltaic which is affected by resistances. The current and voltage at the maximum power are Imp and Vmp in the fourth quadrant of the current–voltage curve, respectively.

$$\eta e = (V_{OC} * I_{SC} * FF) / Pin$$

$$FF = Imp * Vmp / V_{OC} * I_{SC}$$

1.8.4. Electrochromic Devices

Electrochromic device technology is becoming more and more popular due to combination of ambient stability, high contrast ratio, fast response time, easy processability and color tuning. Polymer electrochromic devices can be mainly separated into two: Reflective devices and absorptive/ transmissive devices [74].

Electrochromic devices simply have three components; an ion-conducting electrolyte, transparent substrates and two electrochromic materials. For absorption/transmission type ECDs, one of the electrochromic material changes its color anodically whereas the other changes the color cathodically upon applied an external potential [41]. Optical shutters, smart windows and window-type displays are the applications of absorption/transmission type ECDs. For reflective type devices, light is decreased or prevented with one optically transparent electrode and one metal layer. Car rear view mirror is one of the application of reflective type electrochromic devices.

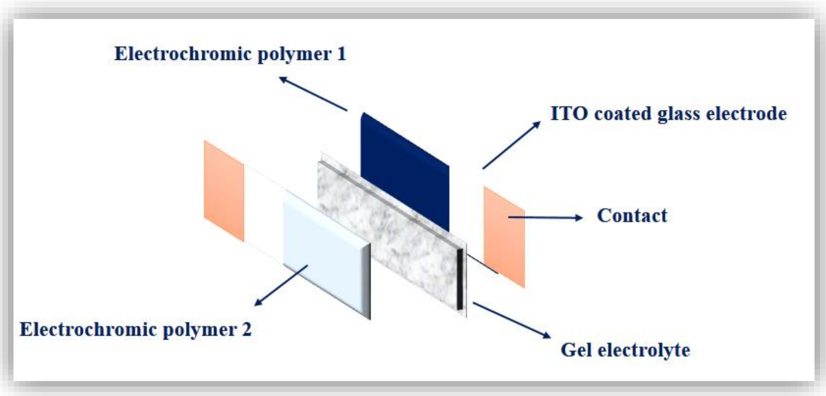

Figure 1.24: Schematic representation of an electrochromic device

1.8.4.1. Device Fabrication and Characterization of an Electrochromic Device

1.8.4.1.1. Gel electrolyte preparation

Tetrabutylammonium hexafluorophosphate ($TBAPF_6$), polymethylmethacrylate (PMMA) and propylene carbonate (PC) are mixed and stirred in acetonitrile. ACN is used to dissolve the PMMA (stiffener) and $TBAPF_6$ while the homogeneous mixture is plasticized by PC introduced in the medium. Stirring and heating continued until gel formation by evaporation of ACN is observed.

1.8.4.1.2. Device Fabrication

For an absorptive/transmissive type ECD, one of the materials is cathodically coloring in its fully oxidized state whereas the other material is anodically coloring when fully reduced. The device operation is based on switching between a colored state and a bleached state. An absorptive/transmissive type electrochromic device consists of two electrodes. Electrochemically active species which are anodically and cathodically coloring materials are spray coated onto ITO coated glass electrodes. Gel electrolyte is placed between two electrodes in order to provide ionic conduction before sandwiching the electrodes.

1.8.4.1.3. Characterization of an Electrochromic Device

Color stability, fast response time, optical contrast, coloration efficiency and long-term stability are some important parameters for an electrochromic device characterization. Coloration efficiency is the change in optical absorbance divided by electrochemical charge density at a specific wavelength. Electrochromic contrast of an electrochrome is the change in percent transmittance at a specific wavelength that can be measured by stepping sequential potential in spectroelectrochemistry experiments or stepping square wave potential. Electrochromic memory of a material can be defined as the ability to maintain its colored state in the absence of external potential [74]. In contrast to viologens, conjugated polymers have good optical memories. Cyclic voltammetry, spectroelectrochemistry, chronoamperometry and electrochemical impedance spectroscopy are some techniques to characterize an electrochromic device. Spectroelectrochemistry studies allow to monitor the optical properties of electrochromic devices. Potential is applied sequentially to the device using the counter and the reference electrodes in a short cut. Working electrode is directly connected to anodically coloring material. To investigate switching time and stability of an electrochromic device, square-wave potential method combined with optical spectroscopy are used. Three electrode system is used to carry out stability experiments using repeated potential steps. The long term switching stability test can be operated on transparent conducting oxide coated glass electrode up to million cycles. Colorimetry studies define the color according to light across the visible region at which the human eye is sensitive. From those studies, a set of color coordinates are obtained. In the CIE color coordinates, a represents the wavelength at which maximum contrast occurs, b stands for the color saturation and L corresponds to brightness [75, 76, 77].

1.9. Aim of the Study

As an acceptor unit, strong electron withdrawing moeities decrease LUMO levels resulting in low band gap polymers. Benzooxadiazole is one of the strongest electron acceptor units in the literature. The idea of syntheses of air stable polymers makes this moeity popular due to its ability to adopt quinoid form and its strong electron accepting property. π-Conjugation is enhanced which results in extended absorption and low band gap when incorporated into the polymer backbone due to planar structure and polymers of this unit have planar structure. Hence, 2,1,3-benzooxadiazole bearing conjugated polymers were designed and synthesized via both Stille and Suzuki polycondensation reactions to be used in electrochromic devices, solar cells and organic light emitting diodes. In this thesis, six donor- acceptor-donor type monomers bearing 2,1,3-benzooxadiazole as the acceptor unit and 3-hexylthiophene, thiophene, 3,4-ethylenedioxythiophene, selenophene, thienothiophene and furan as the donor units were synthesized. Electropolymerization of the thiophene, 3-hexylthiophene and 3,4-ethylenedioxythiophene containing monomers were achieved to investigate electrochemical and optical properties of homopolymers. Four alternating copolymers having different π-bridges were also synthesized to show different electron donating ability of thiophene, selenophene, furan and thienothiophene. Alternating copolymers showed great properties in terms of band gap, solubility and electronic properties. All polymers revealed multichromic behavior. The broad absorption of the chemically synthesized polymers makes them good candidates for organic photovoltaic devices. Hence, selenophene based polymer was used as the donor and [6,6]-phenyl-C_{71}-butyric acid methyl ester (PCBM) which is a soluble derivative of fullerene, was used as the acceptor in photovoltaic devices. The other three alternating copolymers will be used as the active materials in photovoltaic devices.

CHAPTER 2

EXPERIMENTAL

2.1. Materials

All chemicals were purchased from Aldrich except tetrahydrofuran which was purchased from Acros. All reactions were carried out under argon atmosphere unless otherwise mentioned. THF and toluene were dried over Na/benzophenone ketyl and freshly distilled. 5,6-bis(octyloxy)benzo[c][1,2,5]oxadiazole, 4,7-dibromo-5,6-bis(octyloxy)benzo[c][1,2,5]oxadiazole were synthesized according to previously described methods [78, 79, 80].

2.2. Methods and Equipments

A three-electrode cell was used to achieve electropolymerization of monomers in which a platinum wire was the counter electrode, Ag wire was the reference electrode and Indium Tin Oxide (ITO) doped coated glass was the working electrode under ambient conditions. To keep a constant voltage between the working and reference electrodes and to compensate the decrease in voltage, potentiostats were used during the electrolysis. Electrochemical studies for homopolymers were performed using Voltalab 50 potentiostat to provide constant potential in the electrochemical polymerization. To record cyclic voltammetry studies of alternating and random copolymers, GAMRY Reference 600 potentiostat was used. All measurements were carried out at room temperature and were recorded under nitrogen atmosphere for the n-doped states. The reference electrode was calibrated wrt Fc/Fc$^+$. The spectroelectrochemical properties of the polymers were examined using Varian Cary 5000 UV–Vis spectrophotometer. HOMO-LUMO values were calculated considering the value of NHE as -4.75 eV vs vacuum. $CDCl_3$ was used as the solvent to run ^1H and ^{13}C NMR spectra on Bruker Spectrospin Avance DPX-400 Spectrometer and tetramethylsilane was the internal reference. High resolution mass spectroscopy was performed to determin exact mass of the monomers using Waters Synapt MS System.

2.3. Monomer Syntheses

2.3.1. Synthesis of 1,2-bis(octyloxy)benzene

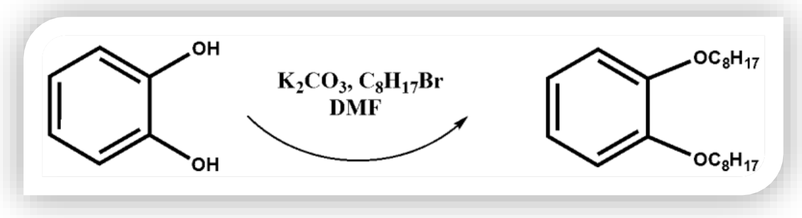

Figure 2.1: Synthetic route of 1,2-bis(octyloxy)benzene

Pyrocatechol (3.96 g, 36.0 mmol), K_2CO_3 (13.0 g, 94.0 mmol) and $C_8H_{17}Br$ (14.1 g, 75.0 mmol) were mixed in DMF and stirred at 115 °C for 40h under inert atmosphere. The mixture was cooled to room temperature and poured into excess distilled water. The milky-brown product was extracted with methylene chloride several times. The organic phases were combined and dried over $MgSO_4$. The evaporation of solvent under reduced pressure affords a crude product which was recrystallized from MeOH to obtain white solid. Yield: 86%

^{1}H NMR (400 MHz, $CDCl_3$): δ 6.82 (s, 4H), 3.92 (t, *J*=6.7 Hz, 4H), 1.74 (m, *J*= 6.8 Hz, 4H), 1.21-1.41 (m, 20H), 0.81 (t, *J*= 6.7 Hz, 6H)

^{13}C NMR (100 MHz, $CDCl_3$): δ 147.9, 119.7, 112.9, 68.01, 30.54, 28.11, 28.06, 27.99, 24.76, 21.38, 12.80

HR-MS (ESI) for $C_{22}H_{38}O_2$ calculated 334.2872, found 334.2888

2.3.2. Synthesis of 1,2-dinitro-4,5-bis(octyloxy)benzene

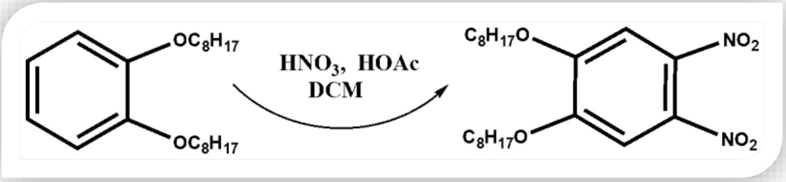

Figure 2.2: Synthetic route of 1,2-dinitro-4,5-bis(octyloxy)benzene

In a two-neck round bottom flask, 1,2-bis(octyloxy)benzene (1.70 g, 5.00 mmol), glacial acetic acid (24 ml) and dichloromethane (24 ml) were mixed and the mixture was cooled to 10 °C. After the drop wise addition of 65 % HNO_3 (4 ml) was completed, the mixture was warmed to room temperature and stirred for 1.5 h. The reaction medium was again cooled to 10 °C and 100 % HNO_3 (11 ml) was added drop wise. The mixture was cooled to room temperature and stirred for 40 h. The orange mixture was poured into ice-water and extracted with dichloromethane. The organic layer was then washed with $NaHCO_3$, water and brine. The organic phase was dried over $MgSO_4$, the evaporation of solvent under reduced pressure afford a crude solid. The crude product was recrystallized from ethanol to obtain yellow solid. Yield: 93%

^{1}H NMR (400 MHz, $CDCl_3$): δ 7.23 (s, 2H), 4.03 (t, *J*=6.5 Hz, 4H), 1.80 (m, *J*= 6.6 Hz, 4H), 1.22-1.44 (m, 20H), 0.82 (t, *J*= 6.53 Hz, 6H)

^{13}C NMR (100 MHz, $CDCl_3$): δ 150.8, 135.5, 107.1, 69.23, 30.74, 28.17, 27.71, 24.80, 21.62, 13.05

HR-MS (ESI) for $C_{22}H_{36}N_2O_6$, calculated 425.2573 $[M+H]^+$, found 425.2652

2.3.3. Synthesis of 5,6-bis(octyloxy)benzo[c][1,2,5]oxadiazole

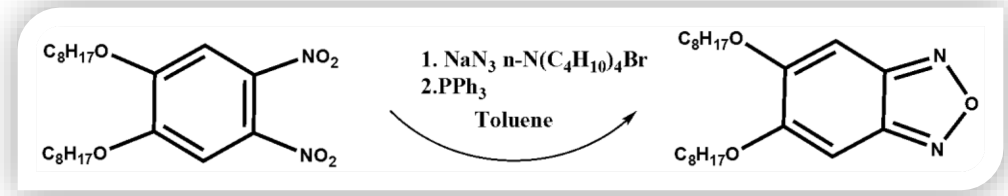

Figure 2.3: Synthetic route of 5,6-bis(octyloxy)benzo[c][1,2,5]oxadiazole

A mixture of 1,2-dinitro-4,5-bis(octyloxy)benzene (5.50 g, 15.0 mmol), NaN_3 (4.02 g, 62.0 mmol) and tetra-n-butylammonium bromide (0.71 g, 2.20 mmol) was refluxed in 50 ml toluene under argon atmosphere for 20 h at 125 °C. Then, triphenylphosphine (3.90 g, 15.2 mol) was added and the mixture was refluxed for an additional 20 h. The reaction mixture was cooled to room temperature and the solvent was evaporated under reduced pressure. The crude product was purified by column chromatography on silica gel using 3:1 hexane: dichloromethane. Evaporation of solvent and recrystallization with ethanol afforded a yellow solid. Yield: 34%

^{1}H NMR (400 MHz, $CDCl_3$): δ 6.74 (s, 2H), 4.01 (t, *J*=6.5 Hz, 4H), 1.82 (m, *J*= 6.6 Hz, 4H), 1.25-1.48 (m, 20H), 0.82 (t, *J*= 6.6 Hz, 3H)

^{13}C NMR (100 MHz, $CDCl_3$): δ 153.3, 145.1, 89.01, 67.68, 30.08, 27.56, 27.53, 26.90, 24.27, 20.95, 12.37

HR-MS (ESI) for $C_{22}H_{36}N_2O_3$ calculated 377.2804, found 377.2816

2.3.4. Synthesis of 4,7-dibromo-5,6-bis(octyloxy)benzo[c][1,2,5]oxadiazole

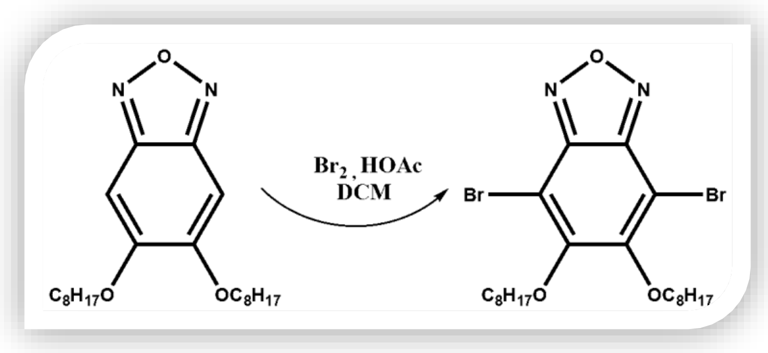

Figure 2.4: Synthetic route of 4,7-dibromo-5,6-bis(octyloxy)benzo[c][1,2,5]oxadiazole

5,6-Bis(octyloxy)benzo[*c*][1,2,5]oxadiazole (2.40 g, 6.40 mmol) was dissolved in dichloromethane (50 ml) and glacial acetic acid (15.93 ml) was added to the solution. The reaction mixture was stirred at room temperature and Br_2 (3.57 g, 45.0 mmol) was added. The mixture was stirred at room temperature for 72 h. The excess acid was quenched by aqueous NaOH solution. The CH_2Cl_2 layer was separated and washed with brine. The organic layer was dried over $MgSO_4$. The evaporation of solvent under reduced pressure afforded a solid product which was then purified by column chromatography on silica gel using 3:1 hexane: methylene chloride. The product was a white solid. Yield: 58%

^{1}H NMR (400 MHz, $CDCl_3$): δ 4.08 (t, *J*=6.6 Hz, 4H), 1.72 (m, *J*= 6.8 Hz, 4H), 1.23-1.44 (m, 20H), 0.83 (t, *J*= 6.6 Hz, 6H)

^{13}C NMR (100 MHz, $CDCl_3$): δ 153.9, 145.6, 97.76, 75.19, 73.59, 29.98, 28.38, 27.51, 24.07, 20.73, 12.26

HR-MS (ESI) for $C_{22}H_{34}N_2O_3Br_2$, calculated 533.0936 $[M+H]^+$, found 533.1014

2.3.5. Synthesis of tributyl(thiophen-2-yl)stannane

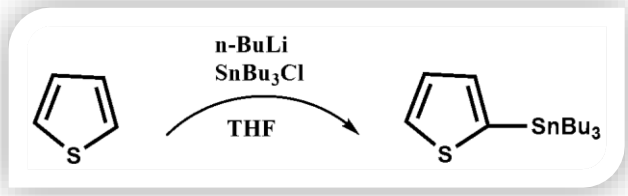

Figure 2.5: Synthetic route of tributyl(thiophen-2-yl)stannane

Thiophene (3.0 g , 30 mmol) and 42 ml freshly distilled THF were added in a 100 ml three-necked flask under argon atmosphere. At -78 °C, n- butyl lithium (17 ml 2.5 M in hexane, 0.184 mol) was added drop wise and the solution was stirred for 1h while the temperature was maintained at - 78 °C. Then tributyltin chloride (11.7 ml, 43.0 mmol) was added drop wise. The mixture was allowed to reach room temperature and stirred for another 24 h. After evaporation of solvent under reduced pressure, dichloromethane was added to the crude product and the mixture was washed with NH_4Cl, brine and water. The organic layers were mixed and dried over anhydrous $MgSO_4$. Through removal of solvent by rotary evaporation, a yellow liquid was obtained without further purification. Yield: 93%

^{1}H NMR (400 MHz, $CDCl_3$): δ 7.58 (d, *J*=4.7 Hz, 1H), 7.19 (t, *J*= 3.3 Hz, 1H), 7.12 (d, *J*= 3.2 Hz, 1H), 1.50 (m, *J*=7.8 Hz, 6H), 1.28 (m, *J*= 7.3 Hz, 6H), 1.03 (t, *J*= 8.4 Hz, 6H), 0.82 (t, *J*= 7.3 Hz, 9H)

^{13}C NMR (100 MHz, $CDCl_3$): δ 134.8, 133.8, 129.2, 126.5, 27. 94, 27.61, 25.90, 12.30, 9.458

2.3.6. Synthesis of tributyl (4-hexylthiophen-2-yl) stannane

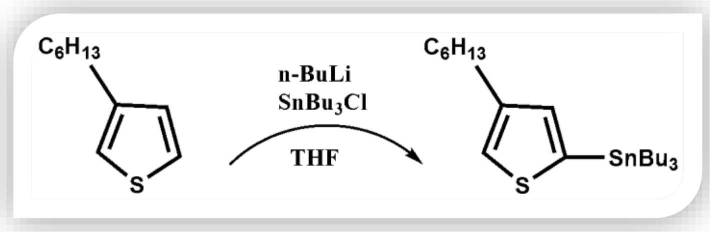

Figure 2.6: Synthetic route of tributyl (4-hexylthiophen-2-yl) stannane

3-Hexylthiophene (2.50 g, 15.0 mol) and 50 ml freshly distilled THF were added in a 100 ml three-necked flask under argon atmosphere. At -78 °C n- butyl lithium (13.04 ml 2.5 M in hexane, 14.2 mmol) was added drop wise and the solution was stirred for 1.5 h while maintaining the temperature at - 78 °C. Then tributyltin chloride (4.50 ml, 16.0 mmol) was added drop wise. The mixture was allowed to reach room temperature and stirred for another 24 h. After evaporation of solvent under reduced pressure, dichloromethane was poured into the crude product and the mixture was washed with NH_4Cl, brine and water. The organic layers were combined and dried over anhydrous $MgSO_4$. After removal of solvent by rotary evaporation, a yellow liquid was obtained without further purification. Yield: 82%

^{1}H NMR (400 MHz, $CDCl_3$): δ 7.11 (s, 1H), 6.89 (s, 1H), 2.58 (t, *J*= 7.7 Hz, 2H), 1.78 (m, *J*= 3.1 Hz, 8H), 1.45-1.59 (m, 10H), 1.25 (m, *J*=7.4 Hz, 8H), 1.10 (t, *J*= 8.4 Hz, 9H), 0.82 (t, *J*=7.3 Hz, 3H)

^{13}C NMR (100 MHz, $CDCl_3$): δ 144.5, 136.9, 136.3, 125.5, 31.74, 30.70, 30.00, 29.15, 28.98, 27.84, 27.28, 26.87, 22.65, 14.11, 10.76

2.3.7. Synthesis of tributyl (2,3-Dihydrothieno[3,4-b][1,4]dioxin-5-yl) stannane

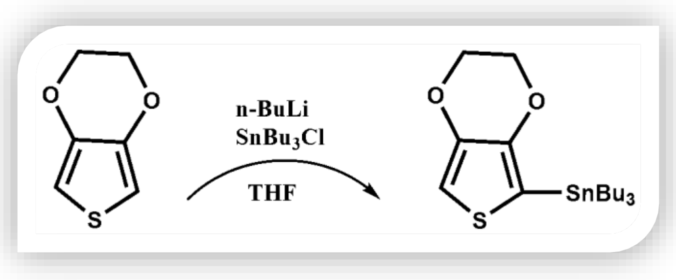

Figure 2.7: Synthetic route of tributyl (2,3-dihydrothieno[3,4-b][1,4]dioxin-5-yl) stannane

3,4-Ethylenedioxythiophene (2.00 g, 14.0 mmol) and 50 ml freshly distilled THF were added into a 100 ml three-necked flask under argon atmosphere. At -78 °C, n- butyl lithium (5.8 ml 2.5 M in hexane, 63.0 mmol) was added drop wise and the solution was stirred for 1.5 h while maintaining the temperature at -78 °C. Then tributyltin chloride (3.83 ml, 14.0 mmol) was added drop wise. The mixture was allowed to reach room temperature and stirred for another 24 h. After evaporation of solvent under reduced pressure, dichloromethane was poured into the crude product and the mixture was washed with NH_4Cl, brine and water. The organic layers were combined and dried over anhydrous $MgSO_4$. After removal of solvent by rotary evaporation, a yellow liquid was obtained. This material was used in the next step without further purification. Yield: 90 %

^{1}H NMR (400 MHz, $CDCl_3$): δ 6.25 (s, 1H), 4.08 (m, 4H), 1.79 (m, *J*= 6.6 Hz, 6H), 1.02 (t, *J*= 8.3 Hz, 6H), 1.40- 1.59 (m, 6H) 0.82 (t, *J*= 7.3 Hz, 9H)

^{13}C NMR (100 MHz, $CDCl_3$): δ 146.1, 107.4, 104.3, 98.07, 63.13, 63.06, 27.41, 25.62, 12.13

2.3.8. Synthesis of 5,6-bis(octyloxy)-4,7-di(thiophen-2-yl)benzo[c][1,2,5]oxadiazole

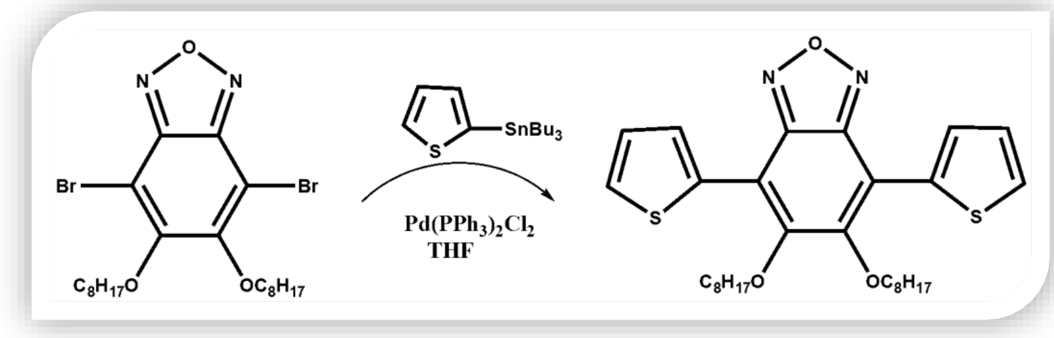

Figure 2.8: Synthetic route of 5,6-bis(octyloxy)-4,7-di(thiophen-2-yl)benzo[c][1,2,5]oxadiazole

4,7-Dibromo-5,6-bis(octyloxy)benzo[c][1,2,5]oxadiazole (0.750 g, 14.0 mmol) and tributyl(thiophen-2-yl)stannane (2.60 g, 7.00 mmol) were dissolved in dry THF (80 ml). The reaction mixture was heated to reflux under argon atmosphere for 1 h and then $Pd(PPh_3)_2Cl_2$ (120 mg, 0.171 mmol) was added. The mixture was stirred under inert atmosphere at 125 °C for 2 days. The product was concentrated on rotary evaporator and the crude product was purified by column chromatography eluting with hexane/methylene chloride (3:1) to afford orange crystalline solid. Yield: 91%

^{1}H NMR (400 MHz, $CDCl_3$): δ 8.40 (d, *J*=5.1 Hz, 2H), 7.44 (d, *J*= 5.2 Hz, 2H), 7.16 (t, *J*=3.9 Hz, 2H), 4.08(t, *J*=7.3 Hz, 4H), 1.93 (m, *J*= 7.3 Hz, 4H), 1.23-1.44 (m, 20H), 0.83 (t, *J*= 6.6 Hz, 6H)

^{13}C NMR (100 MHz, $CDCl_3$): δ 150.7, 145.8, 131.9, 129.9, 127.0, 126.1, 112.1, 73.50, 30.79, 29.26, 28.49, 28.25, 24.86, 21.64, 13.08

HR-MS (ESI) for $C_{30}H_{40}N_2O_3S_2$, calculated 541.2559 $[M+H]^+$, found 541.2574

2.3.9. Synthesis of 4,7-bis(4-hexylthiophen-2-yl)-5,6-bis(octyloxy)benzo[c][1,2,5]oxadiazole

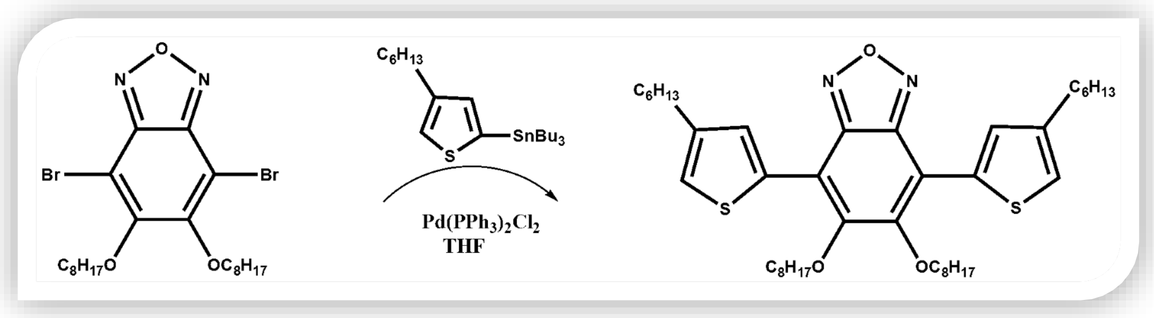

Figure 2.9: Synthetic route of 4,7-Bis(4-hexylthiophen-2-yl)-5,6-bis(octyloxy)benzo[c][1,2,5]oxadiazole

4,7-Dibromo-5,6-bis(octyloxy)benzo[c][1,2,5]oxadiazole (0.750 g, 1.40 mmol) and tributyl(4-hexylthiophen-2-yl)stannane (2.89 g, 6.30 mmol) were dissolved in dry THF (80 ml). The reaction mixture was heated to reflux under argon atmosphere for 1.5 h and then $PdCl_2(PPh_3)_2$ (120.0 mg, 0.171 mmol) was added. The mixture was stirred under inert atmosphere at 125 °C for 2 days. The product was concentrated on rotary evaporator and the crude product was purified by column chromatography eluting with hexane/methylene chloride (3:1) to afford a orange-red solid. Yield: 60 %

^{1}H NMR (400 MHz, $CDCl_3$): δ 8.23 (s, 2H), 7.02(s, 2H), 4.06 (t, *J*=7.2 Hz, 4H), 2.63 (t, *J*=7.8 Hz, 4H), 1.92 (m, *J*= 7.6 Hz, 4H), 1.63 (m, *J*= 7.9 Hz, 4H), 1.23-1.44 (m, 28H), 0.83 (t, *J*= 6.4 Hz, 12H)

^{13}C NMR (100 MHz, $CDCl_3$,): δ 150.1, 145.2, 141.8, 131.0, 130.5, 121.4, 111.4, 72.79, 30.19, 30.08, 28.92, 28.65, 27.90, 27.63, 27.43, 24.27, 21.02, 12.45

HR-MS (ESI) for $C_{42}H_{64}N_2O_3S_2$, calculated 709.4427, found 709.4451

2.3.10. Synthesis of 4,7-bis(2,3-dihydrothieno[3,4-b][1,4]dioxin-5-yl)-5,6-bis(octyloxy)benzo[c][1,2,5]oxadiazole

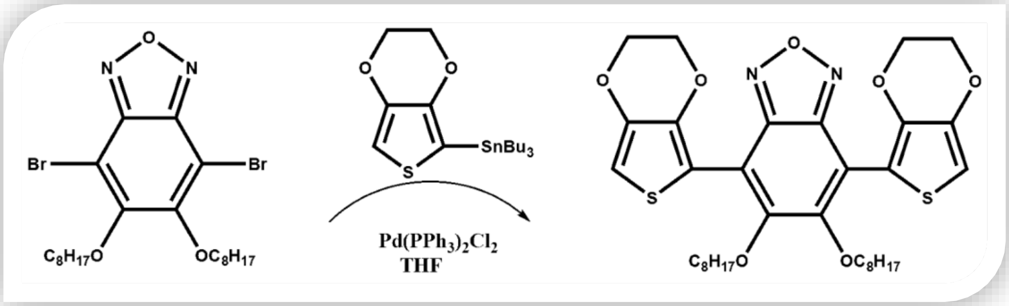

Figure 2.10: Synthetic route of 4,7-Bis(2,3-dihydrothieno[3,4-b][1,4]dioxin-5-yl)-5,6-bis(octyloxy)benzo[c][1,2,5]oxadiazole

4,7-Dibromo-5,6-bis(octyloxy)benzo[c][1,2,5]oxadiazole (0.75 g, 1.40 mmol) and tributyl(2,3-dihydrothieno[3,4-b][1,4]dioxin-5-yl)stannane (2.42 g, 5.60 mmol) were dissolved in dry THF (80 ml). The reaction mixture was heated to reflux under argon atmosphere for 1 h and then $PdCl_2(PPh_3)_2$ (120 mg, 0.171 mmol) was added. The mixture was stirred under inert atmosphere at 125 °C for 3 days. The product was concentrated on rotary evaporator and the crude product was purified by column chromatography eluting with hexane/methylene chloride to afford a pale green solid. Yield: 40%

^{1}H NMR (400 MHz, $CDCl_3$): δ 6.02(s, 2H), 4.17-4.26 (m, 12H), 1.57 (m, *J*=7.4Hz, 4H), 1.23-1.44 (m, 20H), 0.86 (t, *J*= 7.3 Hz, 6H)

^{13}C NMR (100 MHz, $CDCl_3$): δ 139.4, 135.2, 133.3, 128.2, 126.0, 108.1, 95.70, 63.16, 62.77, 26.43, 24.93, 15.45, 11.74

HR-MS (ESI) for $C_{34}H_{44}N_2O_7S_2$ calculated 657.2668, found 657.2776

2.3.11. Synthesis of tributyl(thieno[3,2-b]thiophen-2-yl)stannane

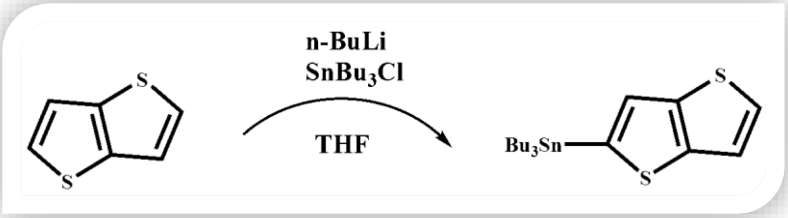

Figure 2.11: Synthetic route of tributyl(thieno[3,2-b]thiophen-2-yl)stannane

Thienothiophene (1.40 g, 9.98 mmol) and 30 ml freshly distilled THF were added in a 100 ml three-necked flask under argon atmosphere. After the system reaches to -78 °C, n- butyl lithium (4.00 ml, 2.5 M in hexane, 10.0 mmol) was added drop wise and the solution was stirred for 1 h while the temperature was maintained at - 78 °C. After 1h, tributyltin chloride (3 ml, 10.0 mmol) was added drop wise. The mixture was maintained at - 78 ^{0}C for 4 h then allowed to reach room temperature. The mixture was stirred for another 24 h. After evaporation of solvent under reduced pressure, distilled water was poured into the crude product and extracted with diethyl ether. The organic layer was dried over anhydrous $MgSO_4$. Through removal of solvent by rotary evaporation, a purple liquid was obtained. Yield: 61%

^{1}H NMR (400 MHz, $CDCl_3$): δ 7.27 (d, *J*= 5.2 Hz, 1H), 7.19 (s, 1H), 7.16 (d, *J*=5.1 Hz, 1H), 1.52 (m, *J*= 7.2 Hz, 6H), 1.27 (m, *J*=7.4 Hz, 6H), 1.07 (t, *J*= 8.3 Hz, 9H)

^{13}C NMR (100 MHz, $CDCl_3$): δ 134.4, 126.9, 126.6, 119.0, 28.96, 22.27, 13.66, 10.93

Two carbons in the aromatic region may overlap.

2.3.12. Synthesis of tributyl(selenophen-2-yl)stannane

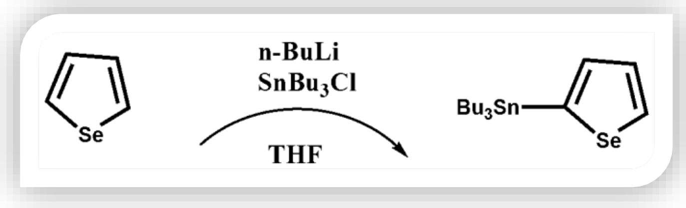

Figure 2.12: Synthetic route of tributyl(selenophen-2-yl)stannane

Selenophene (2.00 g, 15.3 mmol) and 30 ml freshly distilled THF were mixed in a 100 ml three-necked flask under argon atmosphere. The system was allowed to -78 °C then, n- butyl lithium (7.33 ml, 2.5 M in hexane, 15.26 mmol) was added drop wise. Tributyltin chloride (4.43 ml, 16.4 mmol) was added drop wise after the system was maintained at – 78 °C for 1 h. After the addition of tributyltin chloride completed, the mixture was maintained at – 78 °C for 4h. The mixture was stirred for overnight at room temperature. Through removal of solvent by rotary evaporation, dichloromethane was poured into the crude product and the mixture was washed with $NaHCO_3$, water and brine. The organic layers were combined and dried over anhydrous $MgSO_4$. After removal of solvent under reduced pressure, a yellow liquid was obtained. Yield: 63 %

^{1}H NMR (400 MHz, $CDCl_3$): δ 8.28 (d, *J*=4.7 Hz, 1H), 7.44 (t, *J*=3.5 Hz, 1H), 7.42 (d, *J*=4.4 Hz, 1H), 1.50 (m, *J*=6.9 Hz, 6H), 1.28 (m, *J*=7.2 Hz, 6H), 1.03 (t, *J*=8.3 Hz, 9H)

^{13}C NMR (100 MHz, $CDCl_3$): δ 143.6, 137.9, 135.3, 130.6, 28.99, 27.29, 13.67, 11.13

2.3.13. Synthesis of 4,7-bis(5-bromothiophen-2-yl)-5,6-bis(octyloxy)benzo[c][1,2,5]oxadiazole

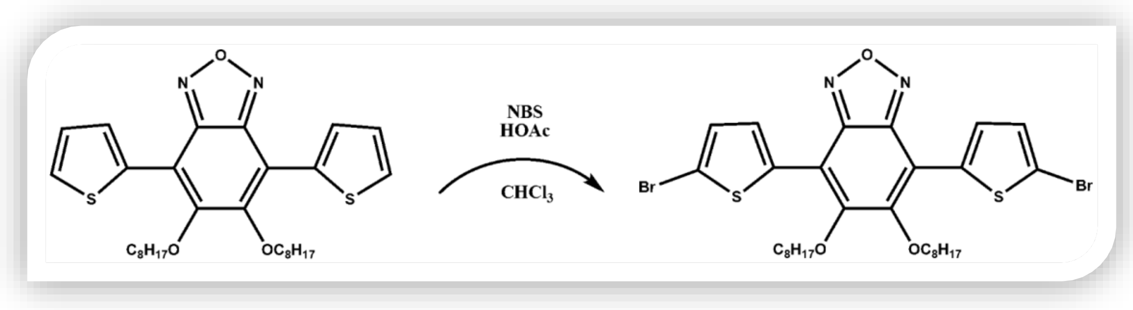

Figure 2.13: Synthetic route of 4,7-Bis(5-bromothiophen-2-yl)-5,6-bis(octyloxy)benzo[c][1,2,5]oxadiazole

5,6-Bis(octyloxy)-4,7-di(thiophen-2-yl)benzo[c][1,2,5]oxadiazole (250 mg, 0.463 mmol), N- bromosuccimide (NBS) (181 mg, 1.02 mmol), glacial acetic acid (10 mL), and chloroform (10 mL) were stirred at room temperature for 24 h in the dark. The solvent was removed using rotary evaporator under reduced pressure. The crude product was chromatographically purified on silica gel column eluting with methylene chloride/ hexane to afford orange-red crystal. Yield: 80 %

^{1}H NMR (400 MHz, $CDCl_3$): δ 8.40 (d, *J*=5.1 Hz, 2H), 7.44 (d, *J*= 5.2 Hz, 2H), 4.08(t, *J*=7.3 Hz, 4H), 1.93 (m, *J*= 7.3 Hz, 4H), 1.23-1.44 (m, 20H), 0.83 (t, *J*= 6.6 Hz, 6H)

^{13}C NMR (100 MHz, $CDCl_3$): δ 150.7, 145.8, 131.9, 129.9, 127.0, 126.1, 112.1, 73.50, 30.79, 29.26, 28.49, 28.25, 24.86, 21.64, 13.08

2.3.14. Synthesis of 5,6-bis(octyloxy)-4,7-di(thieno[3,2-b]thiophen-2-yl)benzo[c][1,2,5]oxadiazole

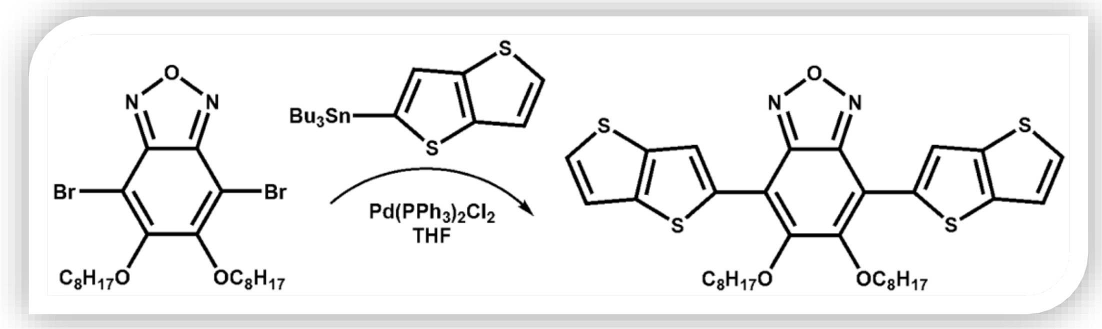

Figure 2.14: Synthetic route of 5,6-bis(octyloxy)-4,7-di(thieno[3,2-b]thiophen-2-yl)benzo[c][1,2,5]oxadiazole

4,7-Dibromo-5,6-bis(octyloxy)benzo[c][1,2,5]oxadiazole (0.75g, 1.40 mmol) and tributyl(thieno[3,2-b]thiophen-2-yl)stannane (1.83 g, 4.20 mmol) were dissolved in dry THF (40 ml). The reaction mixture was heated to reflux under argon atmosphere for 1 h and then $PdCl_2(PPh_3)_2$ (mg, mmol) was added. The mixture was stirred under inert atmosphere at 125 °C for 2 days. The product was concentrated on rotary evaporator and the product was purified by column chromatography to afford red solid. Yield: 66%

^{1}H NMR (400 MHz, $CDCl_3$): δ 8.65 (s, 2H), 7.42 (d, *J*=5.2 Hz, 2H), 7.26 (d, *J*= 5.2 Hz, 2H), 4.12 (t, *J*=7.3 Hz, 4H), 1.98 (q, *J*= 7.5 Hz, 4H), 1.44-1.23 (m, *J*= 4.8 Hz, 20H), 0.83 (t, *J*= 6.6 Hz, 6H)

^{13}C NMR (100 MHz, $CDCl_3$): δ 142.0, 139.6, 135.0, 129.1, 123.1, 119.4, 113.6, 74.91, 31.83, 30.30, 29.54, 29.31, 25.89, 22.69, 14.12

HR-MS (ESI) for $C_{34}H_{40}N_2O_3S_4$ calculated 652.1922 found 652.1909

Two carbons which belong to thienothiophene unit may overlap.

2.3.15. Synthesis of 5,6-bis(octyloxy)-4,7-di(selenophen-2-yl)benzo[c][1,2,5]oxadiazole

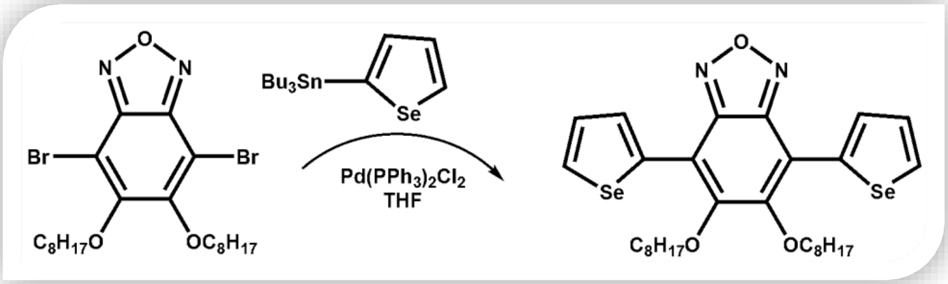

Figure 2.15: Synthetic route of 5,6-Bis(octyloxy)-4,7-di(selenophen-2-yl)benzo[c][1,2,5]oxadiazole

4,7-Dibromo-5,6-bis(octyloxy)benzo[c][1,2,5]oxadiazole (0.75 g, 1.40 mmol) and tributyl(selenophen-2-yl)stannane (1.78 g, 4.20 mmol) were dissolved in dry THF (35 ml). The reaction mixture was heated to reflux under argon atmosphere for 1 h and then $PdCl_2(PPh_3)_2$ (mg, mmol) was added. The mixture was stirred under inert atmosphere at 125 °C for 2 days. The product was concentrated on rotary evaporator and the crude product was purified by column chromatography to afford orange crystalline solid. Yield: 81 %

^{1}H NMR (400 MHz, $CDCl_3$): δ 8.71 (d, *J*= 4.6 Hz, 2H), 8.16 (d, *J*= 5.7 Hz, 2H), 7.41 (dd, *J*= 4.9 Hz, 2H), 4.10 (t, *J*= 7.5 Hz, 4H), 1.95 (q, *J*= 7.410 Hz, 4H), 1.41-1.27 (m, *J*=8.3 Hz, 20H) 0.83 (t, *J*= 6.6 Hz, 6H)

^{13}C NMR (100 MHz, $CDCl_3$): δ 135.5, 132.7, 132.2, 128.9, 73.75, 30.78, 29.52, 28.49, 28.23, 24.81, 21.63, 13.07

HR-MS (ESI) for $C_{30}H_{40}N_2O_3Se_2$ calculated 636.1369 found 636.1354

Three carbons around 126.0 and 103.0 ppm are difficult to see therefore they are not observed.

2.3.16. Synthesis of 4,7-bis(5-bromothieno[3,2-b]thiophen-2-yl)-5,6-bis(octyloxy)benzo[c][1,2,5]oxadiazole

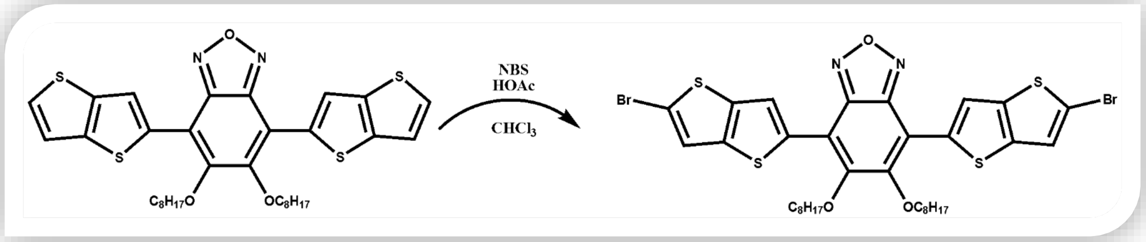

Figure 2.16: Synthetic route of 4,7-bis(5-bromothieno[3,2-b]thiophen-2-yl)-5,6-bis(octyloxy)benzo[c][1,2,5]oxadiazole

5,6-Bis(octyloxy)-4,7-di(thieno[3,2-b]thiophen-2-yl)benzo[c][1,2,5]oxadiazole (200 mg, 0.306 mmol), N- bromosuccimide (NBS) (136.3 g, 0.766 mmol), glacial acetic acid (10 mL), and chloroform (10 mL) were stirred at room temperature for 24 h in the dark. After solvent removal under reduced pressure, chloroform was poured into the product and the mixture was washed with $NaHCO_3$ and water. The crude product was recrystallized with cold ethanol to afford orange-red crystal. Yield: 85%

^{1}H NMR (400 MHz, $CDCl_3$): δ 8.55 (s, 2H), 7.25 (s, 2H), 4.11 (t, *J*= 7.4 Hz, 4H), 1.96 (m, *J*=7.3 Hz 4H), 1.42-1.23 (m, *J*= 6.3 Hz, 20H), 0.83 (t, *J*= 6.6 Hz, 6H)

^{13}C NMR (100 MHz, $CDCl_3$): δ 146.4, 140.7, 139.7, 134.2, 122.5, 122.2, 115.6, 113.3, 74.96, 31.82, 30.29, 29.52, 29.30, 25.87, 22.68, 14.11

2.3.17. Synthesis of 4,7-bis(5-bromoselenophen-2-yl)-5,6-bis(octyloxy)benzo[c][1,2,5]oxadiazole

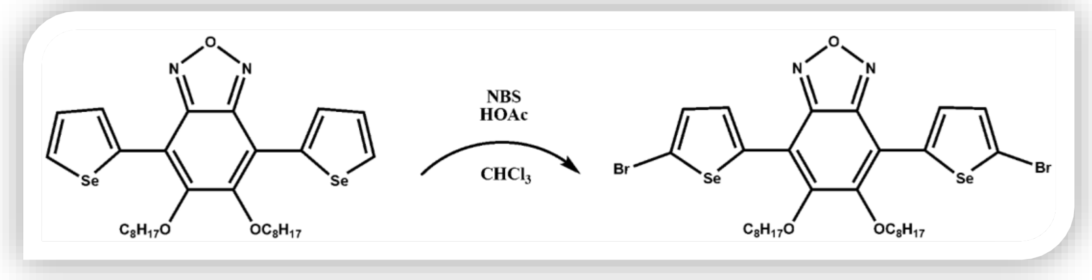

Figure 2.17: Synthetic route of 4,7-bis(5-bromoselenophen-2-yl)-5,6-bis(octyloxy)benzo[c][1,2,5]oxadiazole

5,6-Bis(octyloxy)-4,7-di(selenophen-2-yl)benzo[c][1,2,5]oxadiazole (200 mg, 0.320 mmol), N- bromosuccimide (NBS) (112 mg, 0.630 mmol), glacial acetic acid (8 mL), and chloroform (8 mL) were stirred at room temperature for 24 h in the dark. The solvent was removed using rotary evaporator under reduced pressure. The crude product was chromatographically purified on silica gel column eluting with methylene chloride/ hexane to afford red crystalline solid. Yield: 70 %

^{1}H NMR (400 MHz, $CDCl_3$): δ 8.41 (d, *J*= 4.4 Hz, 2H), 7.33 (d, *J*= 4.4 Hz, 2H), 4.09 (t, *J*= 7.5 Hz, 4H), 1.94 (q, *J*= 8.0 Hz, 4H), 1.40-1.19 (m, *J*=7.8 Hz, 20H) 0.83 (t, *J*= 6.6 Hz, 6H)

^{13}C NMR (100 MHz, $CDCl_3$): δ 149.6, 144.8, 136.9, 132.3, 132.0, 119.5, 113.5, 74.05, 30.78, 29.87, 28.45, 28.24, 24.73, 21.66, 13.09

2.3.18. Synthesis of 5,6-bis(octyloxy)-4,7-di(furan-2-yl)benzo[c][1,2,5]oxadiazole

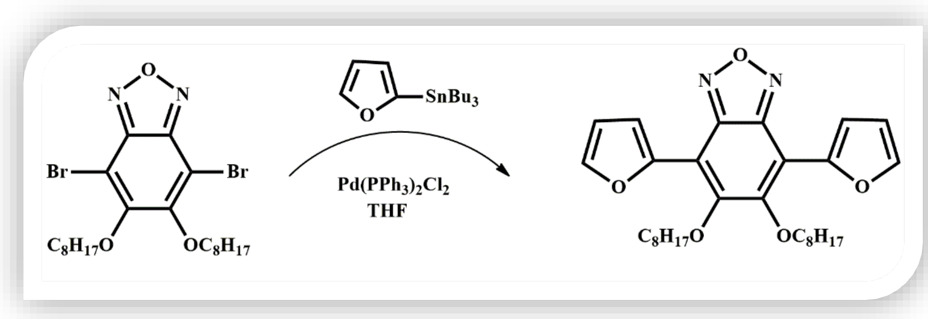

Figure 2.18: Synthetic route of 5,6-bis(octyloxy)-4,7-di(furan-2-yl)benzo[c][1,2,5]oxadiazole

4,7-Dibromo-5,6-bis(octyloxy)benzo[c][1,2,5]oxadiazole (0.83 g, 1.57 mmol) and tributyl(furan-2-yl)stannane (1.65 g, 4.71 mmol) were dissolved in dry THF (25 mL). The reaction mixture was heated to reflux under argon atmosphere for 1h and then $PdCl_2(PPh_3)_2$ (90.0 mg, 0.128 mmol) was added. The mixture was stirred under inert atmosphere at 125 °C for 50 hours. The product was concentrated on rotary evaporator and the crude product was purified by column chromatography to afford dark green solid. Yield: 94 %

^{1}H NMR (400 MHz, $CDCl_3$): δ 7.62 (d, *J*=3.4 Hz, 2H), 7.34 (d, *J*=3.4 Hz, 2H), 6.564 (dd, *J*=3.4 Hz, 2H), 4.04 (t, *J*=6.9 Hz, 4H), 1.83 (q, *J*=7.0 Hz, 4H), 1.41(m, *J*=9.0 Hz, 4H), 1.297-1.224 (m, *J*=3.8 Hz, 16H), 0.83(t, *J*=6.6 Hz, 6H)

^{13}C NMR (100 MHz, $CDCl_3$): δ 152.3, 146.7, 145.7, 143.5, 114.0, 112.0, 109.4, 74.78, 31.82, 30.36, 29.46, 29.27, 26.00, 22.66, 14.08

HR-MS (ESI) for $C_{30}H_{40}N_2O_5$, calculated 508.2937, found 508.2920

2.3.19. Synthesis of 4,7-bis(5-bromofuran-2-yl)-5,6-bis(octyloxy)benzo[c][1,2,5]oxadiazole

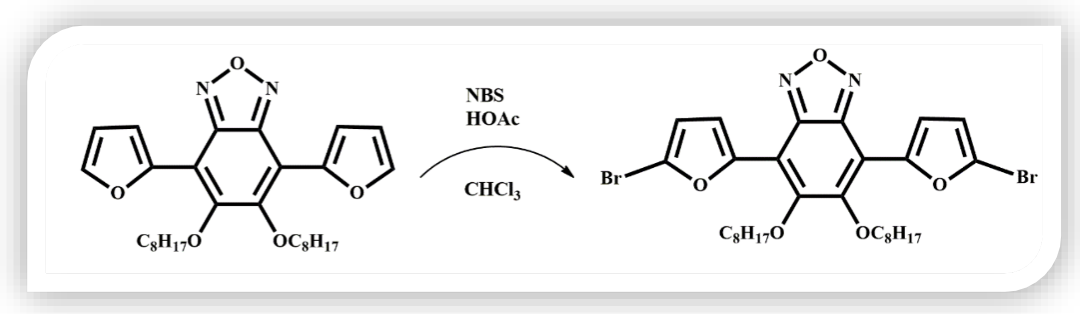

Figure 2.19: Synthetic route of4,7-bis(5-bromofuran-2-yl)-5,6-bis(octyloxy)benzo[c][1,2,5]oxadiazole

4,7-di(furan-2-yl)-5,6-bis(octyloxy)benzo[c][1,2,5]oxadiazole (200 mg, 0.393 mmol), N- bromosuccimide (NBS) (175.1 mg, 0.983 mmol), glacial acetic acid (14 mL), and chloroform (14 mL) were stirred at room temperature overnight in the dark. The solvent was removed using rotary evaporator under reduced pressure. The crude product was chromatographically purified on silica gel column eluting with methylene chloride/ hexane to afford yellow solid. Yield: 80 %

^{1}H NMR (400 MHz, $CDCl_3$): δ 7.32 (d, *J*= 3.5 Hz, 2H), 6.49 (d, *J*= 3.5 Hz, 2H), 4.05 (t, *J*= 6.8 Hz, 6H), 1.872 (m, *J*= 7.2 Hz, 4H), 1.443-1.236 (m, *J*= 7.1 Hz, 20H), 0.83 (t, *J*= 6.6 Hz, 6H)

^{13}C NMR (100 MHz, $CDCl_3$): δ 152.5, 148.5, 145.2, 116.6, 113.9, 108.6, 75.26, 31.84, 30.29, 29.56, 29.27, 26.07, 22.67, 14.09

2.4. Polymer Syntheses

2.4.1. Synthesis of PBOTPh

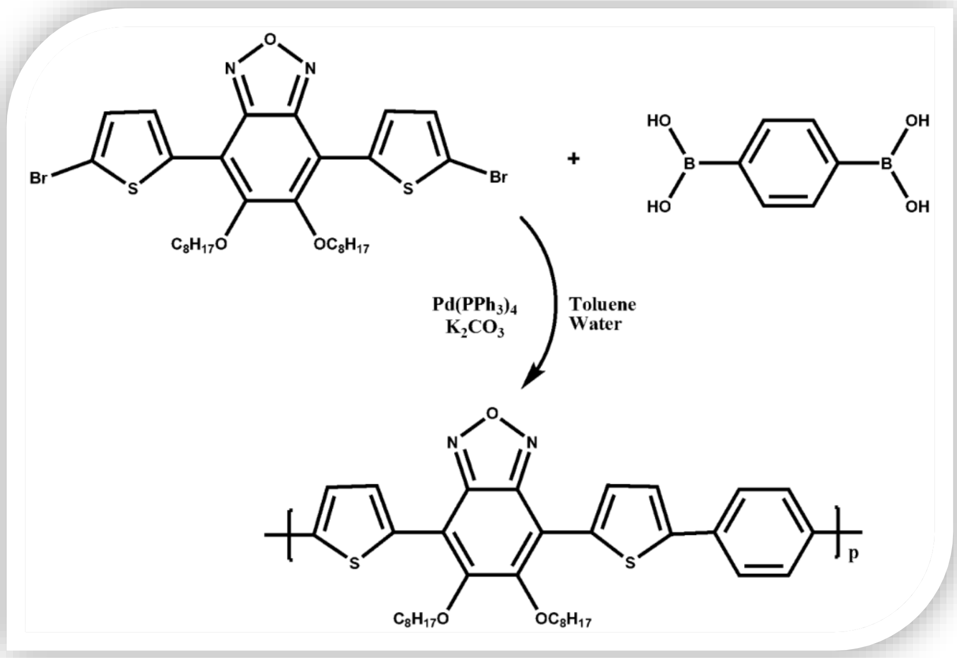

Figure 2.20: Synthetic route of PBOTPh

4,7-Bis(5-bromothiophen-2-yl)-5,6-bis(octyloxy)benzo[c][1,2,5]oxadiazole (250 mg, 0.357 mmol), 1,4-phenylenediboronic acid (59.3 mg, 0.357 mmol), potassium carbonate (K_2CO_3, 2M in H_2O) and toluene (toluene: water 3:2 ratio), $Pd(PPh_3)_4$ (5 mol%) and Aliquat 336 (1 mol%) were mixed. The mixture was refluxed under inert atmosphere for 2 days. The reaction was controlled by TLC. After evaporation of solvent under reduced pressure, the crude product was extracted with $CHCl_3$:H_2O three times to remove alkali solution. The organic layers were collected and dried over $MgSO_4$. The crude product was washed with cold methanol, acetone and hexane to obtain corresponding polymer as purple solid. Yield: 35%

2.4.2. Synthesis of PBOSPh

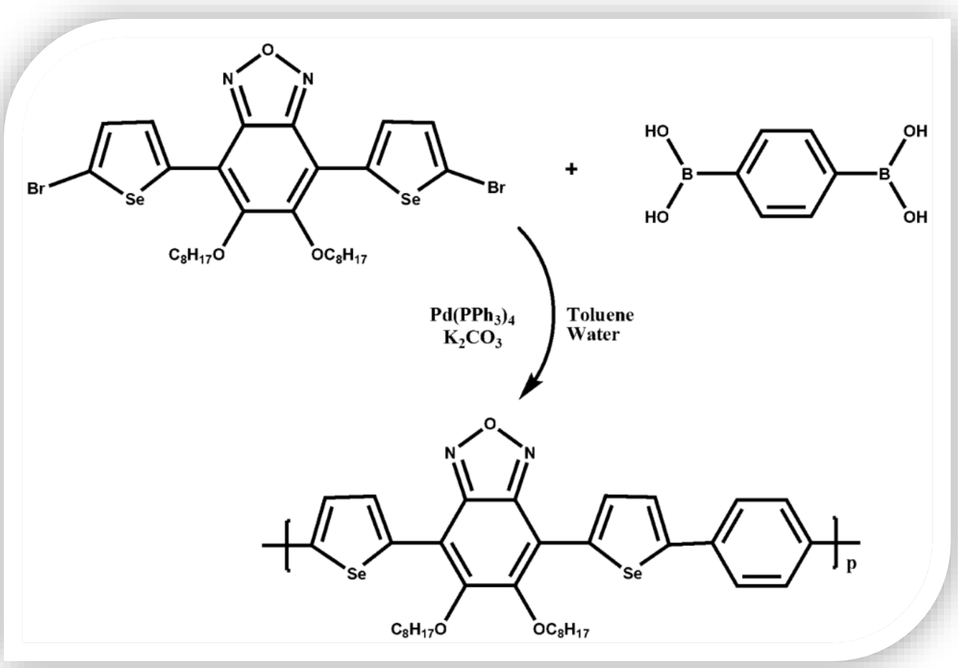

Figure 2.21: Synthetic route of PBOSPh

4,7-Bis(5-bromoselenophen-2-yl)-5,6-bis(octyloxy)benzo[c][1,2,5]oxadiazole (247 mg, 0.389 mmol), 1,4-phenylenediboronic acid (64.5 mg, 0.389 mmol), potassium carbonate (K_2CO_3, 2M in H_2O) and toluene (toluene: water 3:2 ratio), $Pd(PPh_3)_4$ (5 mol%) and Aliquat 336 (1 mol%) were refluxed under inert atmosphere for 50 hours. The reaction was controlled by TLC. After evaporation of solvent under reduced pressure, the crude product was extracted with $CHCl_3$:H_2O three times to remove alkali solution. The organic layers were collected and dried over $MgSO_4$. The crude product was washed with cold methanol, acetone and hexane to obtain corresponding polymer as dark purple solid. Yield: 40%

2.4.3. Synthesis of PBOTTPh

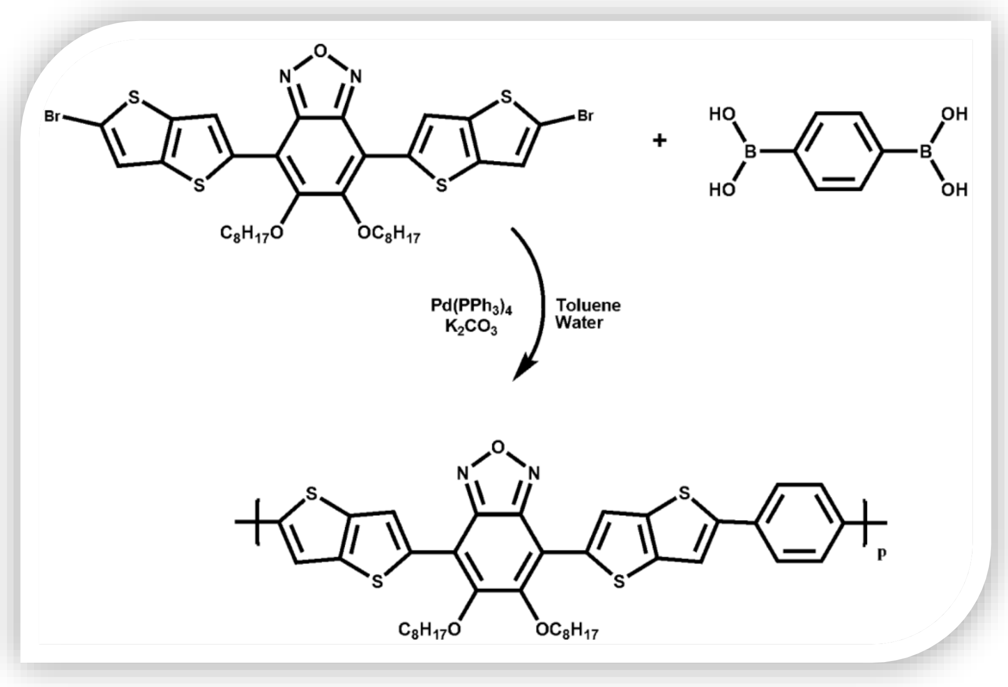

Figure 2.22: Synthetic route of PBOTTPh

4,7-Bis(5-bromothieno[3,2-b]thiophen-2-yl)-5,6-bis(octyloxy)benzo[c][1,2,5]oxadiazole (195 mg, 0.242 mmol), 1,4-phenylenediboronic acid (40.11 mg, 0.242 mmol), potassium carbonate (K_2CO_3, 2M in H_2O) and toluene (toluene: water 3:2 ratio), $Pd(PPh_3)_4$ (5 mol %) and Aliquat 336 (1 mol%) were mixed. The mixture was refluxed under inert atmosphere for 2 days. The reaction was controlled by TLC. After evaporation of solvent under reduced pressure, the crude product was extracted with $CHCl_3$:H_2O three times to remove alkali solution. The organic layers were collected and dried over $MgSO_4$. The crude product was washed with cold methanol, acetone and hexane to obtain corresponding polymer as dark purple solid. Yield: 35%

2.4.4 Synthesis of PBOFPh

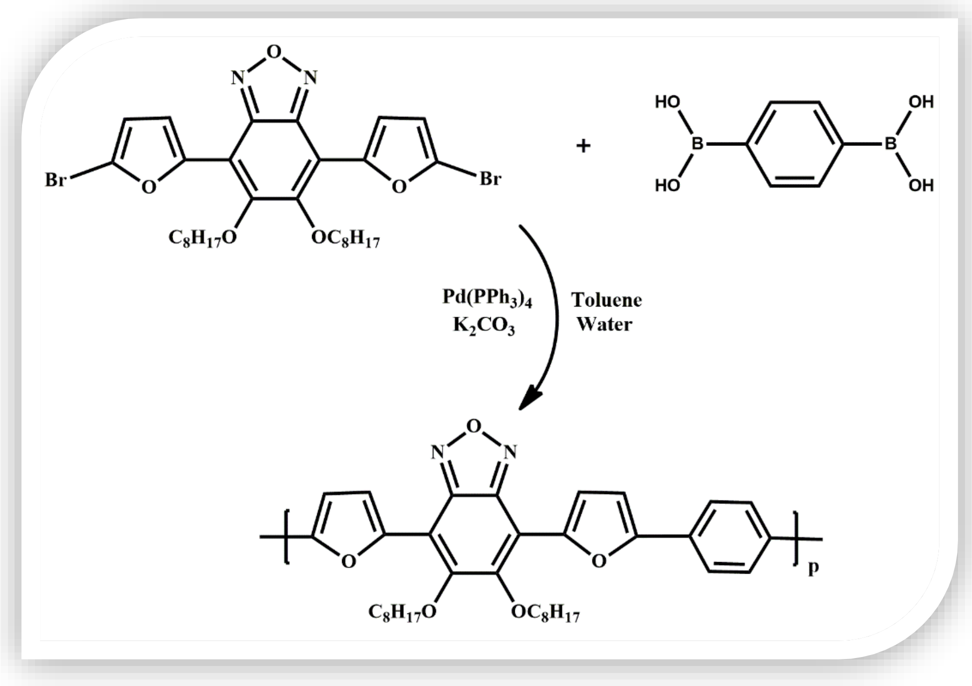

Figure 2.23: Synthetic route of PBOFPh

4,7-Bis(5-bromofuran-2-yl)-5,6-bis(octyloxy)benzo[c][1,2,5]oxadiazole (200 mg, 0.301 mmol), 1,4-phenylenediboronic acid (49.89 mg, 0.301 mmol), potassium carbonate (K2CO3, 2M in H2O) and toluene (toluene: water 3:2 ratio), Pd(PPh3)4 (5 mol %) and Aliquat 336 (1 mol%) were mixed. The mixture was refluxed under inert atmosphere for 2 days. The reaction was controlled by TLC. After evaporation of solvent under reduced pressure, the crude product was extracted with $CHCl_3$:H_2O three times to remove alkali solution. The organic layers were collected and dried over $MgSO_4$. The crude product was washed with cold methanol, acetone and hexane to obtain corresponding polymer as pinkish purple solid. Yield: 30%

2.5. Device Fabrication of the Organic Solar Cell for PBOSPh

Before device fabrication, ITO etching and cleaning is required. ITO was etched using 50% of distilled water, 49% of HCl and 1% of HNO_3 at 100^0C to be able to get anode and cathode contacts seperately with avoiding short circuit. Subsequently, to neutralize ITO slides 10% of K_2CO_3 solution was used. For cleaning, sonication was carried out in an ultrasonic bath using toluene, detergent and water, water, acetone and isopropyl alcohol after etching ITO surface onto glass. To remove dust particles on ITO surface, Oxygen Plasma Cleaner was used. Fabrication and characterization of a solar cell were performed in a nitrogen filled glove box system. PEDOT:PSS was spin coated on ITO substrate as hole transport layer also providing a smoother surface for active layer. The polymer was blended with $PC_{70}BM$ using 1,2-dichlorobenzene as the solvent and spin coated onto PEDOT:PSS layer with various speeds to get different thicknesses. 20 nm Ca and 80 nm Al were thermally evaporated as cathode metals using a shadow mask. Device architecture was ITO/PEDOT:PSS/PBOSPh:$PC_{70}BM$/Ca:Al. Polymer:$PC_{70}BM$ ratio was optimized as 1:2 (ODCB). Keithley 2400 sourcemeter was used to record J-V curve under dark and simulated illumination (AM 1.5G, 100mW/cm^2).

CHAPTER 3

RESULTS and DISCUSSION

3.1. Electrochemical and Electrochromic Properties of Donor-Acceptor-Donor Type Polymers

3.1.1 Electrochemistry of Homopolymers

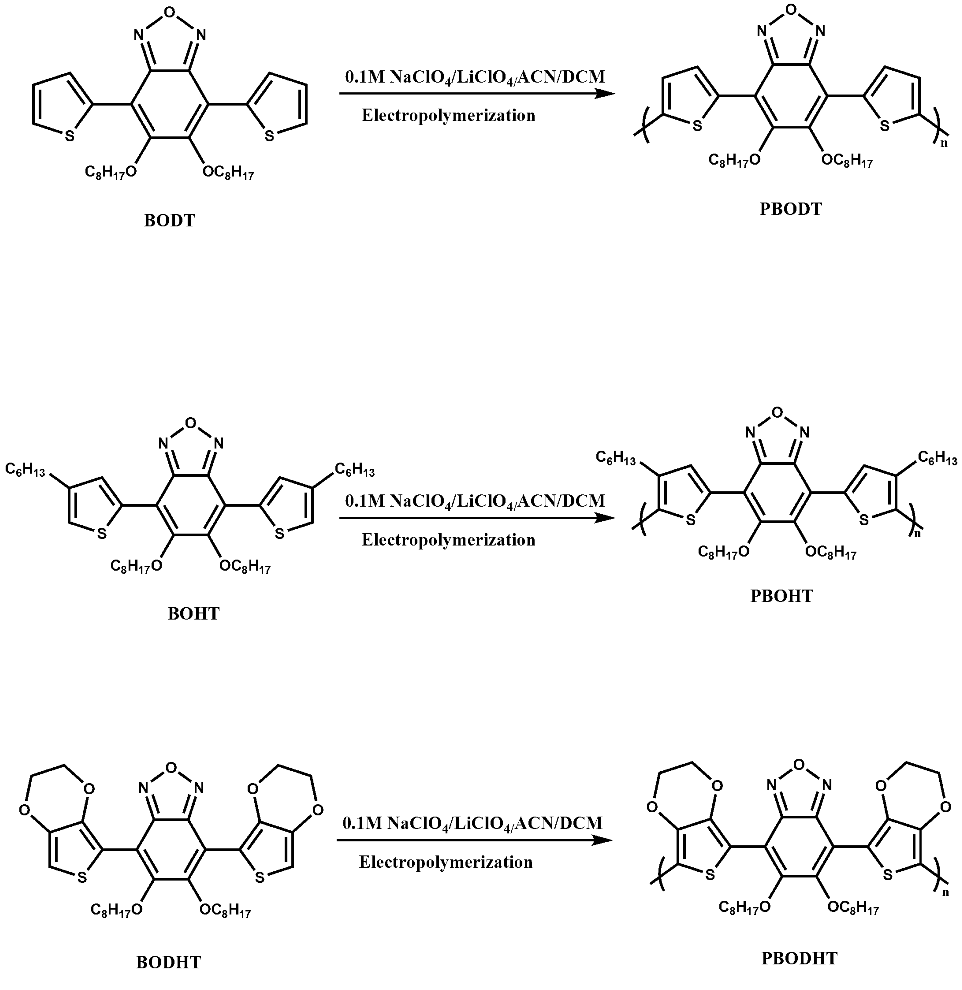

Figure 3.1: Chemical structures and electropolymerizationof BODT, BOHT and BODHT

Cyclic voltammetry studies reveal the reversibility of the electron transfer for the polymers. All electrochemical polymerization reactions were carried out in a dichloromethane (DCM)/ acetonitrile (ACN) (5/95, v/v) solution containing 0.1 M sodium perchlorate/lithium perchlorate ($NaClO_4$ /$LiClO_4$) as the supporting electrolyte with 0.01 M monomer at a scan rate of 100 mV s^{-1} (Figure 1). Monomers have poor solubility in acetonitrile therefore the solvent system was chosen as a mixture of DCM and ACN (5/95, v/v) to obtain good polymer film on ITO coated glass slide (nearly 1 cm^2 area). In the first cycle of voltammograms, irreversible monomer oxidation peaks arouse at 1.27 V for BODT, 1.25 V for BOHT and 0.99 V for BODHT vs. Ag wire pseudo-reference electrode (0.35 V vs. Fc/Fc^+). Continuous polymerization led an increase in anodic and cathodic current densities. This proves the deposition of polymer film on ITO coated glass slides. To investigate the redox behaviors of the resulting polymers (PBODT, PBOHT and PBODHT), cyclic voltammetry was used. Potentiodynamically synthesized polymers were put in a monomer free solution to investigate their p-type and n-type doping properties. In monomer free solution, polymers are p-dopable with reversible redox couple at 1.25 V/0.93 V for PBODT and at 1.23 V/0.88 V for PBOHT and 0.95/ -0.49 V for PBODHT vs. Ag wire as pseudo reference electrode. On account of the electron-rich EDOT units in the PBODHT chains, the polymer film exhibited lower redox potentials compared to other two polymers as expected.

The HOMO energy levels of three polymers were calculated from onset of the corresponding oxidation potentials from the intersection between base line and tangent drawn to the increasing current line. HOMO levels are -5.73 eV for PBODT, -5.54 eV for PBOHT and -4.73 eV for PBODHT respectively. LUMO levels were estimated from the band gap values obtained from spectroelectrochemistry experiment as -6.98 eV for PBODT, -6.81 eV for PBOHT and -6.23 eV for PBODHT.

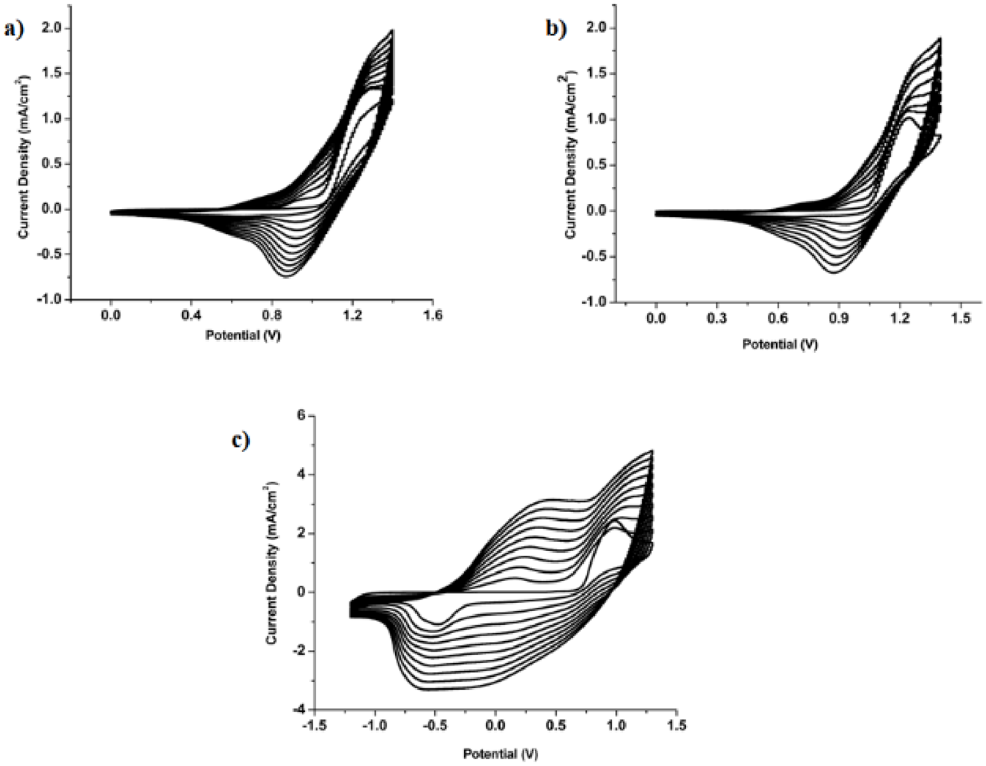

Figure 3.2: Electropolymerization of a) BODT, b) BOHT and c) BODHT on ITO in 0.1M NaClO$_4$/ LiClO$_4$ /DCM/ACN electrolyte/solvent couple at a scan rate of 100 mV.s^{-1}

3.1.2. Spectroelectrochemistry of Homopolymers

Spectroelectrochemistry experiments were performed to investigate electronic and optical changes of conducting polymers upon doping processes. Band gap (E_g), λ_{max}, the intergap states that appear upon doping and formation of polaronic and bipolaronic bands were examined. In situ electronic absorption spectra and kinetic studies of three polymer films were investigated upon doping in a monomer free 0.1 M ACN/NaClO$_4$/LiClO$_4$ solution. To prove formation of polarons and bipolarons, UV–Vis-NIR spectra were obtained as a function of applied potential. Formation of lower energy charge carriers eventuate in absorbance increase in the electronic absorption spectra of the polymer films. Three polymers were potentiodynamically synthesized and put in a monomer free 0.1 M ACN/$NaClO_4$/$LiClO_4$ solution while potential was sweeped between 0.0 V and 1.2 V for PBODT, 0.0 V and 1.15 V for PBOHT and -1.20 V to 0.8 V for PBODHT. To eliminate dopant ions and charges formed throughout electropolymerization of monomers on ITO coated glass slides, the polymers were firstly reduced to their neutral states then oxidation was performed in spectroelectrochemical studies. Moreover, to eliminate unreacted monomers left on surface, polymer films were washed with acetonitrile. The absorption maximum revealed at 551 nm for PBODT, at 577 nm for PBOHT and at 590 nm for PBODHT corresponding to the π-π^* transitions. From these transitions, the band gaps of the polymers were calculated as 1.25, 1.27 and 1.50 eV for PBODT, PBOHT and PBODHT respectively. Alkyl chains at the 3-position of thiophene ring cause steric interactions between repeating units within the polymer backbone hence, decreasing the overlap between π- orbitals. Therefore, distortion of backbone planarity may induce the difference between band gaps of PBOHT and PBOHT.

Electrochromism is important for many commercial applications such as displays, mirrors, windows and sun-glasses. The synthesized polymer films reveal electrochromic properties upon p-doping/dedoping. Thiophene containing polymer switched between purple and blue whereas 3-hexylthiophene containing polymer switched between blue and pale green and EDOT containing polymer switched between dark blue and pale blue. For the scientific expression of the color, colorimetric measurements of the polymer films were performed and CIE (Commission Internationale de l'Eclairage) coordinates were determined. In CIE coordinates, L represent the brightness of the color (L= 0 yields black and L= 100 indicates diffuse white), a represents its color between red/magenta and green, b represents its color between yellow and blue.

Table 1: Colorimetric measurements of the homopolymer films

PBODT	**0.0 V**	**1.2 V**	**1.4 V**
	L: 55.786	**L:** 76.860	**L:** 75.451
	a: 10.048	**a:** -9.822	**a:** -16.152
	b: -13.948	**b:** 19.619	**b:** 9.624
PBOHT	**0.0 V**	**1.2 V**	**1.4 V**
	L: 42.308	**L:** 51.496	**L:** 57.751
	a: 3.222	**a:** -2.489	**a:** -17.344
	b: -26.159	**b:** -6.410	**b:** 8.169
PBODHT	**-1.2 V**	**0.5 V**	**0.7 V**
	L: 31.190	**L:** 53.190	**L:** 61.190
	a: 3.452	**a:** -2.890	**a:** -21.760
	b: -24.210	**b:** -7.978	**b:** -5.132

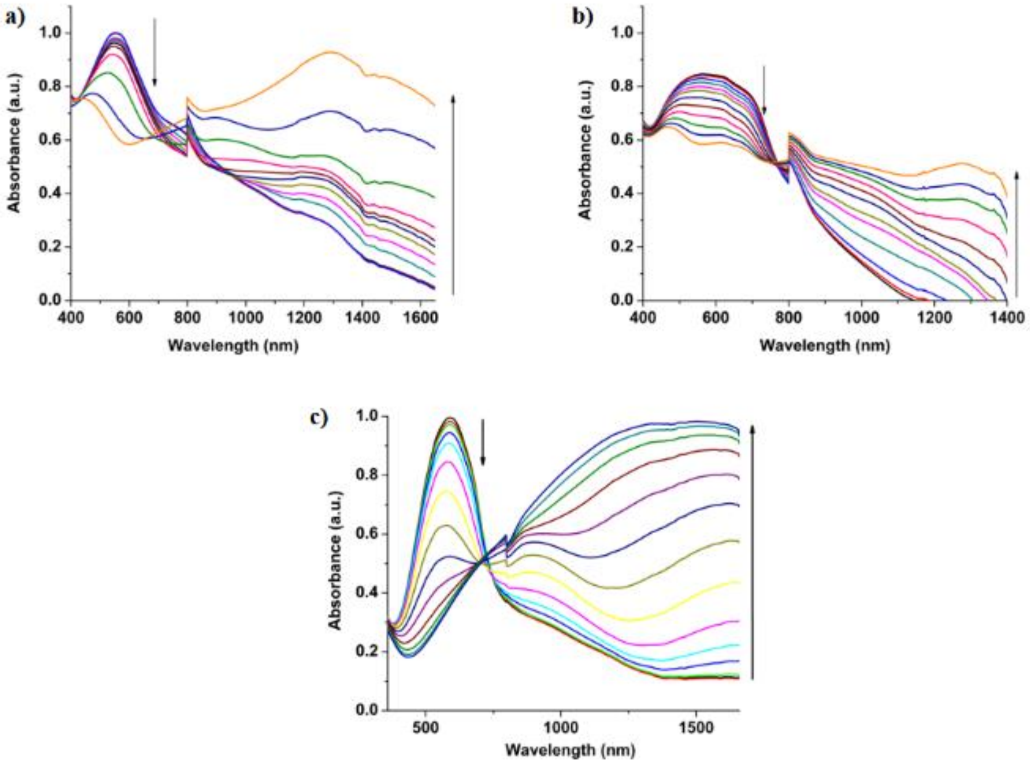

Figure 3.3: Change in the electronic absorption spectra of a) PBODT, b) PBOHT and c) PBODHT upon oxidative doping at potentials between 0.0/1.40 V , 0.0 /1.25 V and -1.20/+1.0V respectively

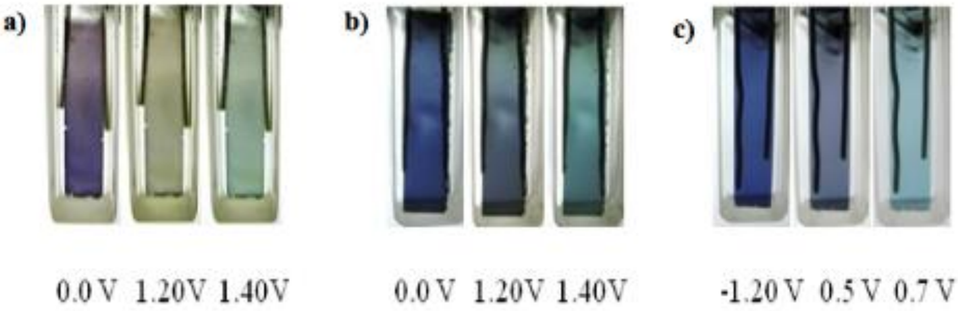

Figure 3.4: Colors upon oxidative doping a) PBODT, b) PBOHT and c) PBODHT

Table 2: The structures of benzooxadiazole based D-A-D type polymers and their electrochemical and optical properties

Structure	$E^{ox}m$ Ep,a Ep,c	λmax (nm)	E_g^{op} (eV)	Color	Optical Contrast/ Switching Time
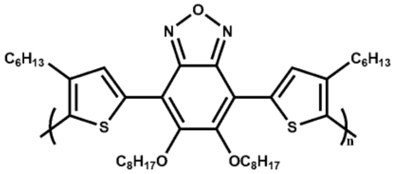	**1.25** **1.23** **0.88**	**577**	**1.27**	**Blue/ Green**	**17% (580 nm)** **2.5 s** **33%(1290 nm)** **1.5 s**
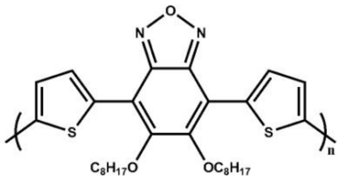	**1.27** **1.25** **0.93**	**551**	**1.25**	**Purple/ Pale Green**	**18% (555 nm)** **1.1 s** **37% (1300 nm)** **0.5 s**
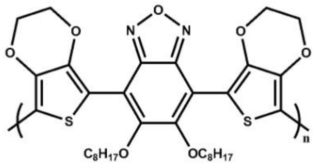	**0.99** **0.95** **-0.49**	**590**	**1.50**	**Dark blue/ Pale blue**	**75% (590 nm)** **0.9s** **88% (1500 nm)** **1.1 s**

3.1.3. Kinetic Studies of Homopolymers

Kinetic studies were done to show changes in percent transmittance while continuous stepping the potential between fully neutral and oxidized states within a time interval of 5 s. Switching time is often reported as the time required for the coloring/bleaching process of the electrochromic material at a 95 % contrast value since the human eye is sensitive up to 95 % of the full contrast. It is important especially for applications such as dynamic displays and switchable mirrors. The switching speed depends on several factors such as the ionic conductivity of the electrolyte, accessibility of the ions to the electroactive sites (ion diffusion in thin films), magnitude of the applied potential, film thickness, and morphology of the thin film. The time required for a full optical contrast between the neutral and oxidized states and transmittance changes at dominant wavelengths are shown in Table 2. The optical contrasts were calculated as 18 % at 555 nm and 37 % at 1300 nm for PBODT and also 17 % at 580 nm and 33 % at 1290 nm for PBOHT respectively. PBOHT film originating from the long alkyl chains on thiophene units has lower conductivity therefore was switched slower when compared to its thiophene homologue PBODT [25]. The optical contrast values for PBODHT were even better than those of PBODT and PBOHT in the visible region with 75 % transmittance change at 590 nm and 88 % transmittance change at 1500 nm. EDOT and thiophene containing polymers switched very rapidly between their neutral and oxidized states. PBODT revealed switching times of 1.1 s at 555 nm and 0.5 s at 1300 nm. On the other hand, PBOHT revealed switching times of 2.5 s at 580 nm and 1.5 s at 1290 nm whereas PBODHT has switching times of 0.9 s in the visible region (590nm) and 1.1 s in the NIR region (1500 nm). Among all, PBODHT exhibited the shortest switching time as well as the highest optical contrast.

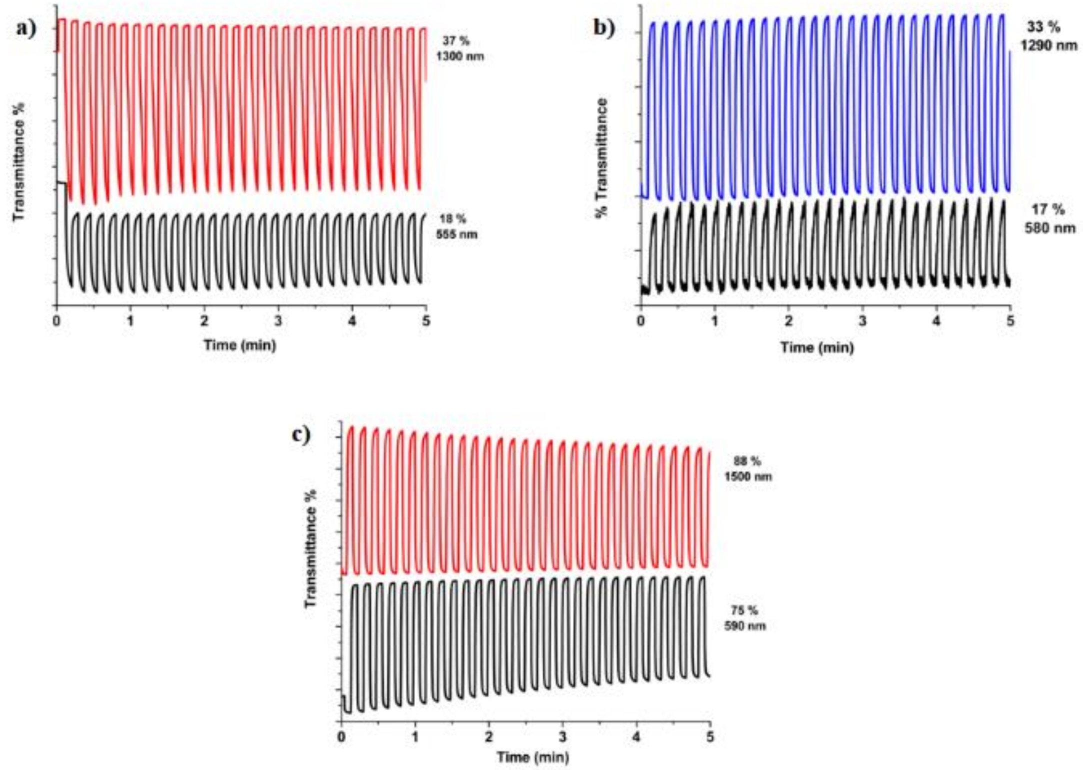

Figure 3.5: Electrochromic switching and percent transmittance changes observed at the absorption maxima of a) PBODT, b) PBOHT and c) PBODHT when switched between in system $NaClO_4/LiClO_4/ACN$

3.2. Electrochromic Properties of Donor-Acceptor-Donor Type Polymers

3.2.1. Electrochemical Properties of PBOTPh

Reversible redox couple was determined from cyclic voltammetry studies at 1.14 V/0.94 V for PBOTP. The HOMO energy level of the polymer was calculated from onset of the corresponding oxidation potential from the intersection between base line and tangent drawn to the increasing current line. HOMO level was found as -5.96 eV. Since the polymer is only p-dopable, LUMO level was estimated from the band gap values obtained from spectroelectrochemistry experiment as -4.11 eV.

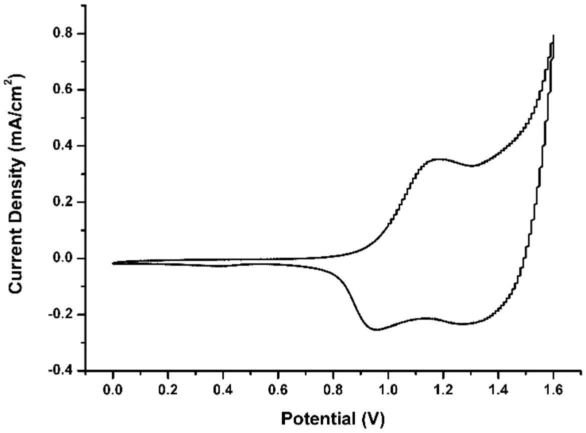

Figure 3.6: Single scan cyclic voltammogram of PBOTP on ITO between 0.0-1.60 V in 0.1 M TBAPF$_6$/ACN solution at a scan rate 100 mV/s

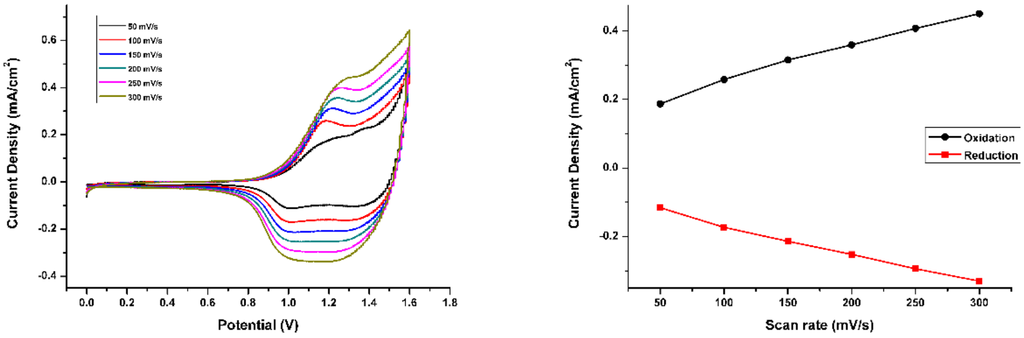

Figure 3.7: Change in cyclic voltammogram of PBOTPh in 0.1 M TBAPF$_6$/ACN electrolyte/solvent couple at different scan rates

Scan rate dependence of the polymers showed that electroactive polymers were stable at different scan rates in the cyclic voltammetry studies. Linear plot was drawn after scan rate dependence test and non-diffusion controlled mass transfer during doping/dedoping process was proven with this plot.

3.2.2. Spectroelectrochemical Properties of PBOTPh

Neutral PBOTP film was spray coated onto ITO coated glass electrode from a solution of 5 mg/mL in chloroform to determine optical properties such as absorption maxima and optical band gap. The UV-vis-NIR spectra was recorded by applying positive potential. The absorbance changes were recorded between 0.0 V and 1.40 V in a monomer free $TBAPF_6$/ACN electrolyte/solvent couple. λ_{max} was observed at 565 nm. The optical band gap was calculated as 1.85 eV. The polymer changes its color from purple to light blue upon oxidative doping.

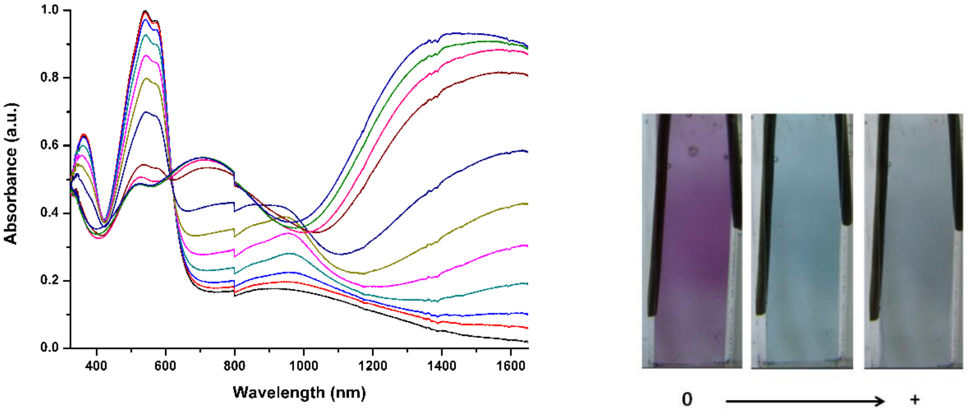

Figure 3.8: Change in the electronic absorption spectra at potentials between 0.0/1.40 V and colors of PBOTPh upon oxidative doping

3.2.3. Electrochemical Properties of PBOSPh

In monomer free solution, the polymer has ambipolar property. The oxidation potential of the polymer appeared at 1.01 V for p-doping and 0.91 V for de-doping and reversible redox couple appeared at -1.48 V /-1.30 V for n-doping. Selenophene provides the polymer n-type doping property. The HOMO and LUMO energy levels of the polymer were calculated from onset of the corresponding oxidation and reduction potentials respectively. HOMO level was found as -5.85 eV. LUMO level was found as -4.02 eV. Electronic band gap of the polymer is calculated from the difference between HOMO and LUMO energy levels and was found as 1.83 eV. The electronic band gap was comparatively higher than the optical one because of the formation of free ions in the cyclic voltammetry studies.

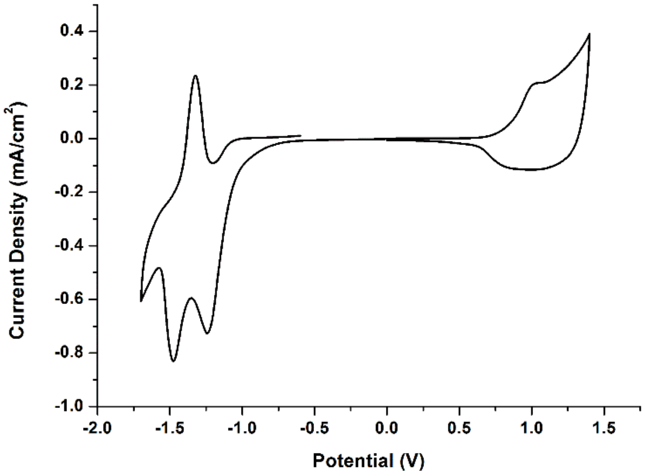

Figure 3.9: Single scan cyclic voltammogram of PBOSPh on ITO between -1.80/1.40 V in 0.1 M TBAPF$_6$/ACN solution at a scan rate 100 mV/s

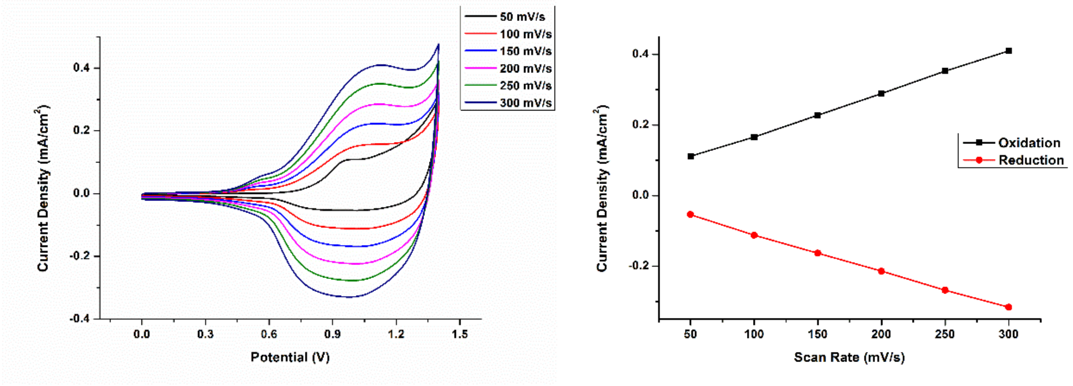

Figure 3.10: Change in cyclic voltammogram of PBOSPh in 0.1 M TBAPF$_6$/ACN electrolyte/solvent couple at different scan rates

Linear relationship between the current density and the scan rate proves the non-diffusion controlled mass transfer during doping-dedoping process in the cyclic voltammetry studies of electroactive polymers.

3.2.4. Spectroelectrochemical and Kinetic Properties of PBOSPh

The optical band gap, absorption maxima and the wavelengths at which polaronic and bipolaronic bands form were determined from spectroelectrochemistry studies. The optical band was calculated using De-Broglie equation as 1.76 eV and the absorption maxima was observed at 532 nm. The spray processable polymer is purple in the neutral state, have multi colored oxidation states. The polymer changes its color to transparent upon negative doping. Since selenophene is stronger donor unit than thiophene, a red shift in absorption occured in the electronic absorption spectra.

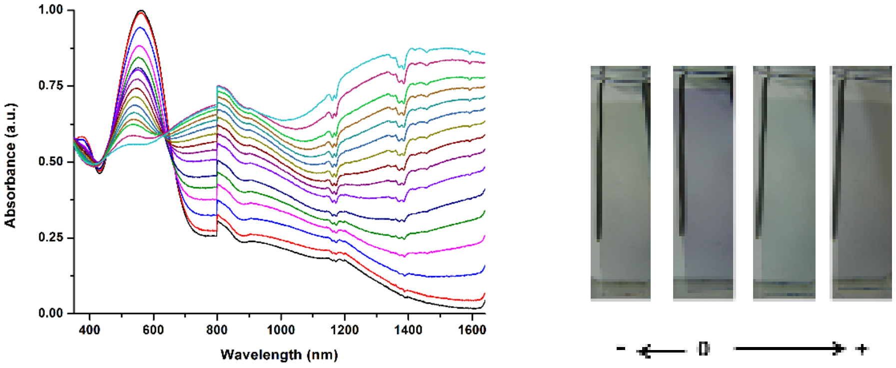

Figure 3.11: Change in the electronic absorption spectra at potentials between 0.0/1.30 V and colors of PBOSPh upon oxidative doping

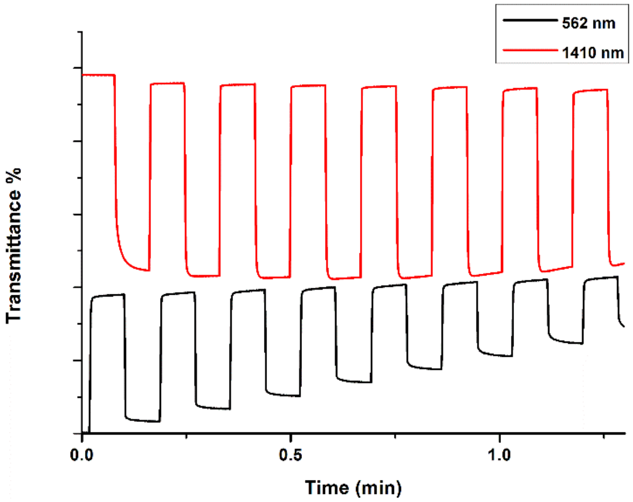

Figure 3.12: Electrochromic switching and percent transmittance changes observed at 562 and 1410 nm in 0.1M TBAPF$_6$/ACN

Percent transmittance change, switching times and the stabilities of the polymer upon electrochromic switching between the neutral and oxidized states were investigated in both visible and near-IR regions. The optical contrasts of the PBOSP film was calculated to be 18 % and 27 % at 532 nm and 1410 nm respectively. The polymer has switching times of 0.6 s and 0.4 s at 532 nm and 1410 nm respectively.

3.2.5. Electrochemical Properties of PBOTTPh

The polymer was spray coated onto ITO coated glass electrode and cyclic voltammetry studies were carried out in a monomer free solution. Upon p-doping, the oxidation potential of the polymer appeared at 0.97 V for doping and for de-doping 0.66V. Reversible redox couples appeared at -1.49 V /-1.28 V and -1.91 V/-1.72 V upon n-doping. Thienothiophene has much stronger electron donating ability than thiophene counterpart resulting in different electrochemical properties. The polymer is ambipolar. The HOMO and LUMO energy levels of the polymer were calculated from onset of the corresponding oxidation and reduction potentials respectively. HOMO level was found as -5.63 eV. LUMO level was found as -4.03 eV. Electronic band gap was determined as 1.60 eV. The polymer is multi-colored upon both positive and negative doping.

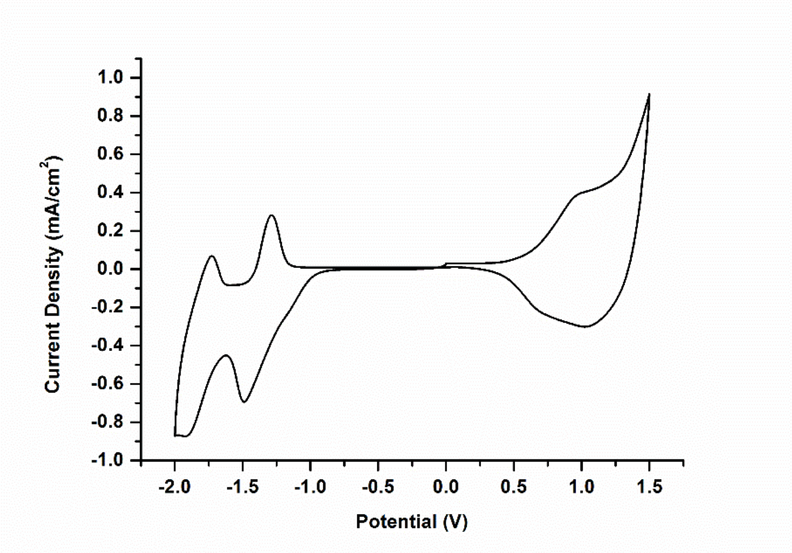

Figure 3.13: Single scan cyclic voltammogram of PBOTTPh on ITO between -2.00/1.50 V in 0.1 M TBAPF$_6$/ACN solution at a scan rate 100 mV/s

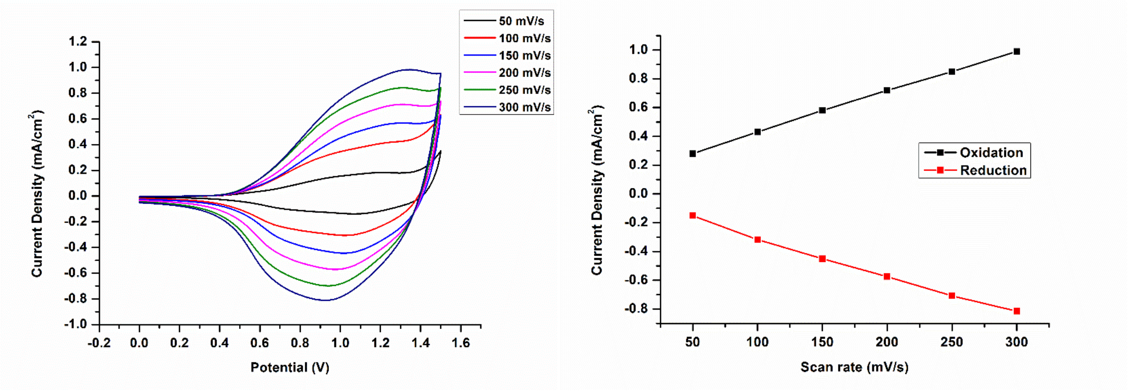

Figure 3.14: Change in cyclic voltammogram of PBOTTPh in 0.1 M TBAPF$_6$/ACN electrolyte/solvent couple at different scan rates

The current density versus scan rate graph revealed that during doping-dedoping process in the cyclic voltammetry studies of electroactive polymer, the mass transfer is non-diffusion controlled.

3.2.6. Spectroelectrochemical and Kinetic Properties of PBOTTPh

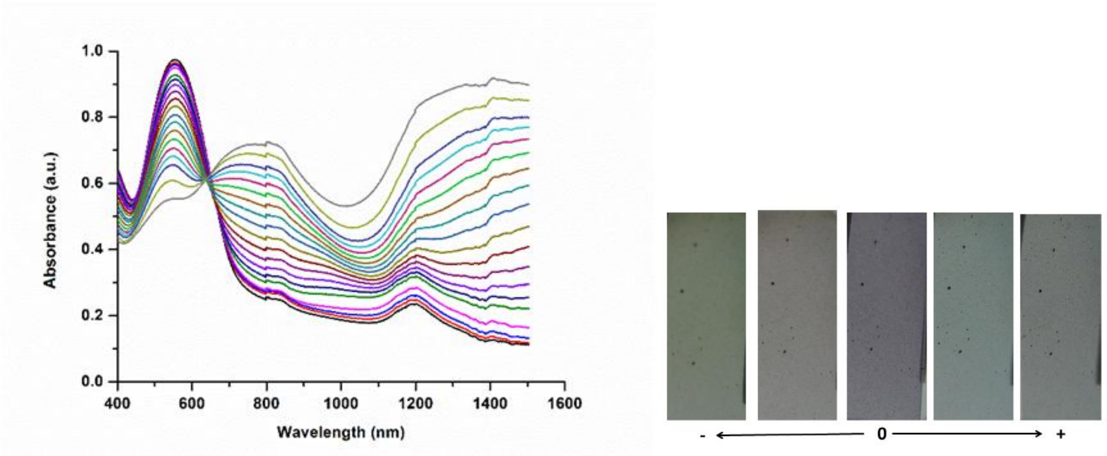

Figure 3.15: Change in the electronic absorption spectra at potentials between 0.0/1.20 V and colors of PBOTTPh upon oxidative doping

Spectroelectrochemistry studies provide to determine the optical band gap, absorption maxima and the wavelengths for the formation of polaronic and bipolaronic bands. The optical band gap of the polymer was 1.58 eV and the absorption maxima was observed at 555 nm which is red shifted compared to other analogs due to strong electron donating ability of thienothiophene. The spray processable polymer is dark purple in the neutral state, changes its color to blue and then gray with stepwise oxidation. Upon successive negative doping, green and gray colors were achieved.

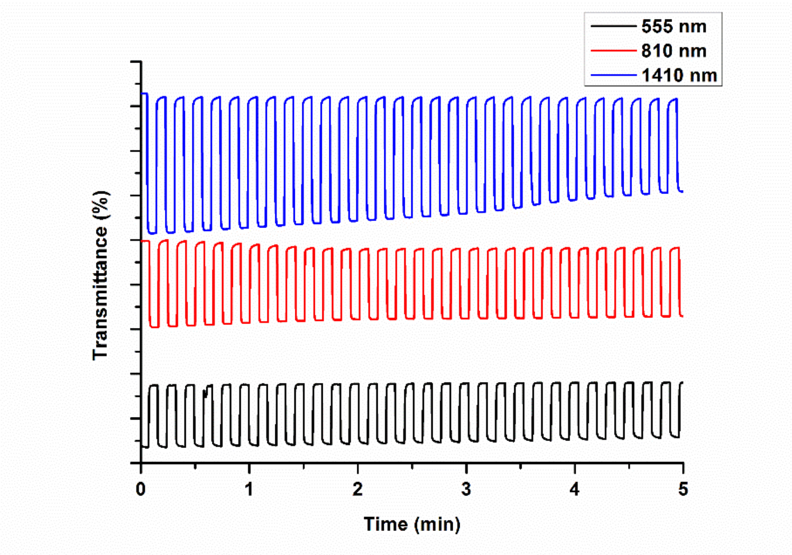

Figure 3.16: Percent transmittance changes of the polymer film in monomer free, 0.1 M TBAPF$_6$/ACN solution at its maximum absorption wavelengths

During chronoamperometry studies, the changes in transmittance as optical contrasts of the polymer film at corresponding wavelengths were recorded as 14% at absorption maxima which is 555 nm, 20% for 810 nm where the polaron bands form and 31% for 1410 nm in which bipolarons appear. The switching times were calculated as of 0.6 s, 0.6 s, 0.5 s at 555 nm, 810 and 1410 nm respectively.

3.2.7. Electrochemical Properties of PBOFPh

The furan based polymer is both p-dopable and n-dopable. The oxidation potential of the polymer was observed at 0.98 V for p-doping and for de-doping 0.77 V. Reversible redox couples appeared at -1.45 V and -1.36 V upon n-doping. Ambipolar character for the polymer may occur due to rich electron donating ability of furan unit. The HOMO and LUMO energy levels of the polymer were calculated as -5.74 eV. LUMO level was found as -3.87 eV. Electronic band gap was 1.87 eV. The polymer is multi-colored upon both positive and negative doping.

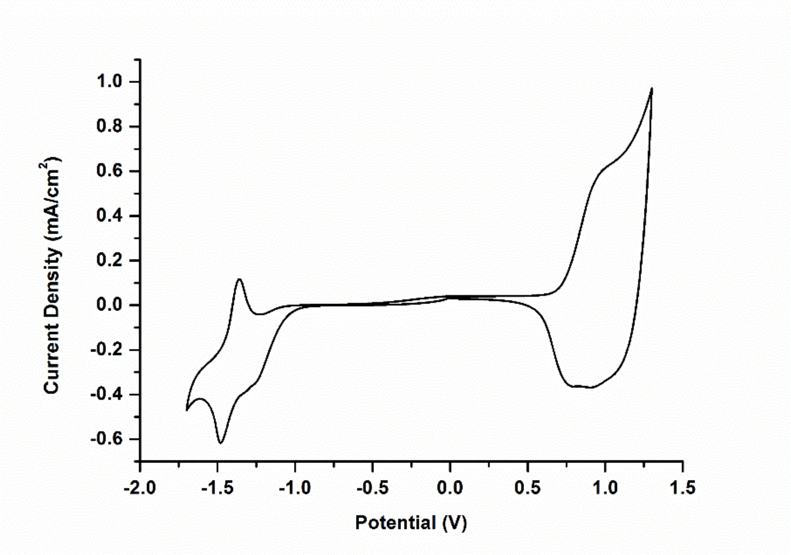

Figure 3.17: Single scan cyclic voltammogram of PBOFPh on ITO between -1.70/1.30 V in 0.1 M TBAPF$_6$/ACN solution at a scan rate 100 mV/s

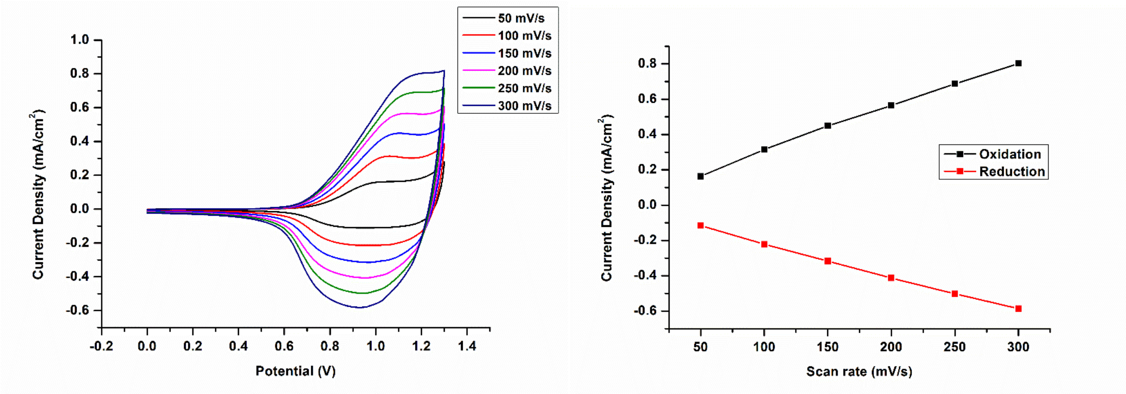

Figure 3.18: Change in cyclic voltammogram of PBOFPh in 0.1 M TBAPF$_6$/ACN electrolyte/solvent couple at different scan rates

3.2.8. Spectroelectrochemical and Kinetic Properties of PBOFPh

Spectroelectrochemical properties of the polymer were carried out in 0.1 M TBAPF$_6$/acetonitrile electrolyte-solvent couple. As the potential was gradually changed, the changes in the absorbance were recorded. PBOFPh has an absorption maxima centered at 535 nm which is blue shifted compared to thienothiophene, selenophene and thiophene counterparts in the visible region. The optical band gap was calculated from the onset of π-π* transition as 1.79 eV. PBOFPh is pinkish purple in the neutral state.

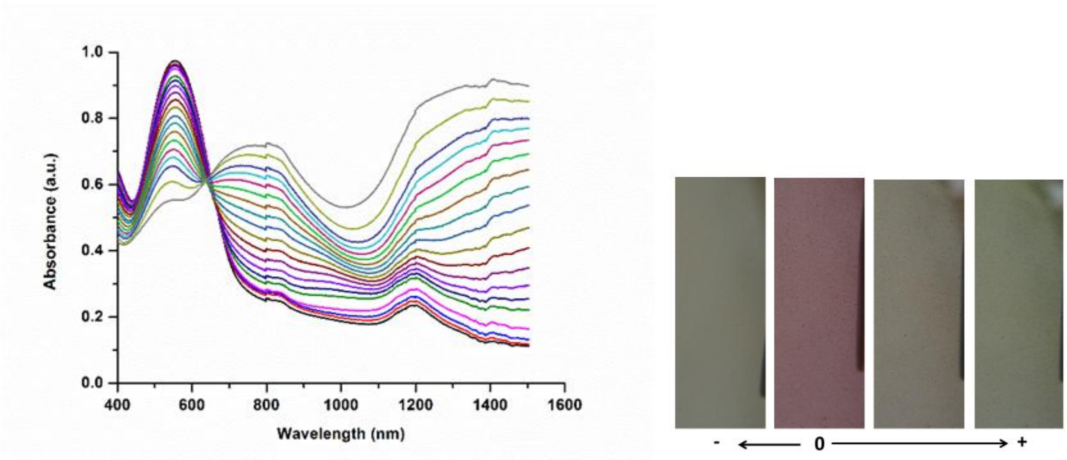

Figure 3.19: Change in the electronic absorption spectra at potentials between 0.0/1.10 V and colors of PBOFPh upon oxidative doping

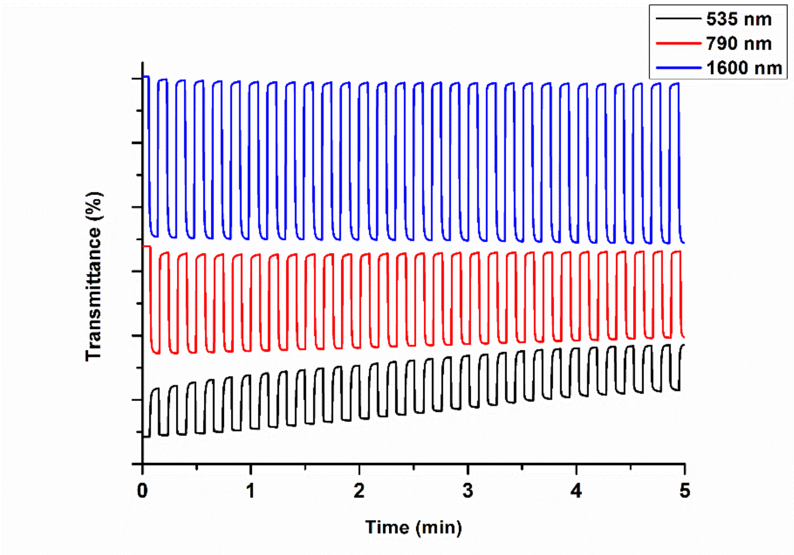

Figure 3.20: Percent transmittance changes of the polymer film in monomer free, 0.1 M TBAPF$_6$/ACN solution at its maximum absorption wavelengths

The optical contrasts of the PBOFP film was calculated to be 16%, 32% and 50% at 535 nm, 790 and 1600 nm respectively in chronoamperometry studies. The polymer has switching times of 1.3 s, 0.6 s and 0.5 s at 535 nm, 790 nm and 1600 nm respectively.

In near IR region, the polymer has almost better stability compared to other chemically synthesized polymers.

Table 3: Summary and comparison of electronic properties of benzooxadiazole comprising alternating polymers

	HOMO (eV)	LUMO (eV)	λmax (nm)	Eg^{el} (eV)	Eg^{op} (eV)	Ep doping (V)	Ep dedoping (V)	En doping (V)	En dedoping (V)
PBOTPh	-5.96	-4.11	565	-	1.85	1.14	0.94	-	-
PBOSPh	-5.85	-4.02	532	1.83	1.76	1.01	0.91	-1.48	-1.30
PBOTTPh	-5.63	-4.03	555	1.60	1.58	0.97	0.66	-1.49 -1.91	-1.28 -1.72
PBOFPh	-5.74	-3.87	535	1.87	1.79	0.98	0.77	-1.45	-1.36

Table 4: Summary and comparison of optical properties of benzooxadiazole comprising alternating polymers

	Optical Contrasts (%T)			Switching Times (s)		
PBOTPh	-			-		
PBOSPh	18% (532 nm)	27% (1410 nm)		0.4	0.6	
PBOTTPh	14% (555 nm)	20% (810 nm)	31% (1410 nm)	0.6	0.6	0.5
PBOFPh	16% (535nm)	32% (790 nm)	50% (1600 nm)	1.3	0.6	0.5

Table 5: Colorimetric measurements of the copolymer films

	0.0 V		**1.2 V**	**1.5 V**	
PBOTPh	L: 73.744 a: 7.774 b: -6.277		L: 73.350 a: -1.260 b: -2.181	L: 72.561 a: -5.384 b:1.521	
	-1.8 V	**-1.4 V**	**0.0 V**	**1.0 V**	**1.4 V**
PBOTTPh	L: 77.816 a: -6.177 b: 1.000	L: 74.635 a: -5.928 b: 1.410	L: 81.071 a: 7.498 b: -11.069	L: 75.014 a: -5.380 b: -1.419	L: 81.620 a: -7.739 b: 1.049
	-1.5 V		**0.0 V**	**1.1 V**	**1.3V**
PBOFPh	L: 79.898 a: -4.838 b: 3.369		L: 72.495 a: 1.911 b: 7.223	L: 78.868 a: -2.025 b: 7.548	L: 87.534 a: -6.753 b: 7.016

3.2.9. Organic Solar Cell Studies of PBOSPh

Selenophene based polymer was blended with $PC_{70}BM$ as active layer in bulk heterojunction solar cell with the device architecture ITO/PEDOT:PSS/PBOSPh:$PC_{70}BM$/Ca/Al. The thickness of hole transport layer, PEDOT:PSS, was 40 nm. 1,2-dichlorobenzene was used as the solvent and the solution was filtered using 0.45µm syringe filter. As cathode metals, Ca and Al were thermally evaporated with 20 nm and 80 nm thicknesses, respectively. Table 6 shows the results of optimization studies. Figure 3.21 reveals J-V Curve of PBOSPh with the best device performance.

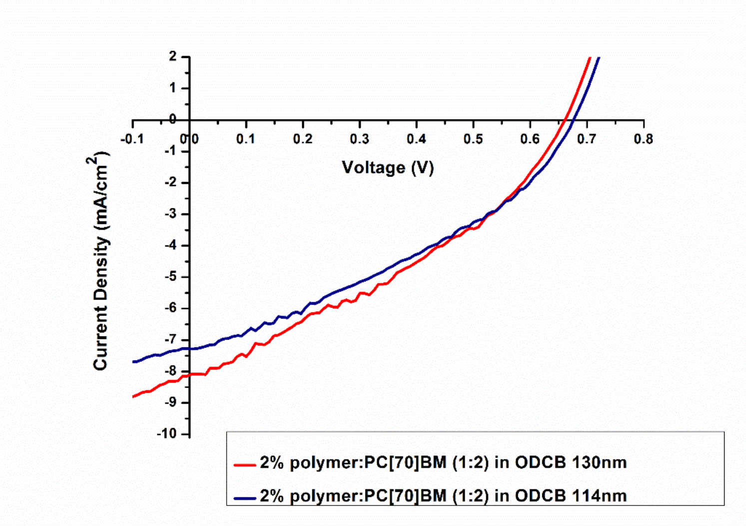

Figure 3.21: J-V Curve of PBOSPh

Table 6: Photovoltaic performance of PBOSPh

Polymer: $PC_{70}BM$ ratio	Thickness (nm)	Voc (V)	Jsc (mA/cm^2)	Vmp (V)	Imp (mA/cm^2)	FF (%)	PCE (%)
1:1	116	0.63	4.10	0.37	2.59	37	0.96
1:1	135	0.63	5.48	0.40	3.29	38	1.32
1:1	102	0.62	4.39	0.32	2.63	31	0.84
1:1	145	0.61	5.18	0.35	3.27	36	1.14
1:2	114	0.68	7.30	0.40	4.29	35	1.74
1:2	**130**	**0.68**	**8.14**	**0.41**	**4.48**	**33**	**1.83**

The optimization studies for photovoltaic device of selenophene based polymer will continue.

CHAPTER 4

CONCLUSION

D-A-D type all monomers were synthesized *via* Stille coupling methods and fully characterized performing nuclear magnetic resonance and high resolution mass spectroscopy. Electropolymerization method was used to synthesize the homopolymers of the thiophene, 3-hexylthiophene and 3,4-ethylenedioxythiophene (EDOT) containing monomers on ITO coated glass slides. Cyclic voltammetry and spectroelectrochemistry experiments and kinetic studies for all the polymers were performed to investigate the optoelectronic properties of the corresponding polymers. Thiophene containing homopolymer (PBODT) showed purple in its neutral state whereas 3-hexylthiophene (PBOHT) and 3,4-ethylenedioxythiophene (PBODHT) containing polymers revealed blue and dark blue colors in their neutral states, respectively. 3-Hexylthiophene based polymer film originating from the long alkyl chains on thiophene units has lower conductivity hence switching experiments were carried slowly compared to the ones for its thiophene homologue. The band gaps of the polymers were calculated from π-π* transitions using De Broglie equation as 1.25, 1.27 and 1.50 eV for PBODT, PBOHT and PBODHT respectively. Among all, EDOT containing polymer exhibited the shortest switching time as well as the highest optical contrast. Optical and electrochemical data showed that EDOT units in the conjugated system exert stronger influence on polymer electronic properties. Due to its electron rich property a red shift in absorption and a decrease in oxidation potential were observed compared to other two homopolymers.

This study was published in Synthetic Metals in 2014 [81]

Furthermore, four novel solution processable benzooxadiazole containing alternating copolymers were synthesized in a chemical way *via* Suzuki polycondensation reaction. To explore the electrochemical and electrochromic properties and the photovoltaic characterizations of the copolymers, cyclic voltammetry, spectroelectrochemistry and kinetic studies were again conducted. Thiophene, selenophene, furan and thienothiophene units were used as a π bridge. Thiophene and selenophene based alternating copolymers showed purple color in its neutral state whereas furan and thienothiophene bearing copolymers were pinkish purple and dark purple in their neutral states respectively. The optical band gap of the polymers were calculated as 1.85, 1.76, 1.58, 1.79 eV for thiophene, selenophene, thienothiophene and furan based copolymers, respectively. Among all the alternating copolymers, the lowest optical band gap corresponds to thienothiophene comprising alternating copolymer which is 1. 58 eV and red shifted in absorption due to the stronger donor character compared to other analogs. HOMO and LUMO levels were calculated from cyclic voltammetry studies using onsets of oxidation and reduction, respectively. PBOTPh is only p-dopable therefore LUMO level was estimated from equality of electronic and optical band gap and it was calculated as -4.11 eV. HOMO levels were calculated as -5.96 eV for PBOTPh, -5.85 eV for PBOSPh, -5.63 eV for PBOTTPh and -5.74 eV for PBOFPh. LUMO levels were determined as -4.02 eV for PBOSPh, -4.03 eV for PBOTTPh and -3.87 eV for PBOFPh. Selenophene has stronger electron donating ability and less aromaticity providing more stable quinoid form. Therefore selenium atom in the polymer backbone lowered the band gap compared to thiophene. Thienothiophene with a stronger electron donor ability has the lowest electronic band gap. The electronic band gaps were 1.83 eV for PBOSPh, 1.60 eV for PBOTTPh and 1.87 eV for PBOFPh. The optical contrasts and switching times were calculated from chronoamperometry studies. Thiophene based copolymer showed very poor stability therefore optical contrast could not been calculated. For PBOSPh, the optical contrast was observed as 18% a 532 nm and 27% at 1410 nm. Switching times were calculated as 0.4 s and 0.6 s at these wavelengths, respectively. For PBOTTPh, the optical contrasts were found as 14% at 555 nm, 20% at 810 nm, 31% at 1410 nm. Switching times were 0.6 s, 0.6 s, 0.5 s at 555, 810 and 1410 nm, respectively. Furan containing polymer showed higher stability in near IR region during kinetic studies. The optical contrasts were 16% at 535 nm, 32% at 790 nm and 50% at 1600 nm. Switching times were calculated as 1.3 s at 535 nm, 0.6 s at 790 nm, 0.5 s at 1600 nm.

Selenophene containing polymer was used as active layer in bulk heterojunction solar cell with a blend of $PC_{70}BM$. The device architecture was: ITO/PEDOT:PSS/PBOSPh:$PC_{70}BM$/Ca/Al. PEDOT:PSS was spin casted onto ITO with 40 nm thickness. The polymer was blended with $PC_{70}BM$ in 1,2-dichlorobenzene as the solvent and filtered using 0.45μm syringe filter. 15 nm Ca and 75 nm Al were thermally evaporated as cathode metals. After optimization studies, best results for 130 nm thickness, Polymer:PCBM with 1:2 ratio, V_{oc}, J_{sc}, FF, PCE (%) were found as 0.68, 8.14 mA/cm^2, 0.33, 1.83 % respectively.

All four polymers have low band gaps which is important for applications such organic light emitting diodes or photovoltaics. Also, the polymers were multicolored electrochromic states.

REFERENCES

[1] W. A. Gazotti, A. F. Nogueira, E. M. Girotto, L. Micaroni, M. Martini, S. das Neves, M.-A. De Paoli, Adv. Mater., 1998, 10, 1, 60-64

[2] J. L. Brédas, R. R. Chance, and R. Silbey, Phys. Rev. B 26, 58, 431 (1982)

[3] J. L. Brédas, J. C. Scott, K. Yakushi, and G. B. Street, Phys. Rev. B 30, 1023 (1984)

[4] J. L. Reddinger, J.R. Reynolds, Advances in Polymer Science, 145, 1999, 57-122

[5] G. Zotti, Handbook of Organic Conductive Molecules and Polymers, ed. H. S. Nalwa, Wiley, Chichester, 1997, Vol. 2, Ch. 4.

[6] M. E. G. Lyons, in Advances in Chemical Physics, Polymeric Systems, ed. I. Prigogine and S. A. Rice, John Wiley & Sons, New York, 1997, 94, 297.

[7] G. Zotti, G. Schiavon, A. Berlin, G. Pagani, Chem. Mater., 1993, 5, 430

[8] P. Audebert, P. Hapiot, Synthetic Metal, 199, 75, 95

[9] K. Yoshino, S. Hayashi and R.Sugimoto, Japanese Journal of Applied Physics, part 2, 23, 1984, L899

[10] N. Miyaura, K. Yamada, A. Suzuki, Tetrahedron Lett., 1979, 3437

[11] N. Miyaura, A. Suzuki, Synth. Commun., 1981, 11, 513

[12] D. Milstein, J. K. Stille, J. Am. Chem. Soc., 1978, 100, 3636

[13] T. Yamamoto, Chem. Lett. 2012, 41, 1422-1424

[14] E. Knoevenagel, Chem. Ber. 1894, 27, 2345

[15] D. C. Forbes, Tetrahedron Letters 47 (2006) 1699–1703

[16] K. Tamao, M. Kumada, J. Am. Chem. Soc.1972, 94, 4374

[17] J. P. Corriu, J. P. Masse, Chem. Commun. 1972, 144

[18] S. Murahashi, J. Organomet. Chem.1975, 91, C39

[19] K. Tamao, J. Organomet. Chem., 2002, 653,

[20] K. Sonogashira, Y. Tohda, N. Hagihara, Tetrahedron Letters, 1975, 50, 4467 - 4470

[21] K.-Y. Jen, M. R. Maxfield, L. W. Shacklette, R. L. Elsenbaumer, J. Chem. Soc., Chem Comm., 1987, 309

[22] R. J. Waltman, J. Bargon, A. F. Diaz, J. Phys. Chem., 1983, 87, 1459

[23] J. M. Toussaint, J. L. Brédas, Synth. Met., 1993, 61, 103

[24] J. Roncali, R. Garreau, A. Yassar, P. Marque, F. Garnier, M. Lemaire, J. Phys. Chem., 1987, 91, 6706

[25] R. D. McCullough, Adv. Mater., 1998, 10, 93

[26] H. Sirringhaus, P. J. Brown, R. H. Friend, M. M. Nielsen, K. Bechgaard, B. M. W. Langeveld-Voss, A. J. H. Spiering, R. A. J. Janssen, E. W. Meijer, P. Hervig, D. M. de Leeuw, Nature, 1999, 401, 685

[27] L. Groenendaal, F. Jonas, D. Freitag, H. Pielartzik, J. R. Reynolds, Adv. Mater., 2000, 12, 481

[28] S. Kirchmeyer, K. Reuter, J. Mater. Chem., 2005, 15, 2077

[29] E. E. Havinga, W. ten Hoeve, H. Wynberg, Polym. Bull. 1992,29, 119

[30] J. Roncali, Macromol. Rapid Commun., 2007, 28, 1761–1775

[31] U. Salzner, J. Phys. Chem. B, 2002, 106, 36

[32] R. J. Mortimer, Chem Soc. Rev. 1997, 26, 147-156

[33] S. K. Deb, Appl. Opt. Suppl., 1969, 3, 192

[34] P. D. Beer, O. Kocian, R. J. Mortimer, C. Ridgway, J. Chem. Soc., Faraday Trans., 1993, 89, 333

[35] H. Byker, in Electrochromic Materials 11, ed. K.-C. Ho and D. A. MacArthur, PV 94-2, pp. 3-13, Electrochem. Soc. Proc. Ser., Penning- ton, New Jersey, 1994

[36] M. Green, Chem. Ind., 1996, 17, 641

[37] A. Kraft, Bull. Hist. Chem., 2008, 33, 61-67

[38] P. M. S. Monk, R. J. Mortimer, D. R. Rosseinsky, Electrochromism: Fundamentals and Applications, VCH, Weinheim, 1995

[39] J. J. Berzelius, Afb. Fys. Kemi Miner., 1815, 4, 293

[40] F. Wöhler, Ann. Phys. 1824, 2, 350

[41] P. M. S. Monk, R. J. Mortimer, D. R. Rosseinsky, 2007, Electrochromism and Electrochromic Devices. Cambridge, UK: Cambridge Univ. Press

[42] C. G. Granqvist, 1995, Handbook of Inorganic Electrochromic Materials. Amsterdam: Elseveir

[43] T. A. Skotheim, J. R. Reynolds, eds. 2007, Handbook of Conducting Polymers. Boca Raton, FL: CRC 3rd ed.

[44] J. Roncali, Chem. Rev., 1992, 92, 4, 711-738

[45] C. Spahn, S. D. Minteer, Enzyme Immobilization in Biotechnology, Recent Patents on Engineering 2008, 2, 195-200

[46] S.Tuncagil, S.K. Kayahan, G. Bayramoglu, M.Y. Arica, L. Toppare, J.Mol. Catal. B-Enzym., 2009, 58, 187-193

[47] Bickerstaff, Immobilization of Enzymes and Cells, 1997, New Jersey: Humana Press.

[48] R.A. Messing, Adsorption and inorganic bridge formations, in Methods in Enzymology, vol. XLIV, Academic, New York, (1976) 148

[49] J. Woodward, Immobilized enzymes: adsorption and covalent coupling, in Immobilized Cells and Enzymes: A Practical Approach, IRL, Oxford, (1985) 3

[50] a) A. N. Pryakhin, E. S. Chukhrai, O. M. Poltorak, Glucose 6-phosphate dehydrogenase immobilized by adsorption on silica gel solid supports. Vest Moskov Univ Ser 2 Khim 1977; 18(1), 125

b) M. Kumakura, I. Kaetsu, Immobilization of cellulase using porous polymer matrix, J Appl Polymer Sci, 2003, 29(9): 2713 - 2718.

[51] G.F. Bickerstaff, Genet. Engineeer Biotechnologist, 15 (1995) 13.

[52] O.R. Zaborsky, Immobilized Enzymes, 1973, CRC Press, Cleveland.

[53] S. Borgmann, G. Hartwich, A. Schulte, W. Schuhmann, Perspectives in Bioanalysis, 2005

[54] G. B. Broun, in Methods in Enzymology, K. Mosbach, ed.; Academic, New York, XLIV (1976) 263

[55] W.H. Scouten, J.H.T. Luong, R.S. Brown, Trends in Biotechnology, 1995, 13, 178.

[56] P. A. Srrere, K. Uyeda, Functional groups on enzymes suitable for bind-to matrices, in Methods in Enzymology, K. Mosbach, ed.; Academic, New York, XLIV (1976) 11

[57] N.C. Kekec, F. Ekiz Kanik, Y. Arslan Udum, C. Gundogdu Hizliates, Y. Ergun, L.Toppare, Sensor Actuat. B-Chem., 2014, 193, 306.

[58] H. Wang, H. Ohnuki, H. Endo, M. Izumi, Sensor Actuat. B-Chem., 2012, 168, 249.

[59] T. Ahuja, I.A. Mir, D. Kumar, Rajesh, Biomaterials, 2007, 28, 791

[60] a) C. W. Tang, S. A. VanSlyke, Applied Physics Letters, 1987, 51, 12, 913

b) M. S. White, M. Kaltenbrunner, E. D. Głowacki, K. Gutnichenko, G. Kettlgruber, I. Graz, S. Aazou, C. Ulbricht, D. A. M. Egbe, M. C. Miron, Z. Major, M. C. Scharber, T. Sekitani, T. Someya, S. Bauer, N. S. Sariciftci, “Ultrathin, highly flexible and stretchable PLEDs”, Nature Photonics, 2013, 7, 811-816

[61] L. Hung and C. Chen, “Recent progress of molecular organic electrolu- minescent materials and devices,” Materials Science and Engineering: R: Reports, 2002, 39, 5, 143–222

[62] M. M. Salleh, T. Hasnan, T. Azis, S. Sepeai, and M.Yahaya,“Fabrication of organic light emitting diodes (oleds) for flat panel displays,” Berkala Ilmiah MIPA, 17, 3, 2008

[63] B. Geffroy, P. le Roy, C. Prat, “Organic light-emitting diode (oled) technology: materials, devices and display technologies,” Polymer International, 2006, 55, 6, 572–582

[64] W. Brütting, J. Frischeisen, T. D. Schmidt, B. J. Scholz, C. Mayr, Phys. Status Solidi A, 2013, 210, 1, 44–65

[65] C. Winder, N. S. Sariciftci, Low bandgap polymers for photon harvesting in bulk heterojunction solar cells, J. Mater. Chem., 2004, 14, 1077–1086

[66] T. M. Clarke, J. R. Durrant, Chem. Rev. 2010, 110, 6736.

[67] G. Yu, J. Gao, J. C. Hummelen, F. Wudl, A. J. Heeger, Science, 1995, 270, 1789

[68] Y. M. Nam, J. Huh, W. H. Jo, Solar EnergyMaterials and Solar Cells, 2010, 94, 1118.

[69] C. J. Brabec, S. Gowrisanker, J. J. M. Halls, D. Laird, S. Jia, S. P. Williams, Adv. Mater. 2010, 22, 3839–3856

[70] R. Po, M. Maggini, N. Camoioni, J. Phys. Chem. C., 2010, 114, 695.

[71] M. Theander, A. Yartsev, D. Zigmantas, V. Sundstroem, W. Manno, M. R. Andersson and O. Inganaes, Phys. Rev. B, 2000, 61, 12957

[72] G. Greczynski, Th. Kugler, M. Keil, W. Osikowicz, M. Fahlman and W. R. Salanck, J. Electron Spectrosc. Relat. Phenom., 2001, 121, 1.

[73] J. S. Kim, M. Granstrom, R. H. Friend, N. Johansson, W. R. Salaneck, R. Daik, W. J. Feast and F. Cacialli, J. Appl. Phys., 1998, 84, 6859

[74] P. M. Beaujuge, J. R. Reynolds, Chem. Rev., 2010, 110, 268–320

[75] Simge doktora tez

[76] G. Sonmez, C. K. F. Shen, Y. Rubin, F. Wudl, Angew. Chem. Int. Ed. 43 (2004)1498

[77] B. C. Thompson, P. Schottland, K. Zong, J. R. Reynolds Chem. Mater. 2000, 12 (2000) 1563.

[78] P. Ding, C. Zhong, Y. Zou, C. Pan, H. Wu, Y. Cao, 5,6-Bis(decyloxy)-2,1,3-benzooxadiazole-Based Polymers with Different Electron Donors for Bulk-Heterojunction Solar Cells, J. Phys. Chem. C, 115, (2011), 16211

[79] J. M. Jiang, P. A. Yang, T. H. Hsieh, K. H. Wei, Crystalline Low-Band Gap Polymers Comprising Thiophene and 2,1,3-Benzooxadiazole Units for Bulk Heterojunction Solar Cells, Macromolecules, 44, (2011), 9155

[80] J. Bouffard, T. M. Swager, Fluorescent Conjugated Polymers That Incorporate Substituted 2,1,3-Benzooxadiazole and 2,1,3-Benzothiadiazole Units, Macromolecules, 41, (2008), 5559

[81] S. Goker, G. Hizalan, Y. Udum and L. Toppare, Electrochemical and optical properties of 5,6-bis(octyloxy)-2,1,3 benzooxadiazole containing low band gap polymers, Synthetic Metals, 191, (2014), 19

APPENDICES

A. NMR Spectra of Synthesized Monomers

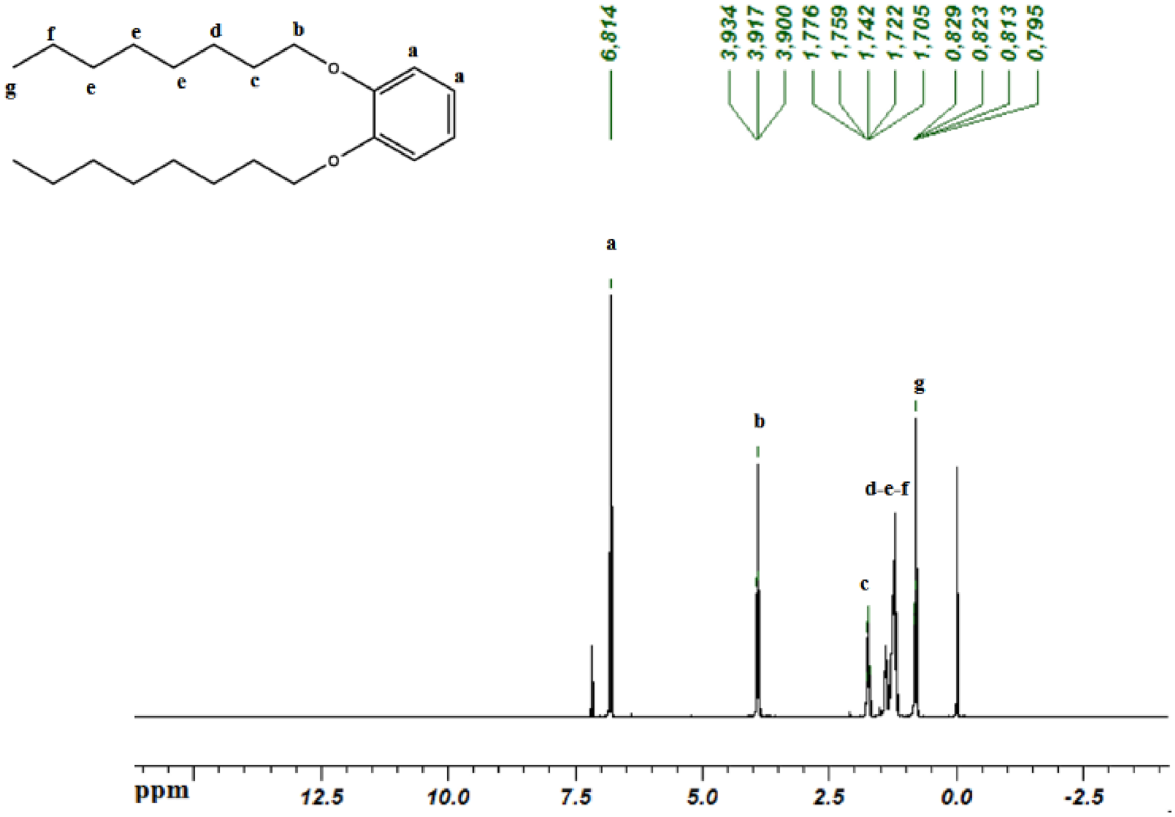

Figure A.1: ^{1}H-NMR spectrum of 1,2-bis(octyloxy)benzene

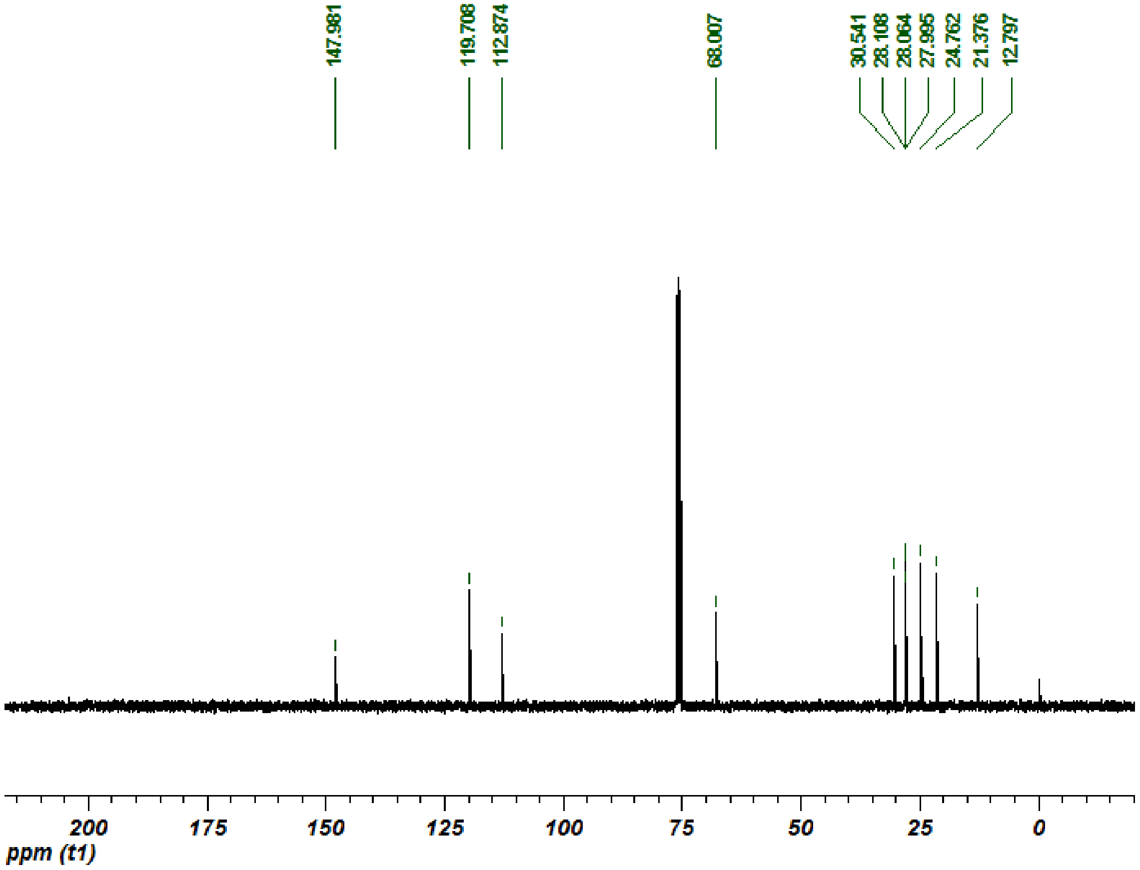

Figure A.2: ^{13}C-NMR spectrum of 1,2-bis(octyloxy)benzene

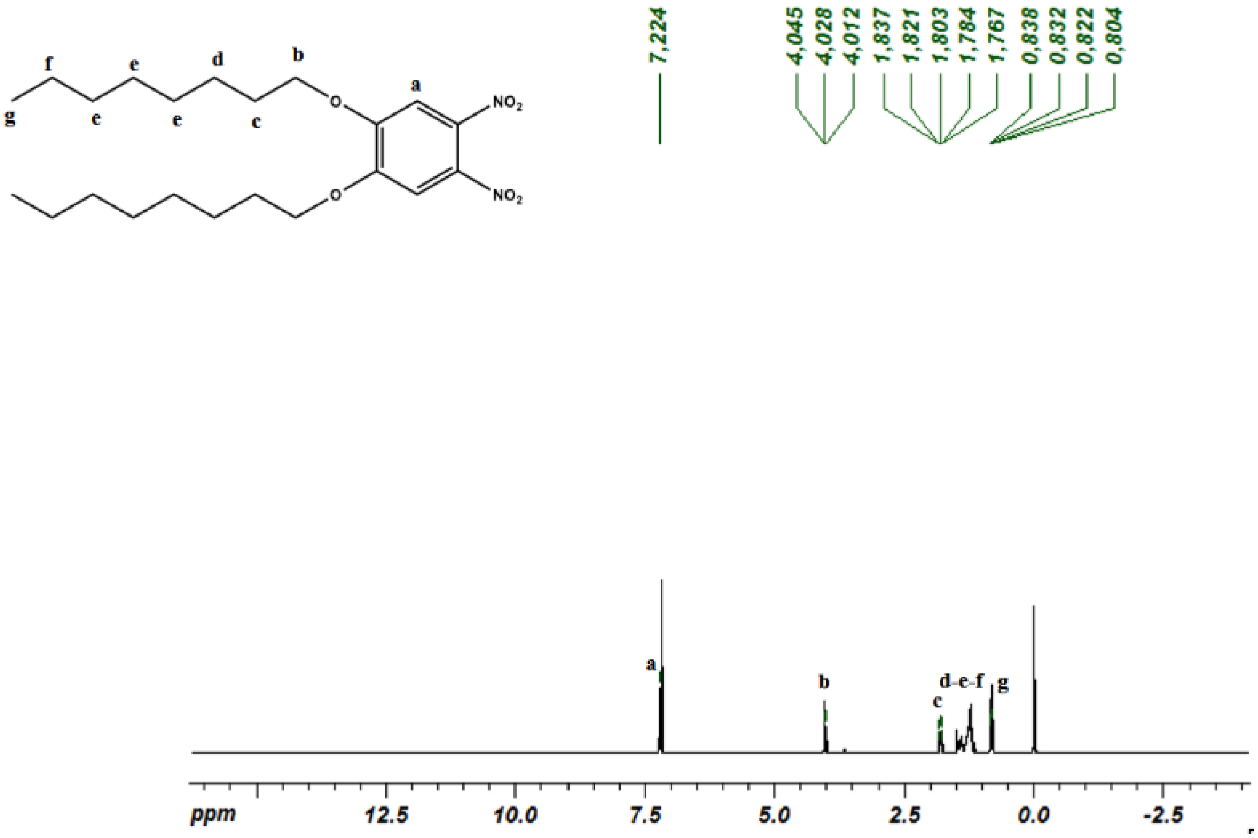

Figure A.3: ^{1}H-NMR spectrum of 1,2-dinitro-4,5-bis(octyloxy)benzene

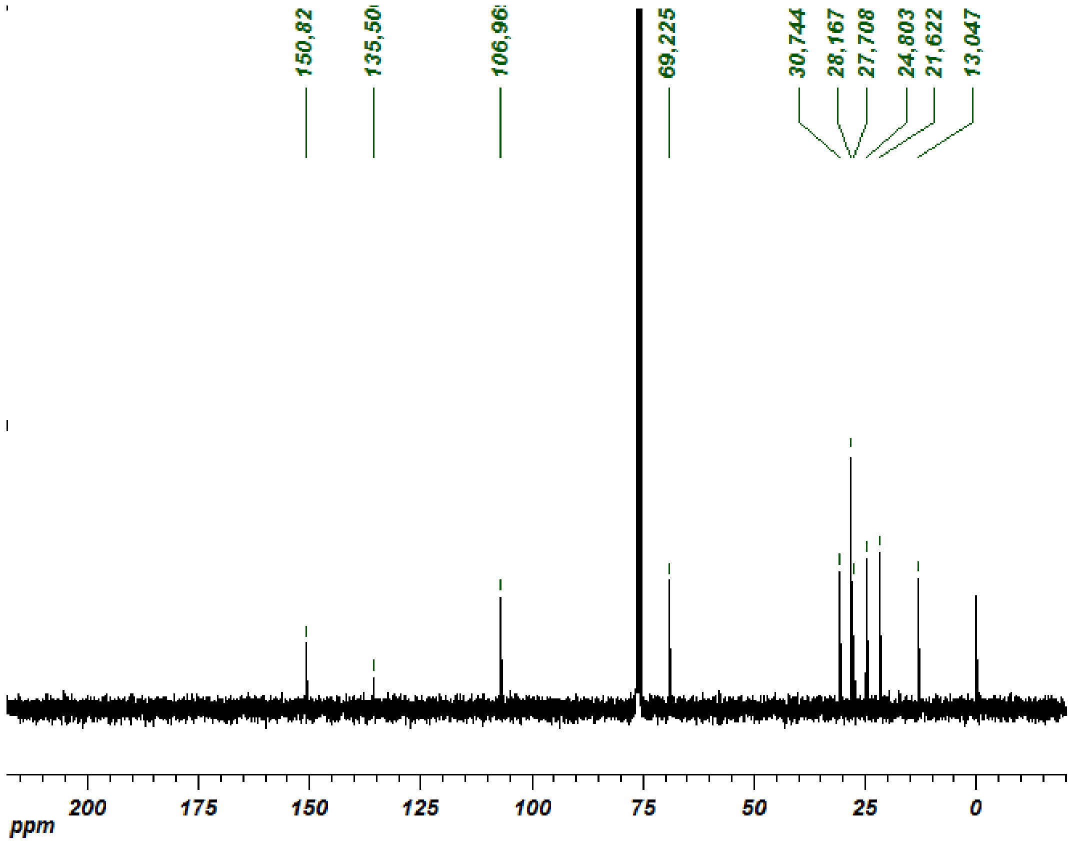

Figure A.4: ^{13}C-NMR spectrum of 1,2-dinitro-4,5-bis(octyloxy)benzene

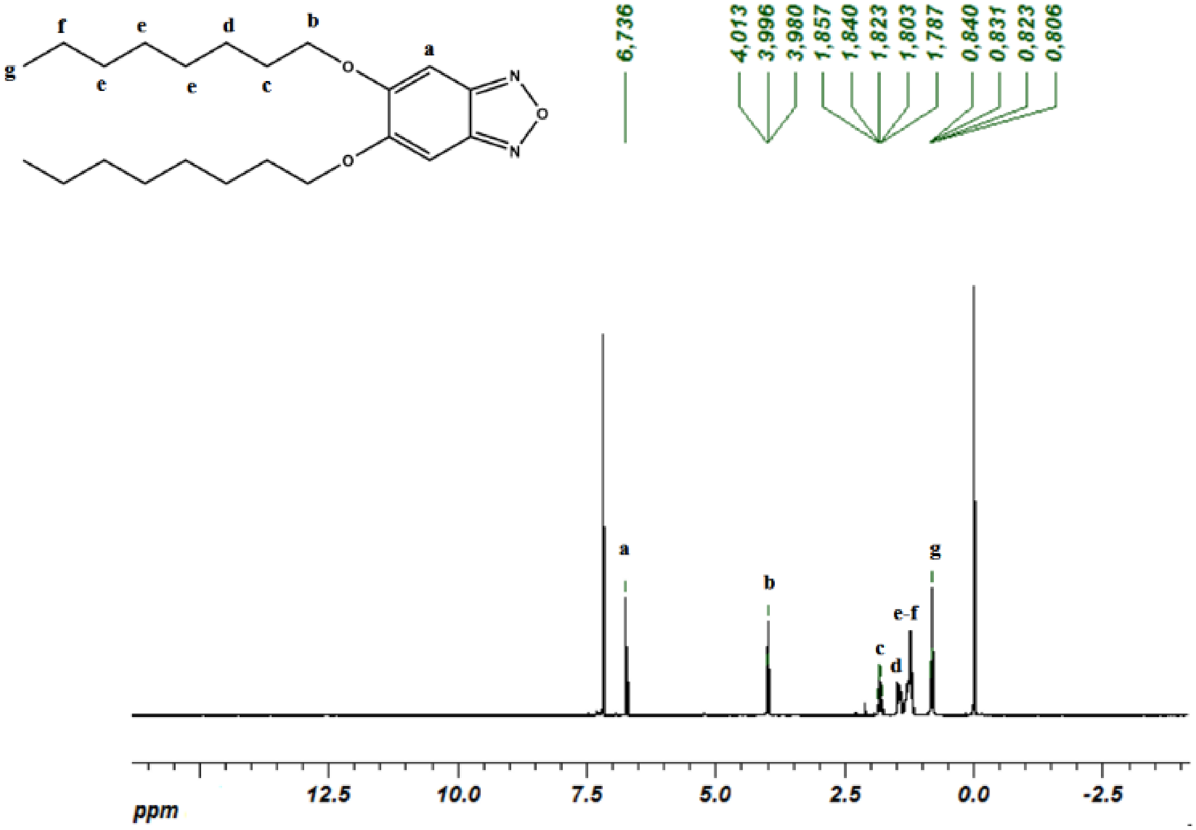

Figure A.5: ^{1}H-NMR spectrum of 5,6-bis(octyloxy)benzo[c][1,2,5]oxadiazole

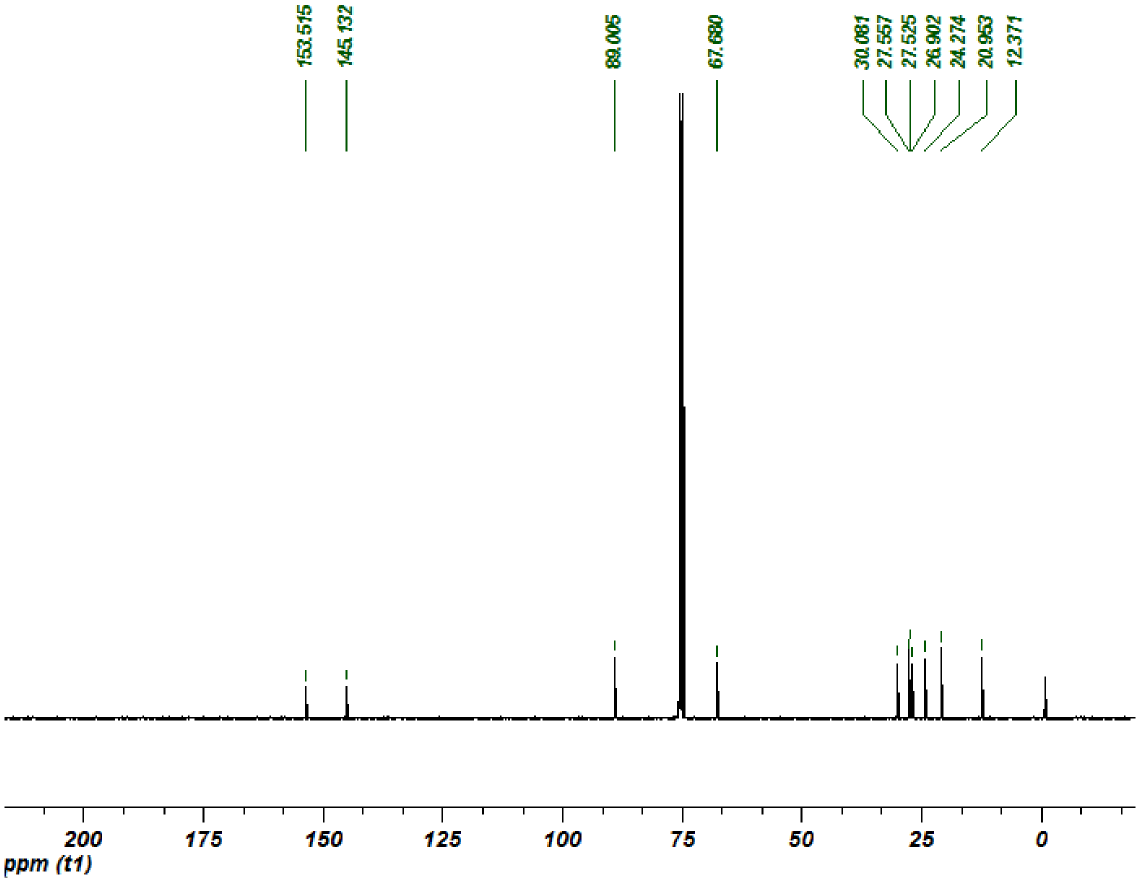

Figure A.6: ^{13}C-NMR spectrum of 5,6-bis(octyloxy)benzo[c][1,2,5]oxadiazole

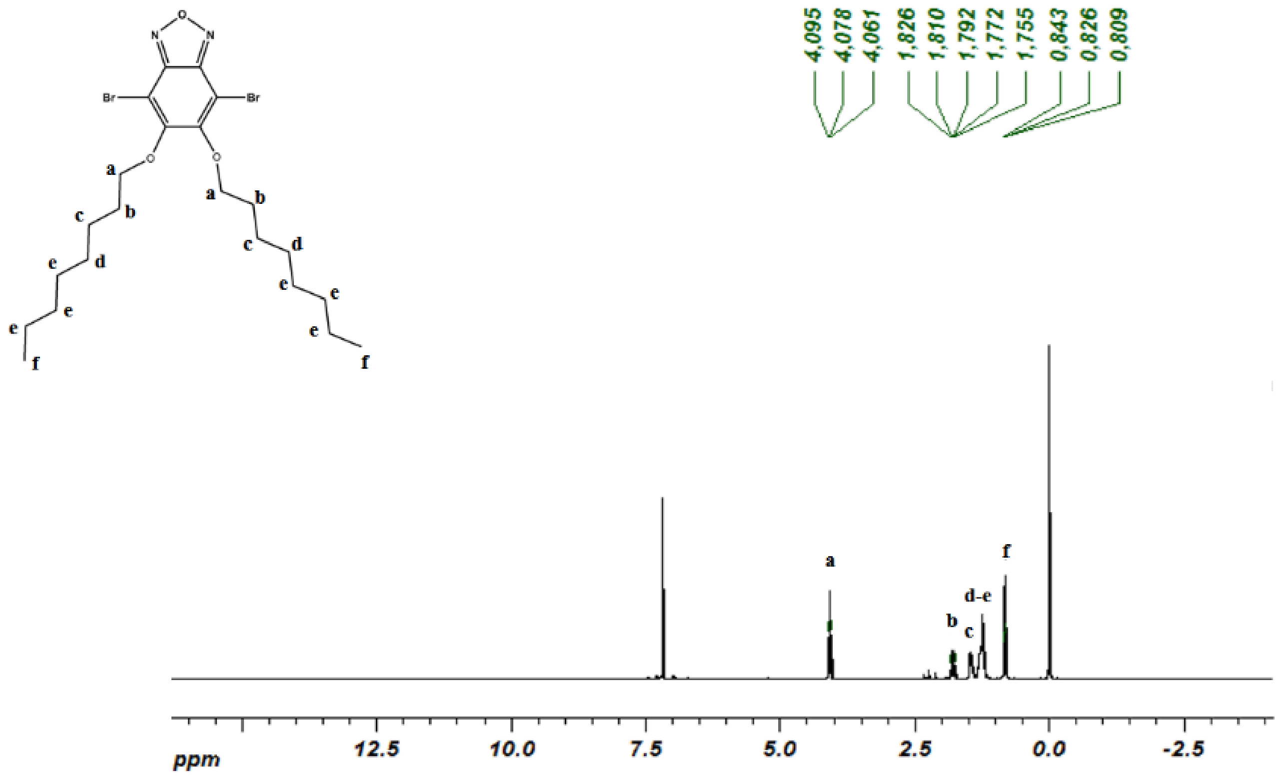

Figure A.7: ^{1}H-NMR spectrum of 4,7-dibromo-5,6-bis(octyloxy)benzo[c][1,2,5]oxadiazole

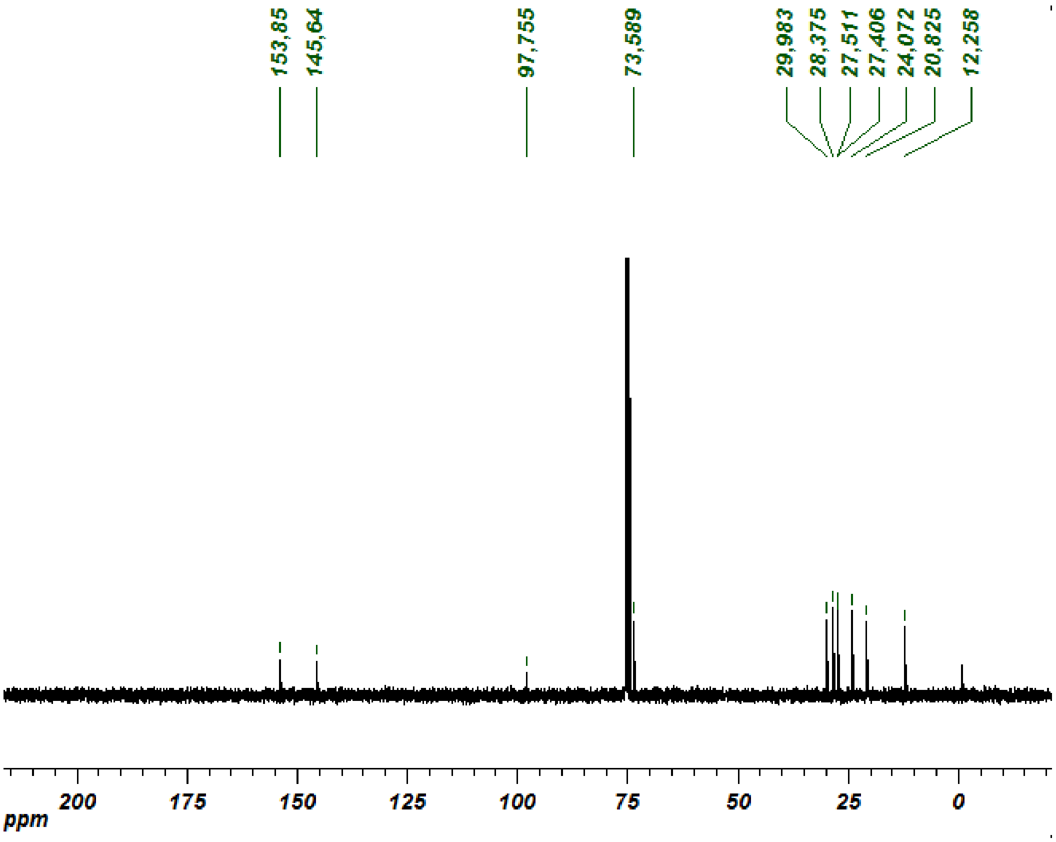

Figure A.8: ^{13}C-NMR spectrum of 4,7-dibromo-5,6-bis(octyloxy)benzo[c][1,2,5]oxadiazole

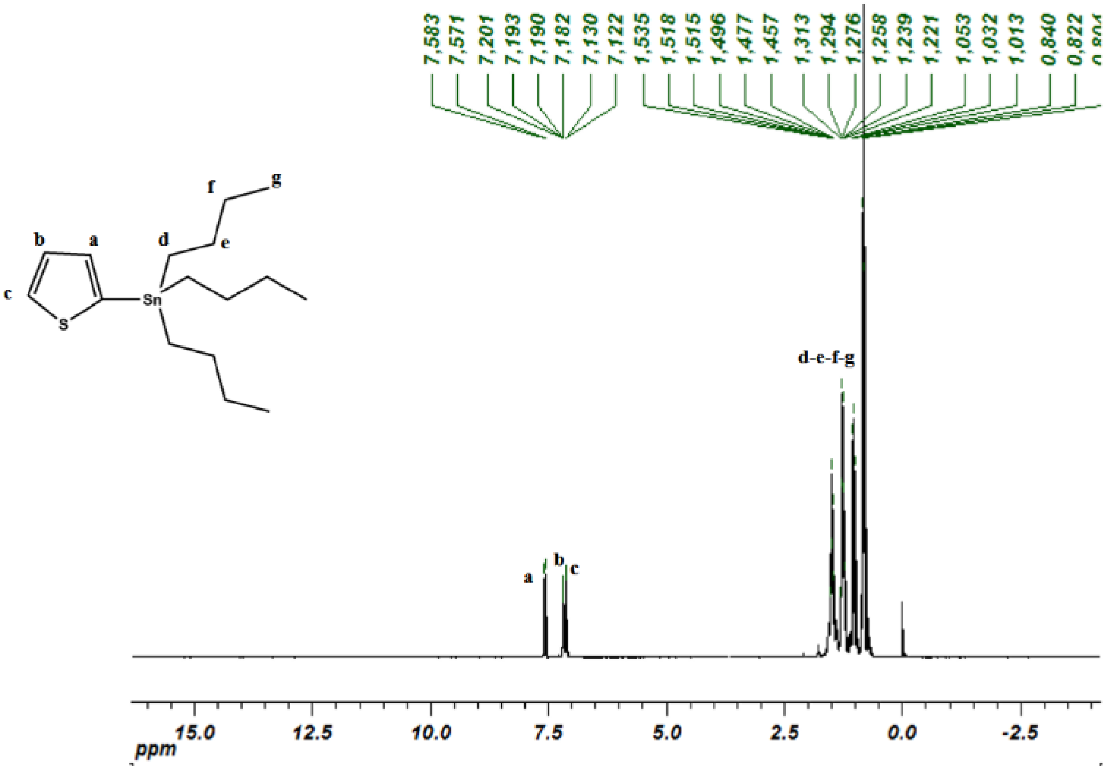

Figure A.9: ^{1}H-NMR spectrum of tributyl(thiophen-2-yl)stannane

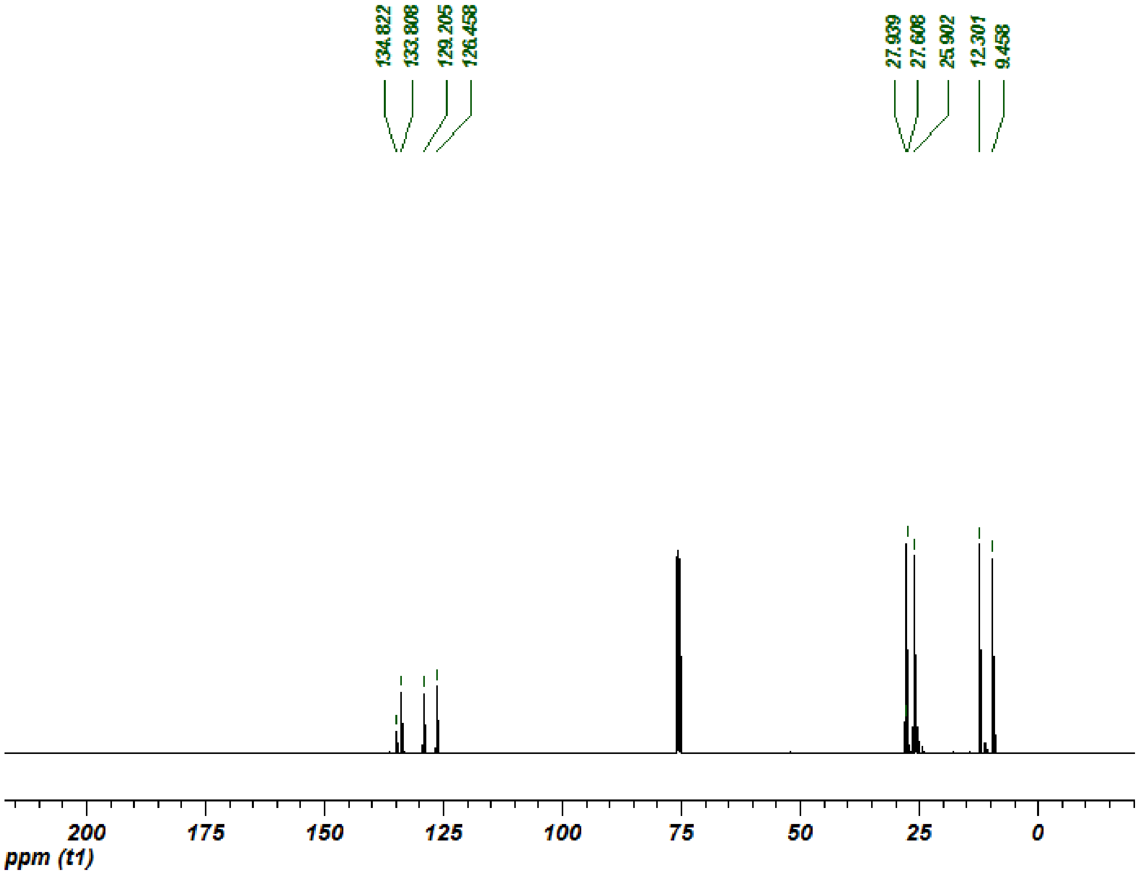

Figure A.10: ^{13}C-NMR spectrum of tributyl(thiophen-2-yl)stannane

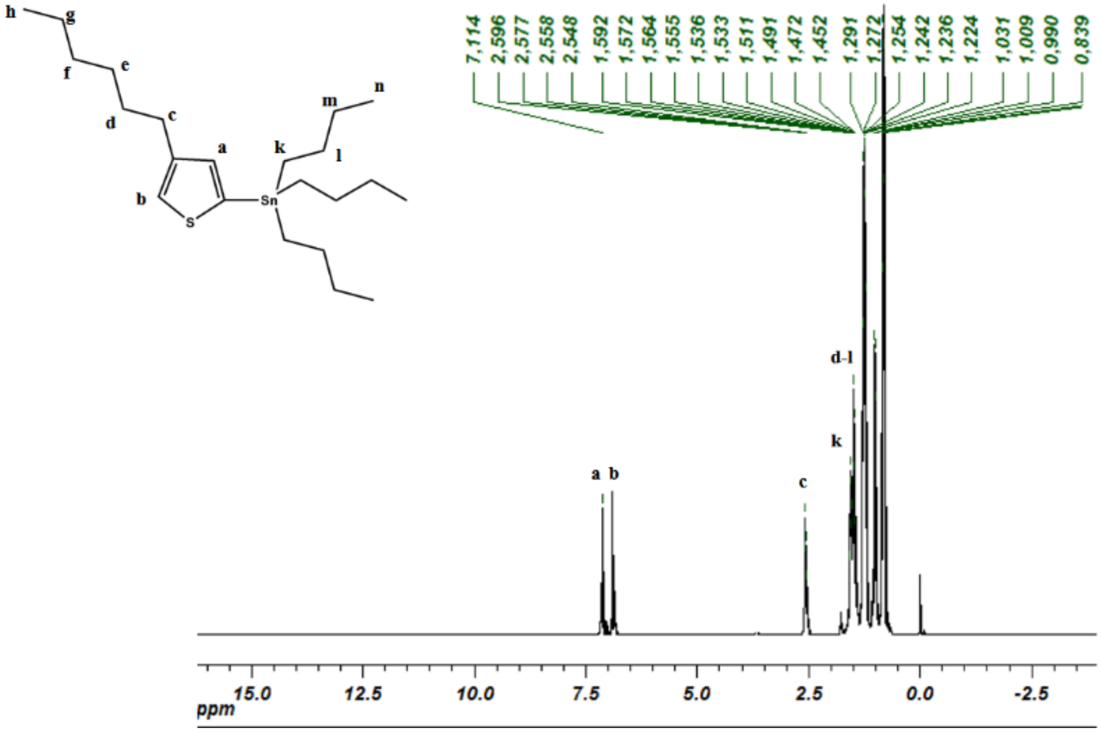

Figure A.11: ^{1}H-NMR spectrum of tributyl (4-hexylthiophen-2-yl) stannane

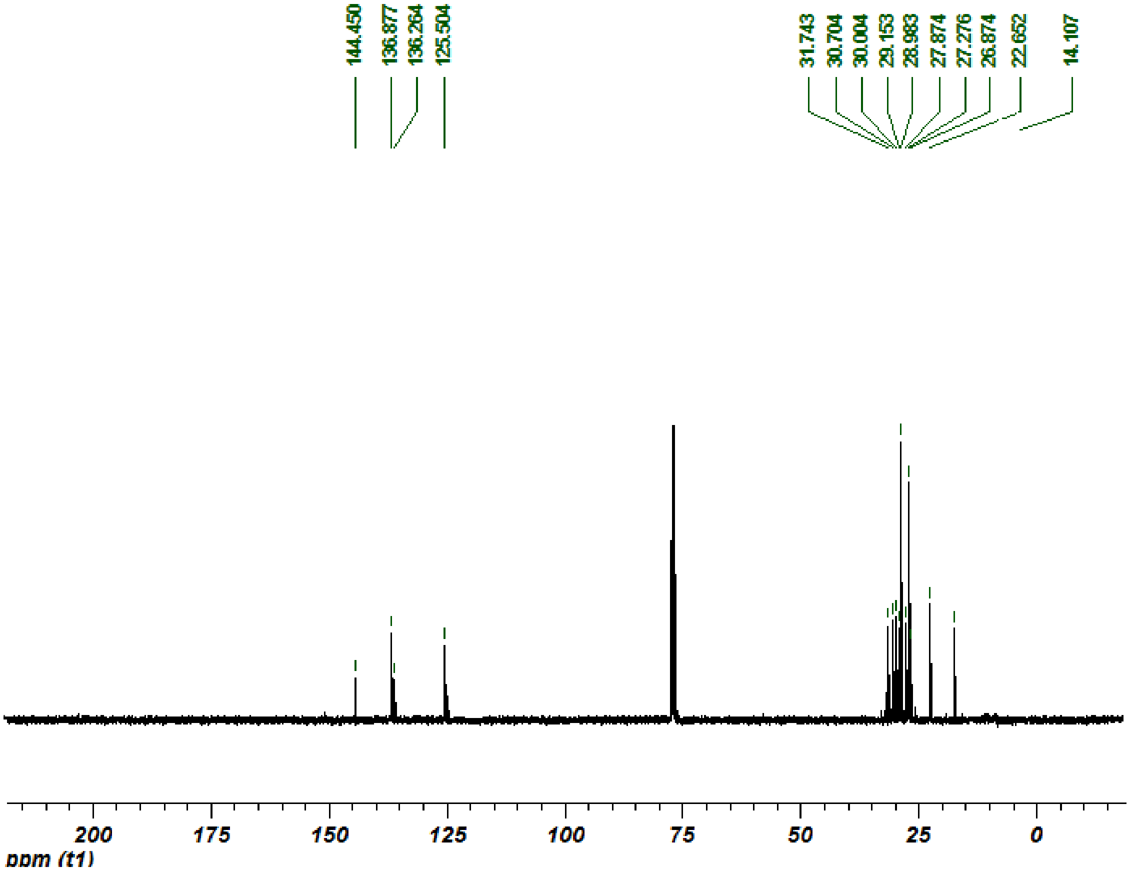

Figure A.12: ^{13}C-NMR spectrum of tributyl (4-hexylthiophen-2-yl) stannane

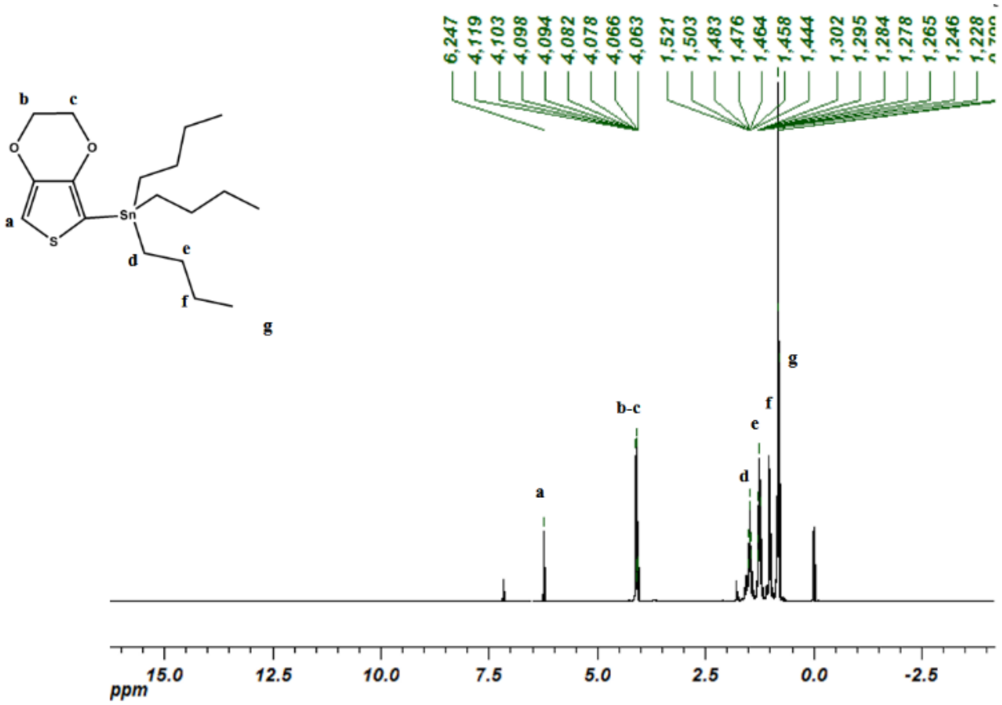

Figure A.13: ^{1}H-NMR spectrum of tributyl (2,3-dihydrothieno[3,4-b][1,4]dioxin-5-yl) stannane

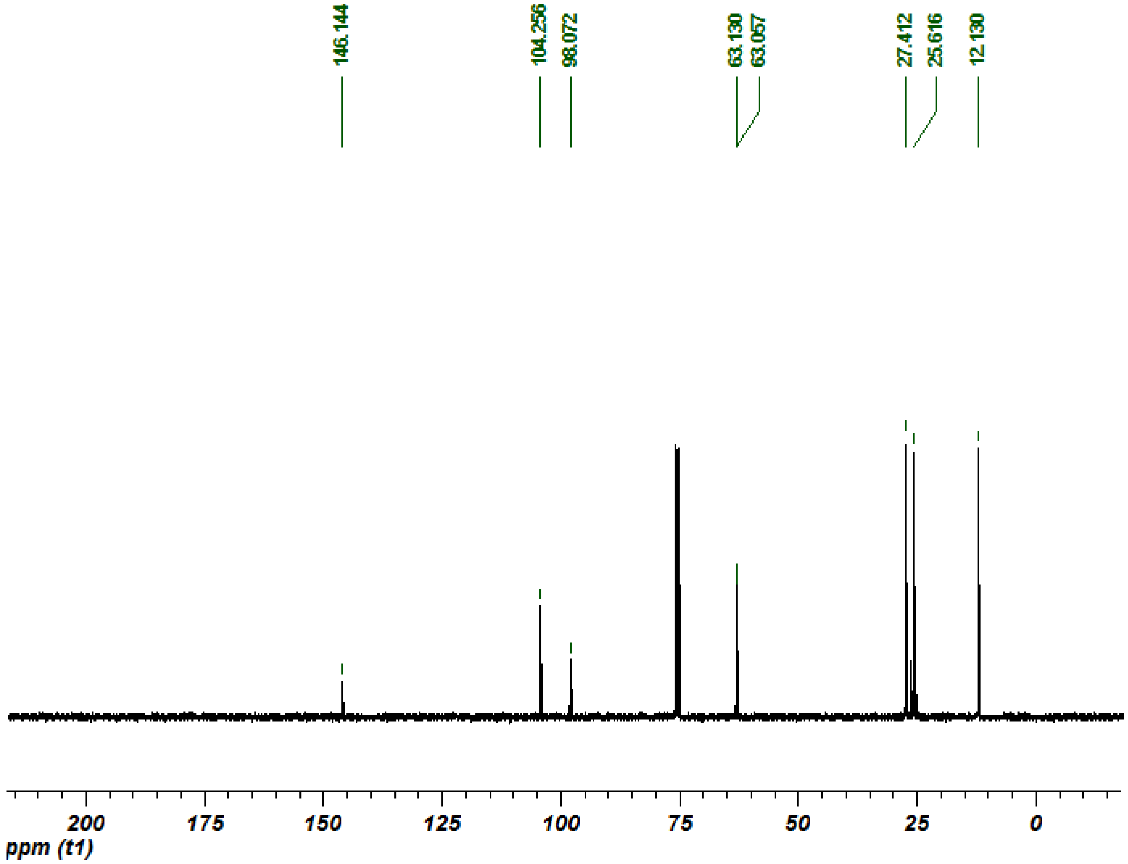

Figure A.14: ^{13}C-NMR spectrum of tributyl (2,3-dihydrothieno[3,4-b][1,4]dioxin-5-yl) stannane

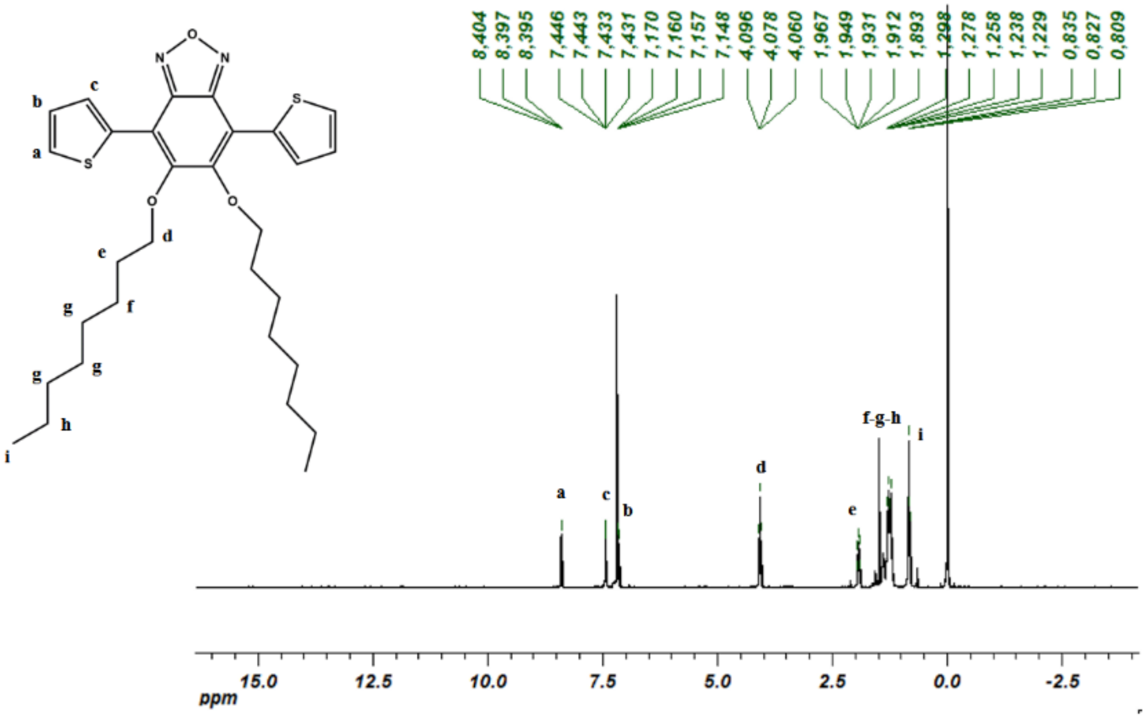

Figure A.15: ^{1}H-NMR spectrum of 5,6-bis(octyloxy)-4,7-di(thiophen-2-yl)benzo[c][1,2,5]oxadiazole

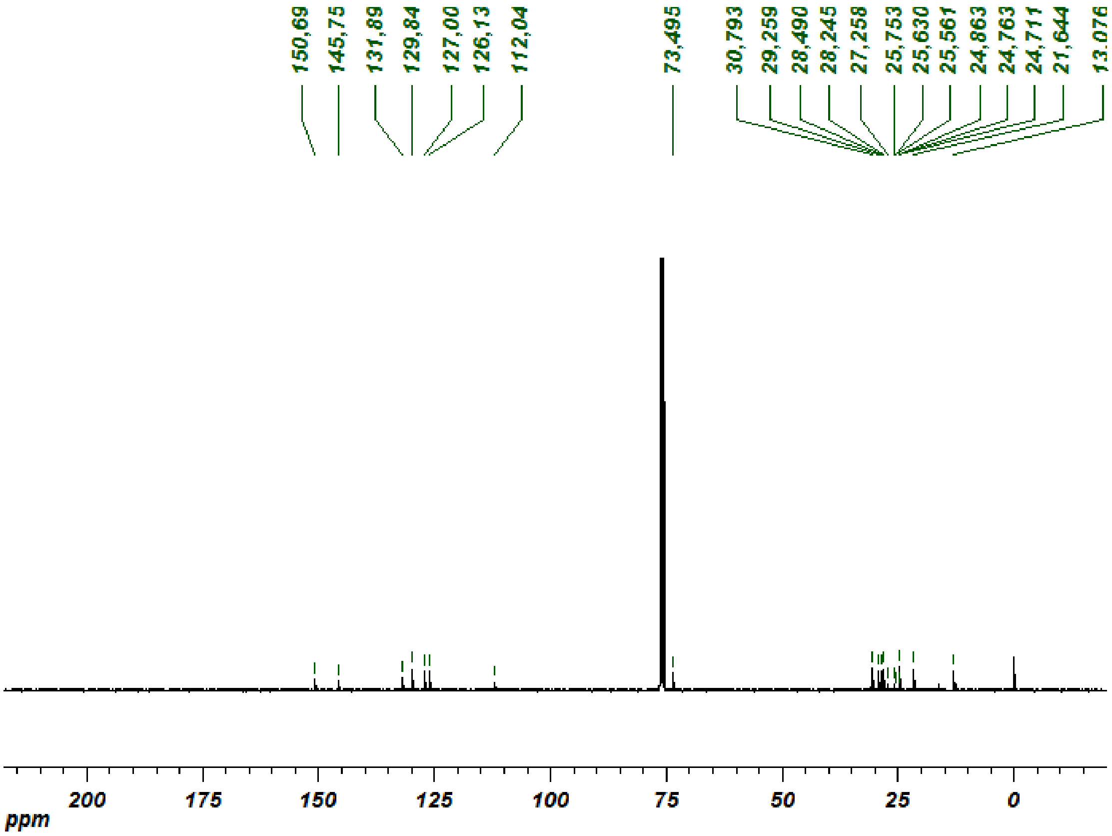

Figure A.16: ^{13}C-NMR spectrum of 5,6-bis(octyloxy)-4,7-di(thiophen-2-yl)benzo[c][1,2,5]oxadiazole

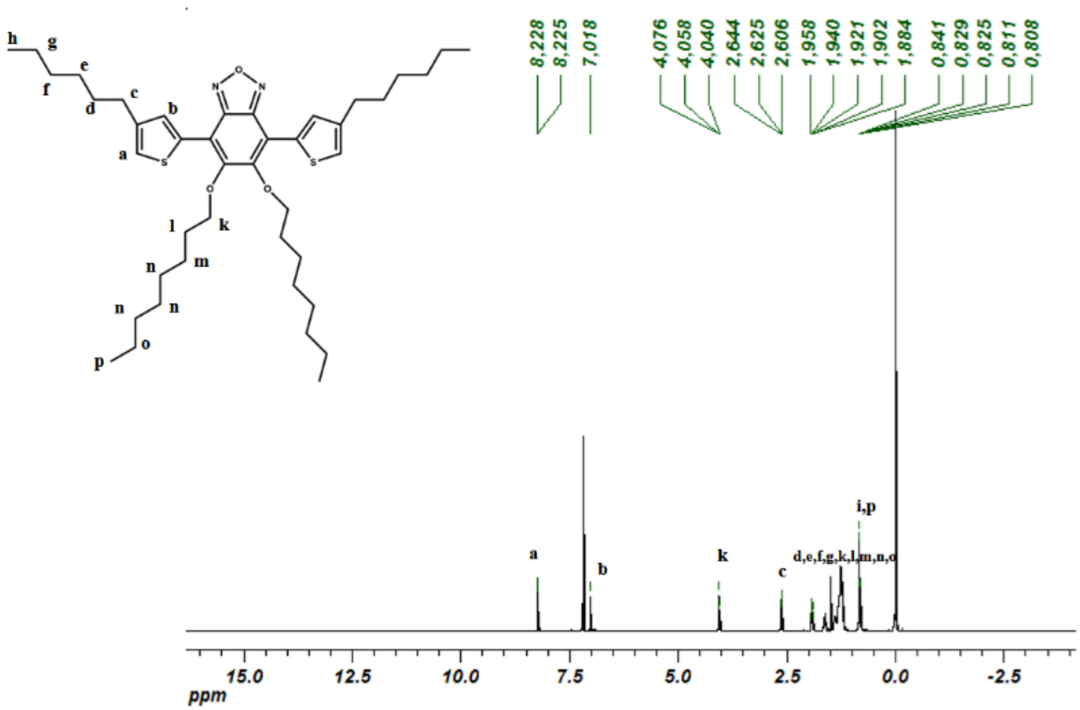

Figure A.17: ^{1}H-NMR spectrum of 4,7-Bis(4-hexylthiophen-2-yl)-5,6-bis(octyloxy)benzo[c][1,2,5]oxadiazole

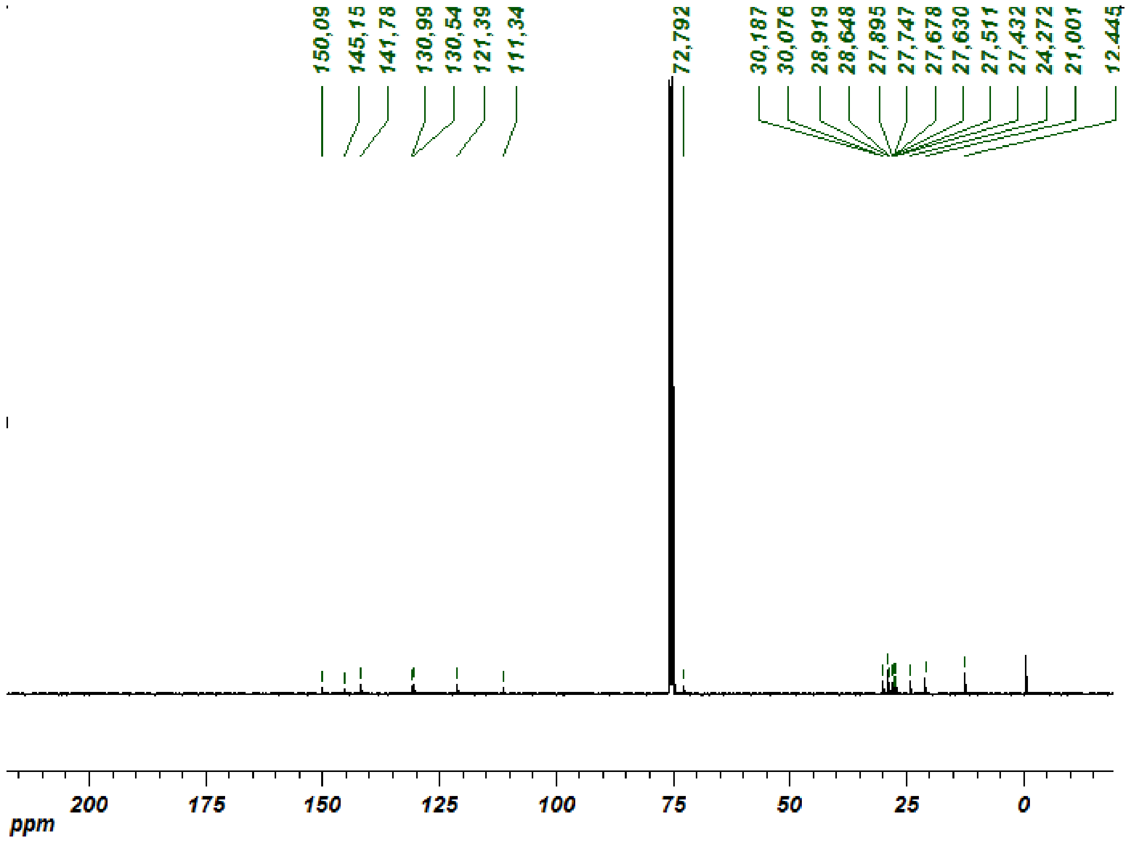

Figure A.18: ^{13}C-NMR spectrum of 4,7-Bis(4-hexylthiophen-2-yl)-5,6-bis(octyloxy)benzo[c][1,2,5]oxadiazole

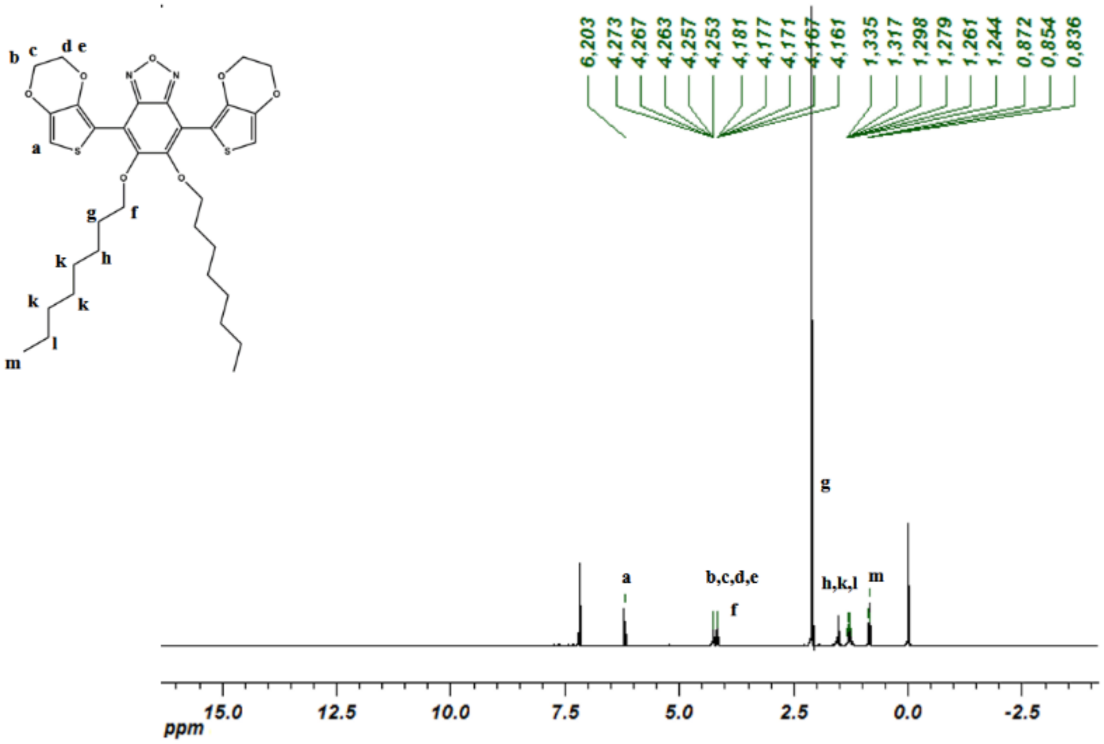

Figure A.19: ^{1}H-NMR spectrum of 4,7-bis(2,3-dihydrothieno[3,4-b][1,4]dioxin-5-yl)-5,6-bis(octyloxy)benzo[c][1,2,5]oxadiazole

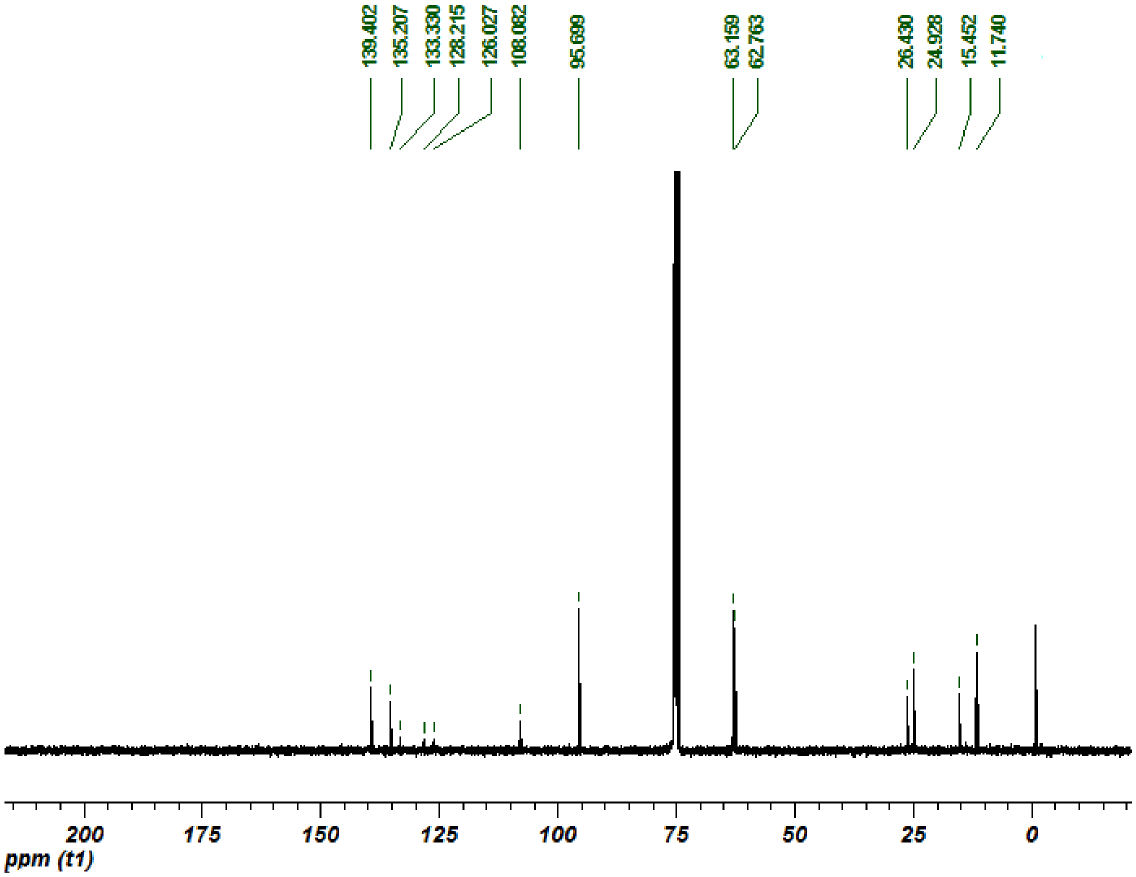

Figure A.20: ^{13}C-NMR spectrum of 4,7-bis(2,3-dihydrothieno[3,4-b][1,4]dioxin-5-yl)-5,6-bis(octyloxy)benzo[c][1,2,5]oxadiazole

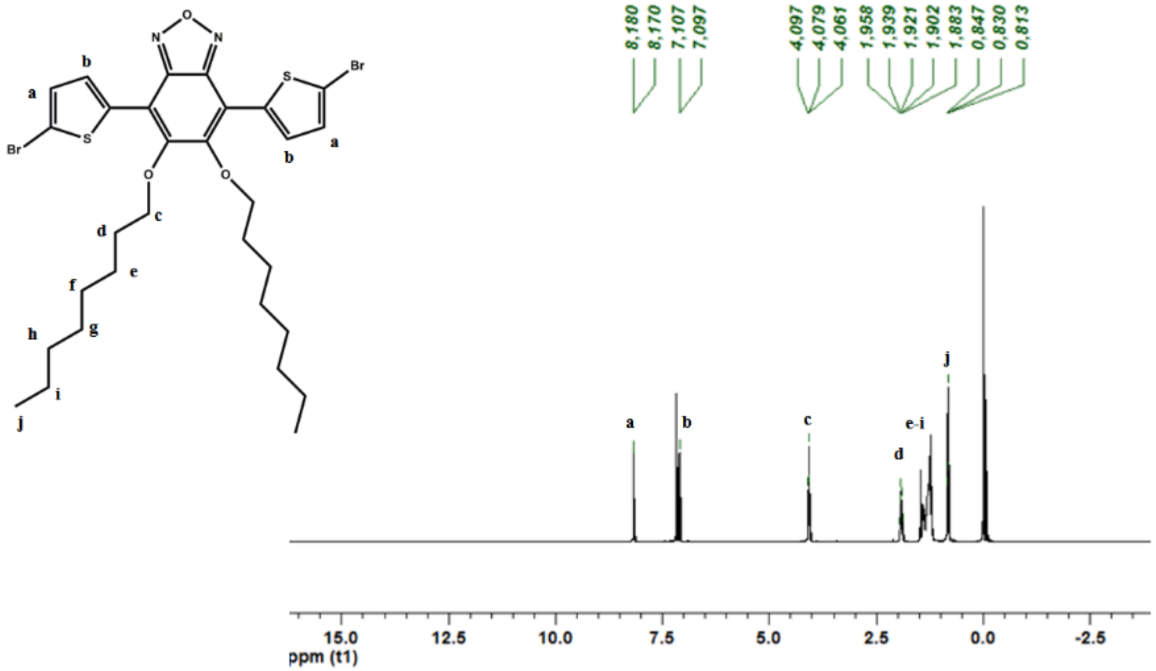

Figure A.21: ^{1}H-NMR spectrum of 4,7-bis(5-bromothiophen-2-yl)-5,6-bis(octyloxy)benzo[c][1,2,5]oxadiazole

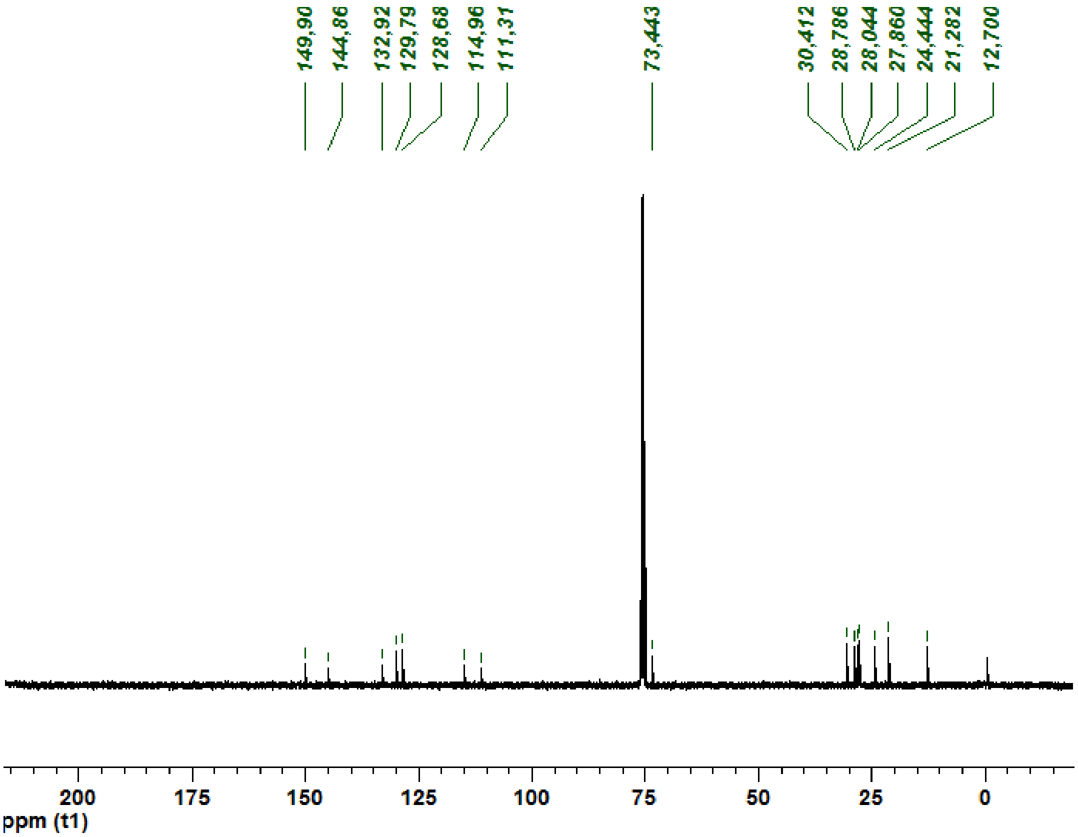

Figure A.22: ^{13}C-NMR spectrum of 4,7-bis(5-bromothiophen-2-yl)-5,6-bis(octyloxy)benzo[c][1,2,5]oxadiazole

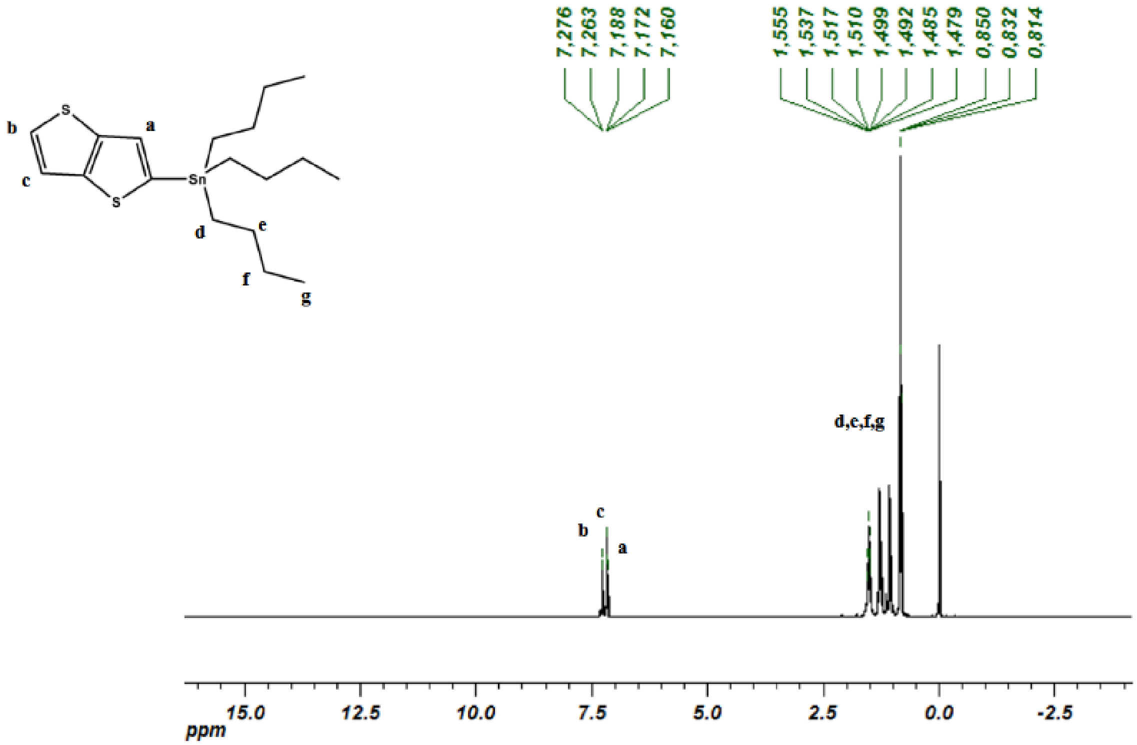

Figure A.23: ^{1}H-NMR spectrum of tributyl(thieno[3,2-b]thiophen-2-yl)stannane

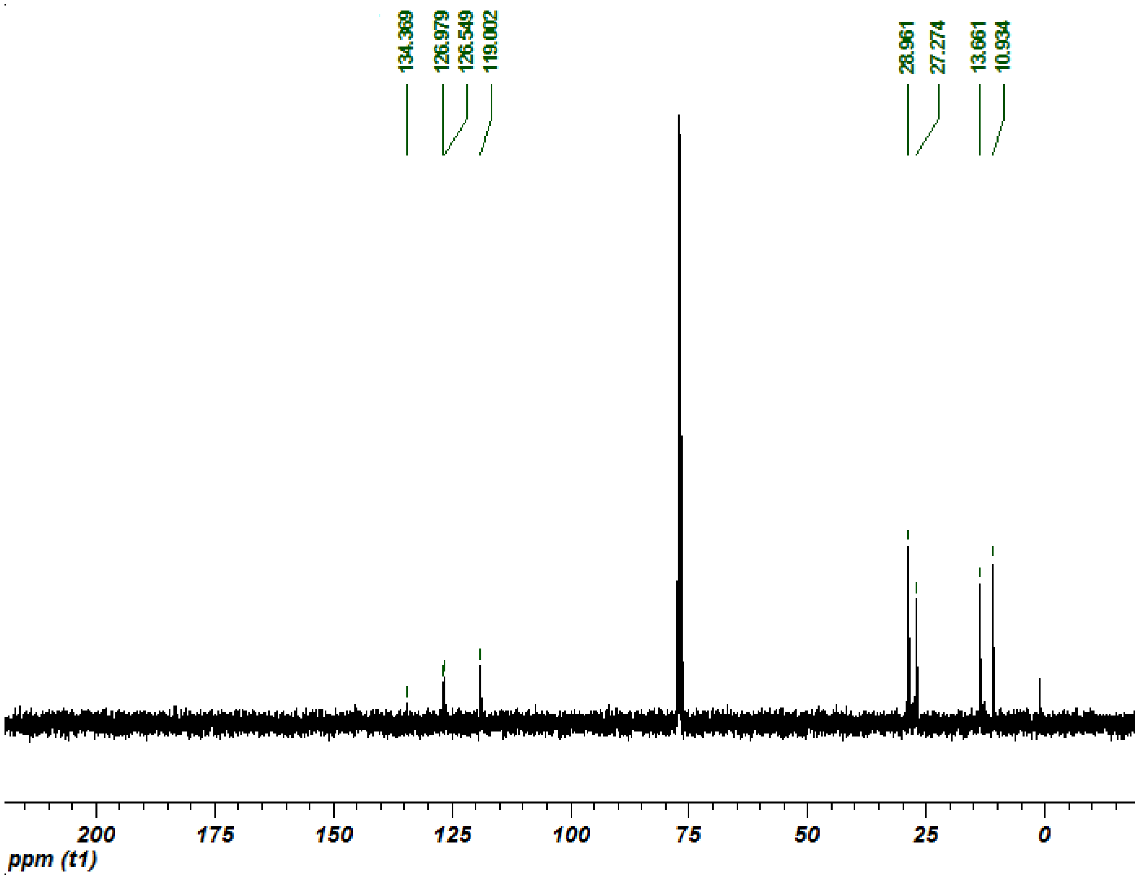

Figure A.24: ^{13}C-NMR spectrum of tributyl(thieno[3,2-b]thiophen-2-yl)stannane

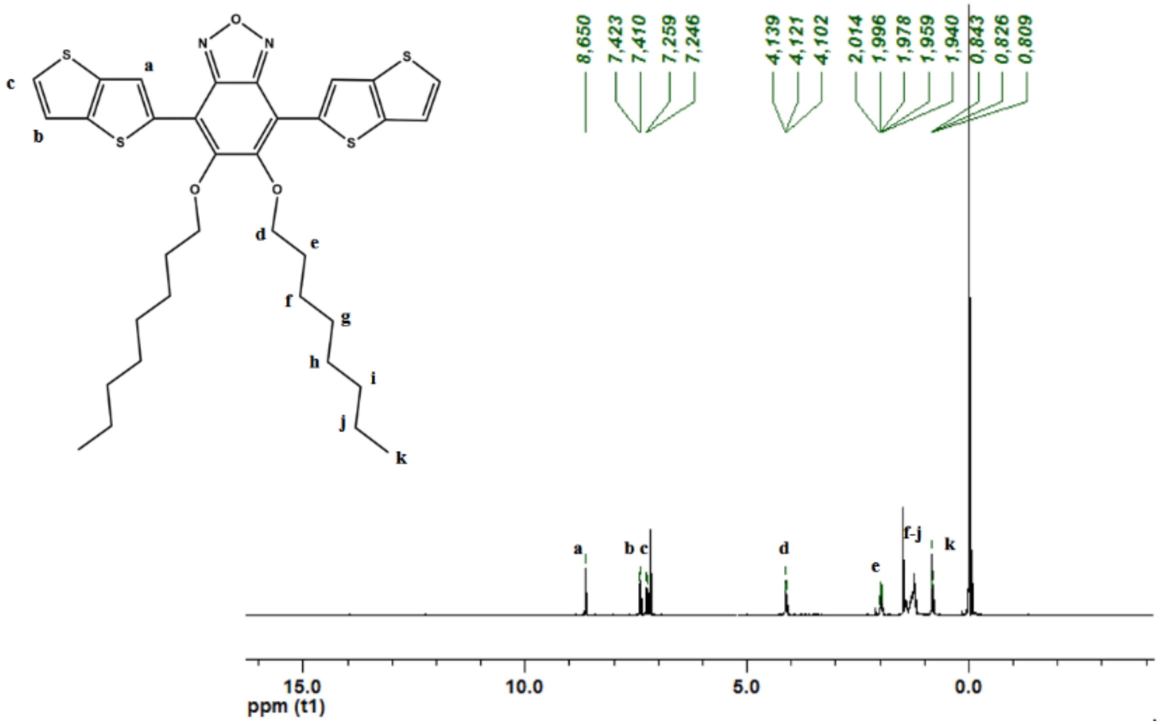

Figure A.25: ^{1}H-NMR spectrum of 5,6-bis(octyloxy)-4,7-di(thieno[3,2-b]thiophen-2-yl)benzo[c][1,2,5]oxadiazole

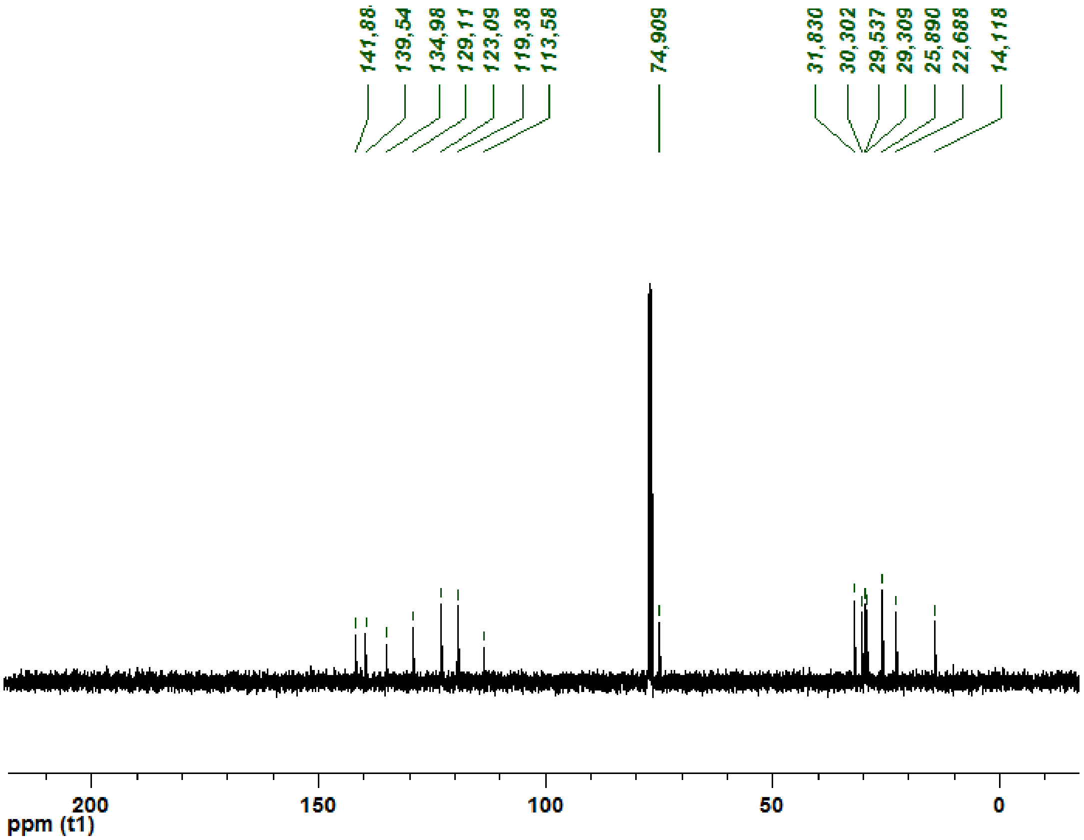

Figure A.26: ^{13}C-NMR spectrum of 5,6-bis(octyloxy)-4,7-di(thieno[3,2-b]thiophen-2-yl)benzo[c][1,2,5]oxadiazole

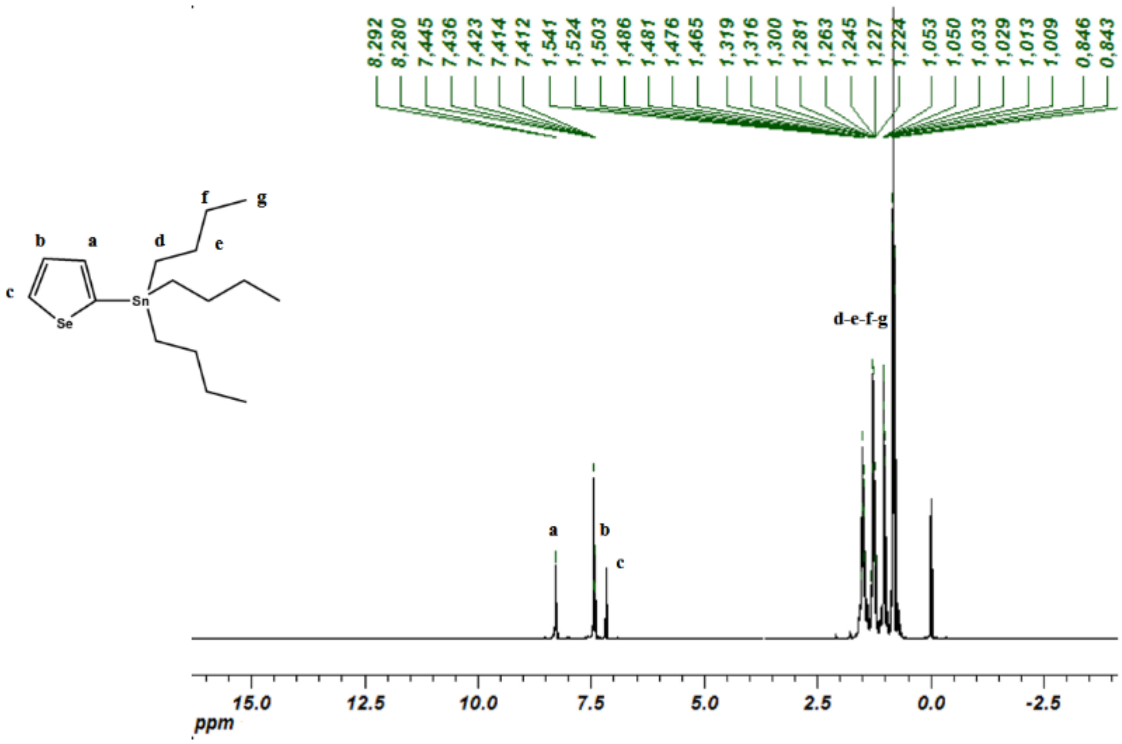

Figure A.27: ^{1}H-NMR spectrum of tributyl(selenophen-2-yl)stannane

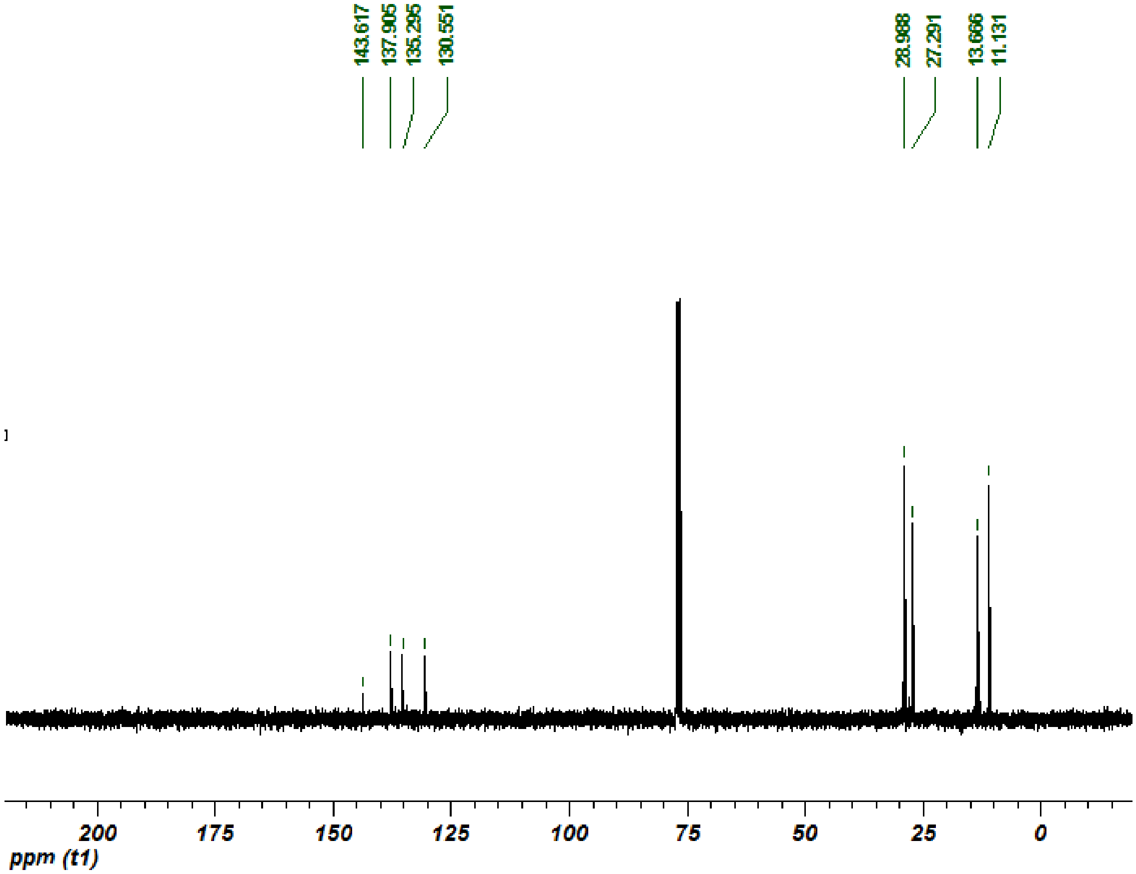

Figure A.28: ^{13}C-NMR spectrum of tributyl(selenophen-2-yl)stannane

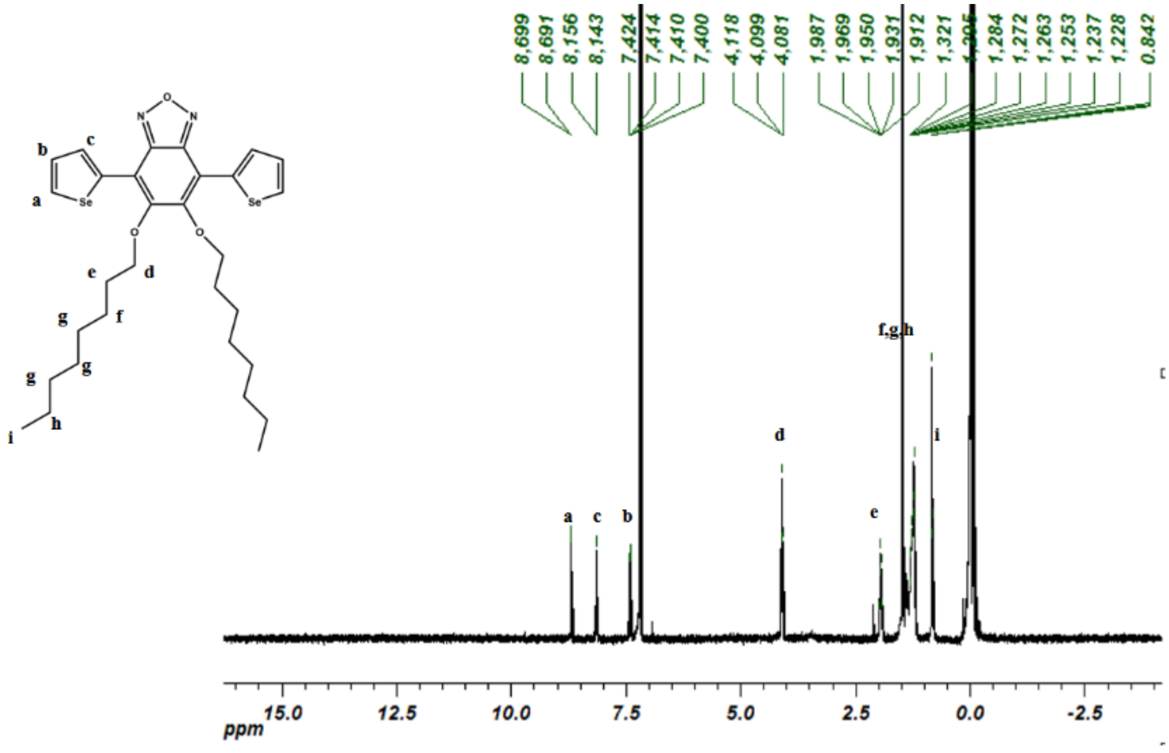

Figure A.29: ^{1}H-NMR spectrum of 5,6-bis(octyloxy)-4,7-di(selenophen-2-yl)benzo[c][1,2,5]oxadiazole

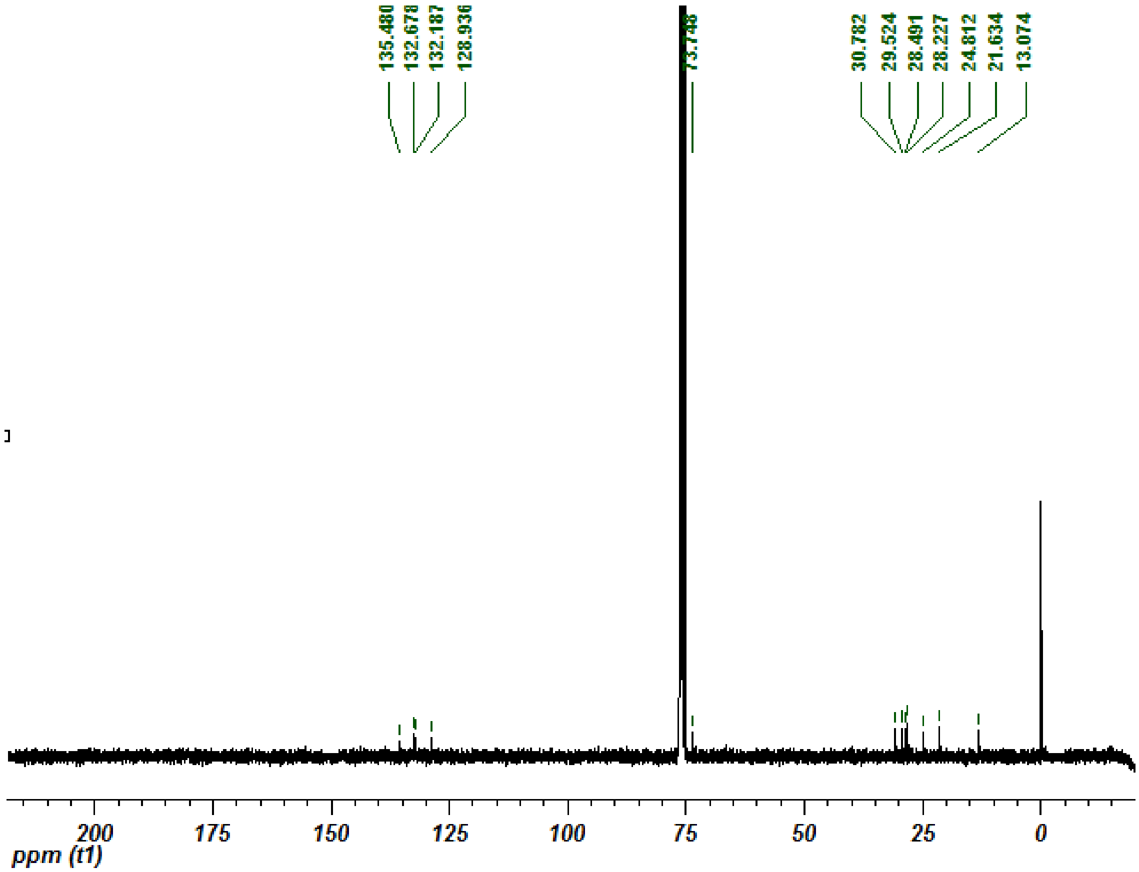

Figure A.30: ^{13}C-NMR spectrum of 5,6-bis(octyloxy)-4,7-di(selenophen-2-yl)benzo[c][1,2,5]oxadiazole

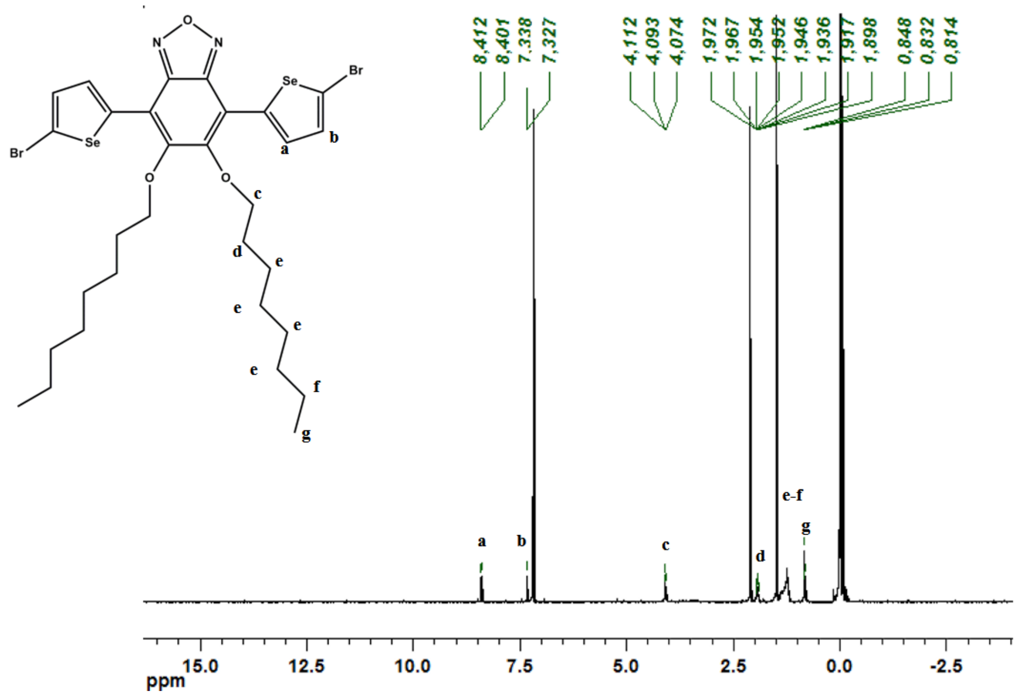

Figure A.31: ^{1}H-NMR spectrum of 4,7-bis(5-bromoselenophen-2-yl)-5,6-bis(octyloxy)benzo[c][1,2,5]oxadiazole

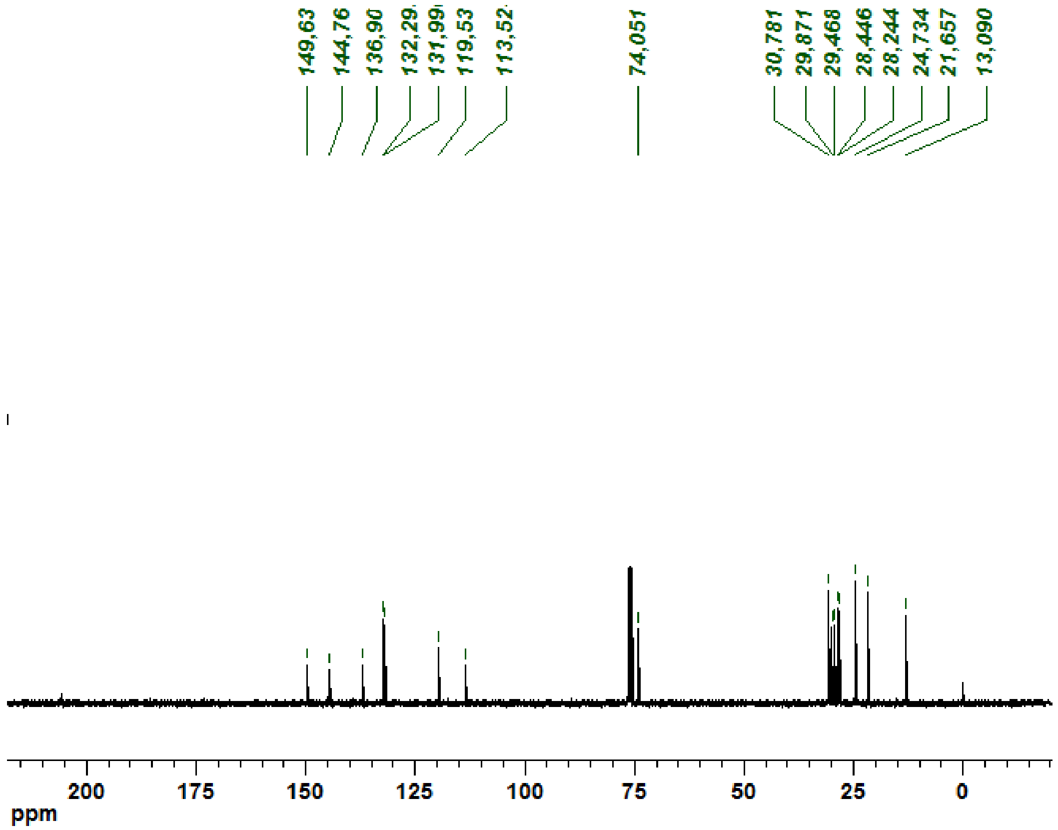

Figure A.32: ^{13}C-NMR spectrum of 4,7-bis(5-bromoselenophen-2-yl)-5,6-bis(octyloxy)benzo[c][1,2,5]oxadiazole

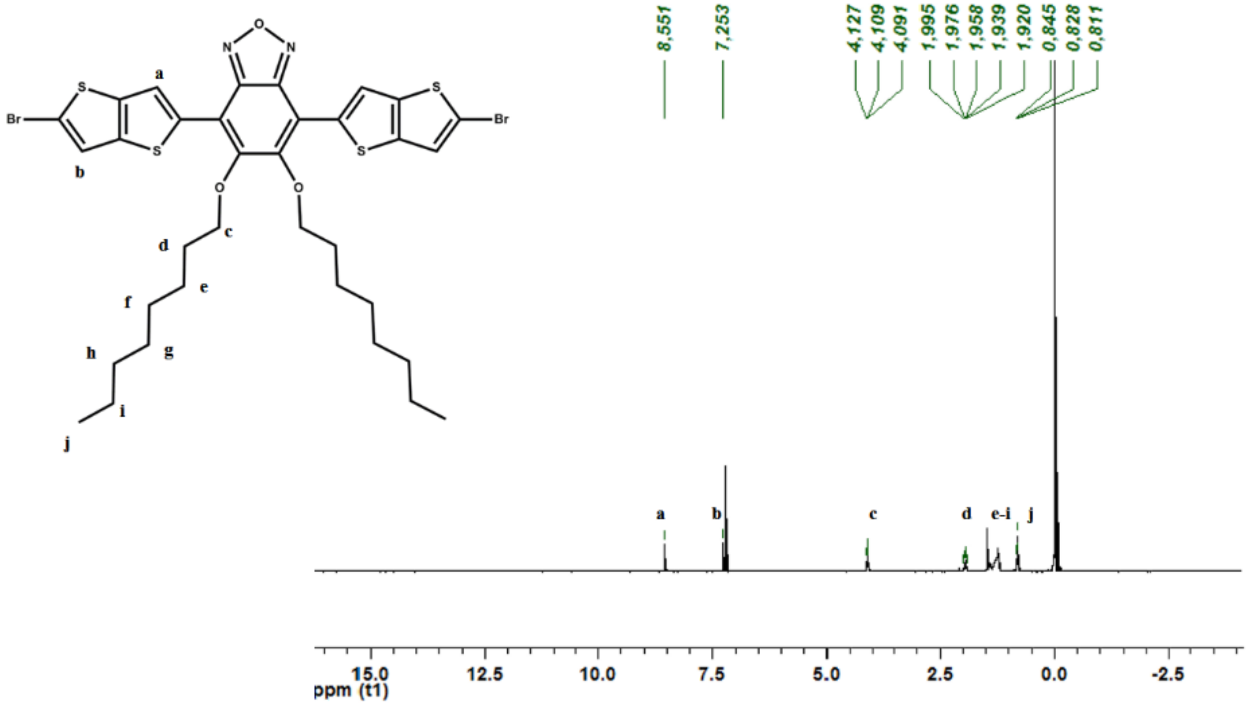

Figure A.33: ^{1}H-NMR spectrum of 4,7-bis(5-bromothieno[3,2-b]thiophen-2-yl)-5,6-bis(octyloxy)benzo[c][1,2,5]oxadiazole

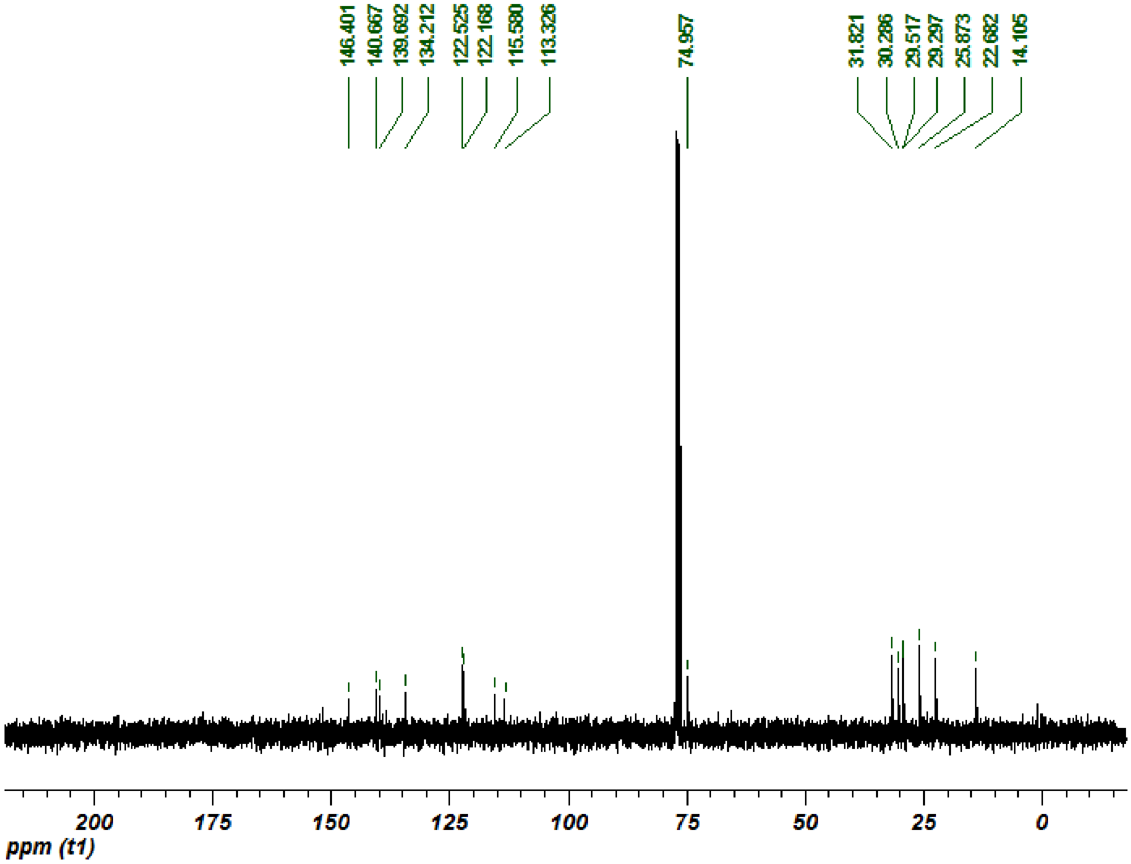

Figure A.34: ^{13}C-NMR spectrum of 4,7-bis(5-bromothieno[3,2-b]thiophen-2-yl)-5,6-bis(octyloxy)benzo[c][1,2,5]oxadiazole

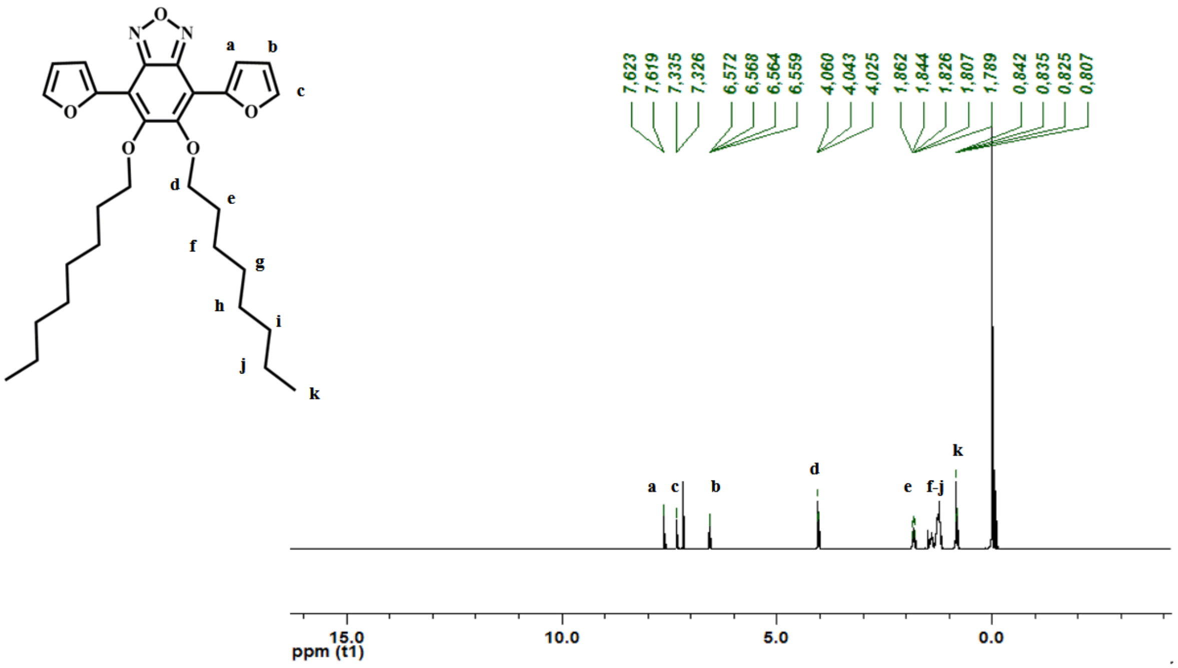

Figure A.35: ^{1}H-NMR spectrum of 5,6-bis(octyloxy)-4,7-di(furan-2-yl)benzo[c][1,2,5]oxadiazole

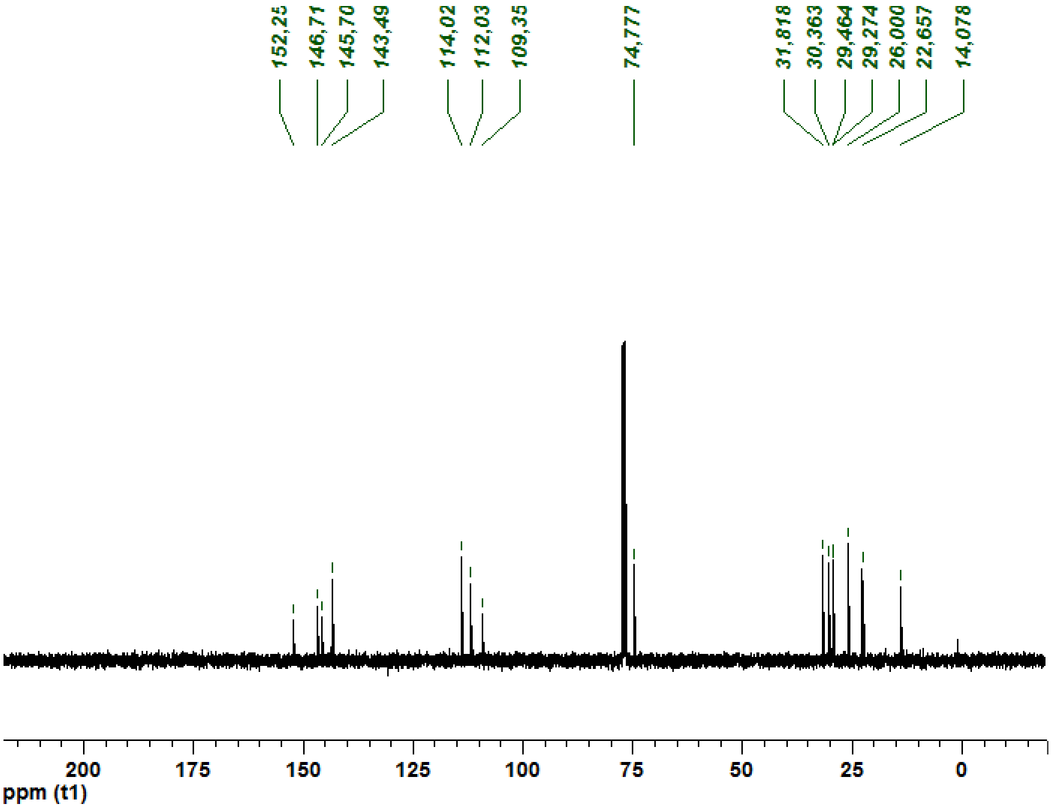

Figure A.36: ^{13}C-NMR spectrum of 5,6-bis(octyloxy)-4,7-di(furan-2-yl)benzo[c][1,2,5]oxadiazole

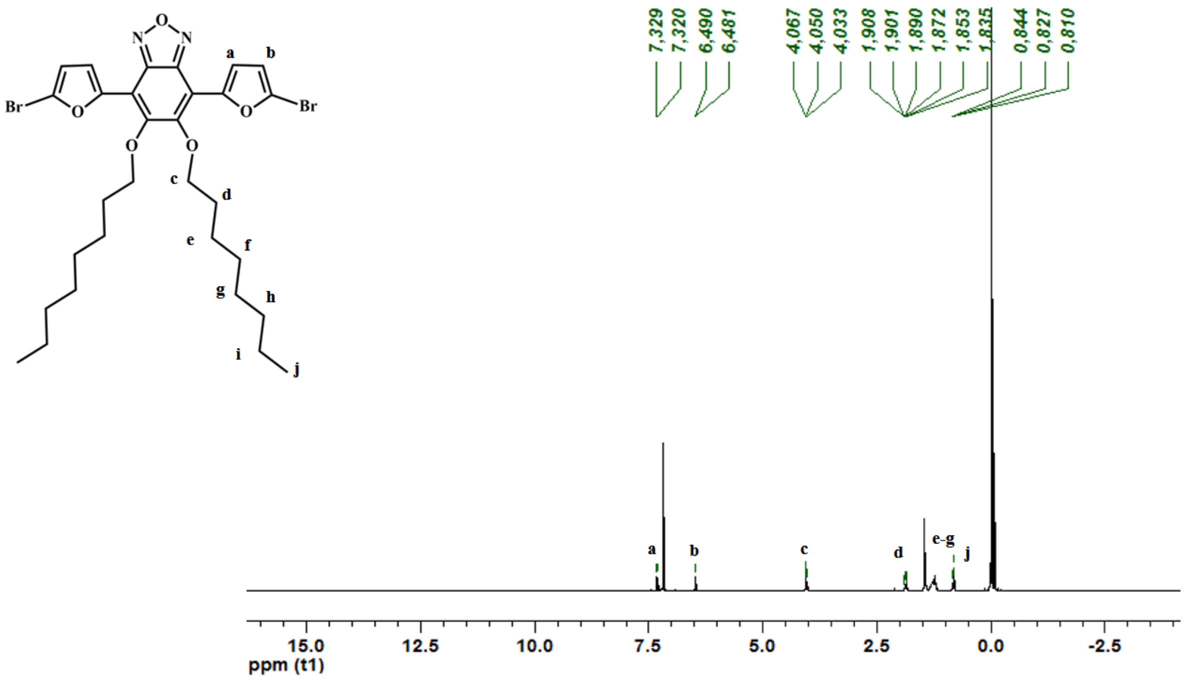

Figure A.37: ^{1}H-NMR spectrum of 4,7-bis(5-bromofuran-2-yl)-5,6-bis(octyloxy)benzo[c][1,2,5]oxadiazole

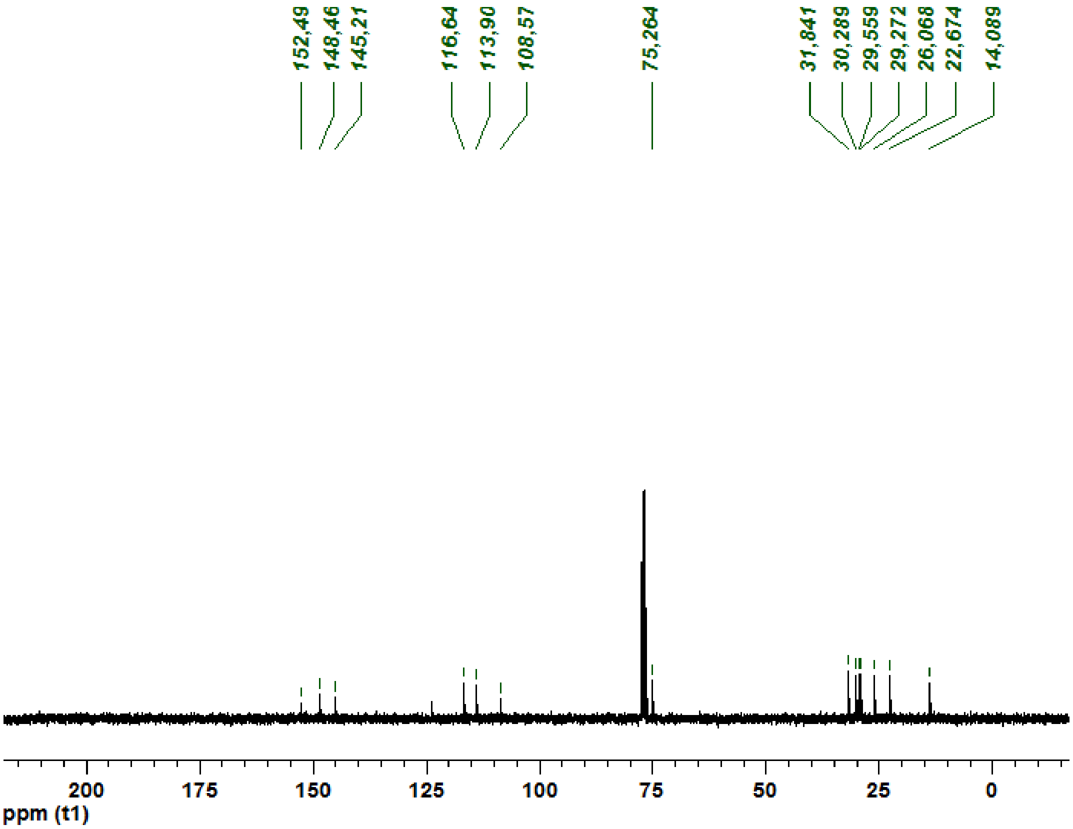

Figure A.38: ^{13}C-NMR spectrum of 4,7-bis(5-bromofuran-2-yl)-5,6-bis(octyloxy)benzo[c][1,2,5]oxadiazole